THE ROLE OF PROTEOME IN CELLULAR Zn^{2+} TRAFFICKING AND IN THE ABILITY OF FLUORESCENT ZINC SENSORS TO IMAGE INTRACELLULAR Zn^{2+}

by

Mohammad R. Karim

A Dissertation Submitted in

Partial Fulfillment of the

Requirements for the Degree of

Doctor of Philosophy

in Chemistry

at

The University of Wisconsin – Milwaukee

August 2016

ABSTRACT

THE ROLE OF PROTEOME IN CELLULAR Zn^{2+} TRAFFICKING AND IN THE ABILITY OF FLUORESCENT ZINC SENSORS TO IMAGE INTRACELLULAR Zn^{2+}

by

Mohammad R. Karim

The University of Wisconsin-Milwaukee, 2016

Under the Supervision of Professor David H. Petering

Zinc is an essential biological trace metal used in as many as 3000 Zn-proteins, about 10% of the eukaryotic proteome, as either a structural constituent or a catalytic cofactor. These proteins include the zinc fingers, the most prevalent transcription factors that bind a wide range of gene promoters and thus regulate gene expression. A eukaryotic cell contains several hundred micromolar of Zn^{2+}- almost all of it is bound to specific Zn-proteins. Recently, Zn^{2+} has been reported to serve as a regulatory signal and a neurotransmitter, suggesting that there also exists a dynamic Zn^{2+} pool in cells. These findings led to the synthesis of a wide range of fluorescent sensors to image intracellular mobile Zn^{2+}. Despite extensive knowledge about thousands of Zn-proteins, the Zn^{2+} trafficking pathway from its entry into the cytosol by transporters to the formation of Zn-proteins is not well understood. This present work has studied the role of proteome in cellular Zn^{2+} trafficking using fluorescent zinc sensors, including FluoZin-3, Zinquin (ZQ), TSQ, Newport Green (NPG) and Zinpyr-1 (ZP1). The titration of proteome pre-treated with FluoZin-3, a relatively high affinity Zn^{2+} sensor with the stability constant of 15 nM, with Zn^{2+} has revealed that proteome contains a significant number of high

affinity, non-specific Zn^{2+} binding sites, with the stability constants on the order of 10^{-10} M. The discovery of these high affinity binding sites of proteome suggested that along with Zn-metallothionein, proteome too can serve as a possible intermediate along the way to the formation of native Zn-proteins. Moreover, this finding raises the question how the majority of the fluorescent zinc sensors with the stability constants ranging from micromolar to nanomolar image intracellular labile Zn^{2+} by circumventing the proteome's high zinc buffering capacity. Interestingly, the thiol binding reagents, N-ethylmaleimide (NEM) and DTNB abolished these high affinity sites, revealing the involvement of proteomic sulfhydryl groups in these Zn^{2+} binding sites. The loss of proteome's zinc buffering capacity upon sulfhydryl modification can explain how the sensors bind the dynamic Zn^{2+} pool by surpassing the proteome's high Zn^{2+} binding affinity. For example, Zinquin, a high affinity sensor with K_d of 2 nM, could bind the mobile Zn^{2+} only when the proteome was significantly modified by the reaction under investigation, such as the liberation of proteomic Zn^{2+} by nitric oxide, which reacts with the sulfhydryl groups and thus reduces proteome's buffering capacity. In case of unperturbed proteome, these sensors either are unable to compete for mobile Zn^{2+} with proteome's high affinity Zn^{2+} binding sites or generate ternary adduct, Proteome•Zn-Sensor, with Zn^{2+} preferentially bound to proteome. Newport Green, for example, with its modest stability constant ($K_d \sim 10^{-5} – 10^{-6}$ M) cannot efficiently compete with proteomic ligands to image mobile Zn^{2+}. It could not bind intracellular Zn^{2+} shuttled into LLC-PK_1 cells using the ionophore, pyrithione. Moreover, when proteomic Zn^{2+} was liberated by the reaction with sulfhydryl binding reagents, NEM and diethylamine NONOate (DEA-NO), in the presence of Newport Green, insignificant amount of Zn-NPG was detected. By contrast, the higher affinity Zn^{2+} sensor

($K_d \sim 0.7$ nM) than Newport Green, ZP1 formed ternary adduct Proteome•Zn-ZP1 with the dynamic Zn^{2+}, where Zn^{2+} is adventitiously bound to proteome's high affinity zinc binding sites. Besides with the mobile Zn^{2+}, ZP1 also seems to react with the static distribution of cellular Zn^{2+} in specific Zn-proteins and generates ZP1-Zn-Proteome ternary adduct. Therefore, the effectiveness of the sensors to bind the cellular dynamic Zn^{2+} is a variable of proteome's Zn^{2+} binding characteristics.

TABLE OF CONTENTS

LIST OF FIGURES viii
LIST OF TABLES xi
ACKNOWLEDGEMENTS xiii
1. INTRODUCTION 1
2. MATERIALS AND METHODS 11
2.1 Chemicals and Reagents 11
2.2 Cell Culture 12
2.2.1. Preparation of medium and solutions 12
2.2.2. Cell culture 12
2.3 Synchronization of CCRF-CEM cells at G1 and G2/M phases 13
2.4 Cell counting 14
2.5 Cell viability assay (Trypan blue exclusion assay) 14
2.5.1 Cell viability of LLC-PK_1 cells incubated with Newport Green ester (NPG_E) 14
2.5.2 Cell viability assay of CCRF-CEM cells blocked at G1 and G2/M phases 15
2.6 Flow cytometry of CCRF-CEM cells blocked at G1 and G2/M phases 15
2.7 Fluorescence Spectroscopy of LLC-PK_1 Cells 16
2.7.1 Fluorescence spectroscopy of LLC-PK_1 cells incubated with Newport Green ester (NPG_E) 16
2.7.2 Fluorescence spectroscopy of LLC-PK_1 cells incubated with Zinpyr-1 (ZP1) 17
2.7.3 Fluorescence spectroscopy of LLC-PK_1 cells incubated with Zinquin or TSQ followed by diethylamine NONOate (DEA-NO) 17
2.7.4 Fluorescence spectroscopy of CCRF-CEM cells synchronized in G1 phase incubated with TSQ or Zinquin 18
2.8 Isolation of cell lysate following incubation of cells with sensor (and DEA-NO) and its fractionation using gel filtration column or Centricon filtration 18
2.8.1 Preparation of Sephadex G-75 gel filtration column 18
2.8.2 Isolation of cell lysate following incubation of cells with sensor (and DEA-NO) 19
2.8.3 Fractionation of the cell lysate using Sephadex G-75 gel filtration column or Centricon filtration 19
2.9 Isolation of Proteome Using Sephadex G-75 Chromatography 20

2.10 Reaction of isolated proteome with fluorescent sensors 20
2.12 Isolation of subcellular proteomes from LLC-PK_1 cells 21
2.13 Reaction of LLC-PK_1 cells with Zn(pyrithione)$_2$ in the presence of Newport Green (NPG_E) 22
2.14 Reaction of model Zn-proteins (alcohol dehydrogenase, carbonic anhydrase) with Newport Green or Zinpyr-1 23
2.15 Quantification of Zn^{2+} by Atomic Absorption Spectrophotometry 23
2.16 Quantification of sulfhydryl groups in proteome 24
3.1 Chemical Biology of Newport Green (NPG) 25
3.1.1. Spectral properties of NPG and Zn-NPG 26
3.1.2. Cell viability 26
3.1.3 Reaction of NPG_E with LLC-PK_1 cells 29
3.1.4 Location of NPG_A among cell constituents. 38
3.1.5 Reaction of NPG_E and NPG_A with isolated proteome. 38
3.1.6 Reactions of NPG with model Zn-proteins (alcohol dehydrogenase, carbonic anhydrase). 42
3.1.7 Stability of Zn-NPG_A with proteome. 46
3.1.8 Stability of Zn-NPG_A with Glutathione. 49
3.1.7 Reaction of NPG and Zn-NPG with bovine serum albumin (BSA) 52
3.1.9 Response of intracellular NPG_A to added Zn^{2+} 56
3.1.10 Reaction of proteome with thiol reactive agents NO and NEM in the presence of NPG_A 58
3.2 Chemical Biology of Zinpyr-1 (ZP1) 60
3.2.1 Reaction of ZP1 with $ZnCl_2$ 62
3.2.2 Reaction of LLC-PK_1 cells with ZP1 64
3.2.3 Reaction of ZP1 with isolated proteome 68
3.2.4 Titration of proteome with Zn^{2+} in the presence of ZP1 71
3.2.5 Reaction of proteome with Zn-ZP1 75
3.2.6 Reaction of ZP1 with TSQ-Zn-Proteome 78
3.2.7. Reaction of ZP1 with model zinc proteins, such as alcohol dehydrogenase 83
3.3 Reaction of Zn-proteome with Diethylamine NONOate (DEA-NO) in the presence of Zinquin/TSQ/FluoZin-3 87

3.3.2. Reaction of isolated proteome with DEA-NO in the presence of Zinquin acid (ZQacid). 97
3.3.3. Reaction of the whole LLC-PK_1 cells with DEA-NO in the presence of TSQ. 100
3.3.4. Reaction of isolated proteome with DEA-NO in the presence of TSQ. 106
3.3.5. Reaction of isolated proteome with added Zn^{2+} in the presence of excess TSQ/ZQ. 107
3.3.6. Reaction of isolated proteome with DEA-NO in the presence of FluoZin-3. 112
3.3.7. Reaction of isolated proteome with DEA-NO prior to FluoZin-3. 114
3.3.8 Stability of Zn-FluoZin3 in the presence of proteome 118
3.4 Zinc buffering of proteome and proteomic components responsible for it 122
3.4.1 Titration of proteome incubated with N-ethylmaleimide (NEM) with Zn^{2+} in the presence of FluoZin-3 123
3.4.2 Titration of proteome incubated with N-ethylmaleimide (NEM) with $ZnCl_2$ in the presence of Newport Green (NPG) 127
3.4.3. Titration of proteome incubated with 5,5-dithio-bis-(2-nitrobenzoic acid) (DTNB) with $ZnCl_2$ in the presence of FluoZin-3. 130
3.5 Status of Zn-proteome at different phases in a cell cycle 132
3.5.1 Cell viability assay 133
3.5.2 Reaction of TSQ and CCRF-CEM cells blocked at G1 phase by thymidine 134
3.5.3 Reaction of Zinquin (ZQ) and CCRF-CEM cells blocked at G1 phase by thymidine 138
3.5.4 Reaction of TSQ and proteome isolated from CCRF-CEM cells blocked at G1 phase by thymidine 142
3.5.5 Reaction of Zinquin (ZQ) and proteome isolated from CCRF-CEM cells blocked at G1 phase by thymidine 145
3.5.6 Reaction of TSQ and proteome isolated from CCRF-CEM cells blocked at G2/M phase by nocodazole 149
3.5.7 Reaction of Zinquin (ZQ) and proteome isolated from CCRF-CEM cells blocked at G2/M phase by nocodazole 153
4. DISCUSSION 158
5. SUMMARY 174
6. REFERENCES 176
7. CURRICULUM VITAE 188

LIST OF FIGURES

Figure 1.1 Hypothetical trafficking pathways of Zn^{2+} between and within cellular compartments 2

Figure 1.2 Examples of some commonly used fluorescent sensors to image cellular Zn^{2+} 6

Figure 3.1.1 Change of fluorescence intensity and emission wavelength maximum of NPG_A and Zn-NPG_A with increasing concentration 27

Figure 3.1.2 Titration of NPG with Zn^{2+} 28

Figure 3.1.3 Fluorescence spectra of NPG, Zn-NPG and the quenching by TPEN 29

Figure 3.1.4 Reaction of LLC-PK_1 cells with NPG_E 31

Figure 3.1.5 Separation of the reaction mixture of LLC-PK_1 cells with NPG_E 34

Figure 3.1.6 TPEN effect to the extracellular fluorescence 35

Figure 3.1.7 Efflux of NPG_A from cells 36

Figure 3.1.8 Reaction of CCRF-CEM cells and NPG_E 37

Figure 3.1.9 Interaction of NPG_A with Sephadex beads 39

Figure 3.1.10 Centricon filtration of the reaction mixture of proteome and NPG_A 40

Figure 3.1.11 Reaction of proteome with NPG_E 41

Figure 3.1.12 Centricon filtration of the reaction mixture of proteome and NPG_E 42

Figure 3.1.13 Reaction of alcohol dehydrogenase (ADH) with NPG_E 44

Figure 3.1.14 Reaction of carbonic anhydrase (CA) with NPG_E 45

Figure 3.1.15 Stability of Zn-NPG_A in the presence of proteome 47

Figure 3.1.16 Titration of proteome with $ZnCl_2$ in the presence of NPG_A 48

Figure 3.1.17 Stability of Zn-NPG_A with sub-cellular proteome 50

Figure 3.1.18 Stability of Zn-NPG_A in the presence of glutathione (GSH)

Figure 3.1.19 Titration of NPG_A with $ZnCl_2$ in the presence of glutathione (GSH) 52

Figure 3.1.20 Reaction of NPG_A and Zn-NPG_A with bovine serum albumin (BSA) 54

Figure 3.1.21 Titration of Zn-NPG_A with BSA 55

Figure 3.1.22 Reaction of NPG_E incubated LLC-PK_1 cells with Zn-pyrithione 57

Figure 3.1.23 Reaction of proteome with diethylamine NONOate (DEA-NO) in the presence of NPG_A 59

Figure 3.1.24 Reaction of proteome with N-ethylmaleimide (NEM) in the presence of NPG_A 60

Figure 3.2.1 Titration of ZP1 with Zn^{2+} 63

Figure 3.2.2 Reaction of LLC-PK_1 cells with ZP1 66

Figure 3.2.3 Locating fluorescent species in the reaction of LLC-PK_1 cells and ZP1 67

Figure 3.2.4 Reaction of ZP1 with isolated proteome 69

Figure 3.2.5 Sephadex G-75 gel filtration of the reaction mixture of isolated proteome (10 µM Zn^{2+}) and ZP1 70

Figure 3.2.6 Titration of proteome with Zn^{2+} in the presence of ZP1 73

Figure 3.2.7 Sephadex gel filtration of proteome titrated with $ZnCl_2$ in the presence of ZP1 74

Figure 3.2.8 Reaction of proteome with $ZP1(Zn)_2$ 77

Figure 3.2.9 Reaction of ZP1 and proteome incubated with TSQ 80

Figure 3.2.10 Sephadex gel filtration of proteome reacted with TSQ and ZP1 81

Figure 3.2.11 Integrated fluorescence of high molecular weight (HMW) fractions and TPEN effect 82

Figure 3.2.12 Reaction of ZP1 with alcohol dehydrogenase 86

Figure 3.3.1 Reaction of LLC-PK_1 cells with DEA-NO in the presence of Zinquin ethyl ester 92

Figure 3.3.2 Sephadex G-75 filtration of LLC-PK_1 cells incubated with 20 µM Zinquin ethyl ester (ZQee) followed by 500 µM DEA-NO 96

Figure 3.3.3 Sephadex G-75 filtration of isolated proteome incubated with 20 µM Zinquin acid (ZQacid) followed by 500 µM DEA-NO 99

Figure 3.3.4 Reaction of LLC-PK_1 cells with DEA-NO in the presence of TSQ 103

Figure 3.3.5 Sephadex G-75 filtration of LLC-PK_1 cells incubated with TSQ followed by 500 µM DEA-NO 105

Figure 3.3.6 Reaction of isolated proteome with DEA-NO in the presence of TSQ 106

Figure 3.3.7 Titration of isolated proteome with $ZnCl_2$ in the presence of Zinquin acid 110

Figure 3.3.8 Titration of isolated proteome with $ZnCl_2$ in the presence TSQ 112

Figure 3.3.9 Reaction of isolated proteome with DEA-NO in the presence of FluoZin-3 115

Figure 3.3.10 Sephadex gel filtration of proteome incubated with DEA-NO in the presence of FluoZin-3 116

Figure 3.3.11 Reaction of isolated proteome (5 µM Zn^{2+}) with 500 µM DEA-NO followed by 20 µM FluoZin-3 117

Figure 3.3.12 Stability of Zn-FluoZin3 in the presence of proteome 121

Figure 3.4.1 Reaction of N-ethylmaleimide (NEM) with thiolate anion 122

Figure 3.4.2 Reaction of DTNB with sulfhydryl group of a thiol 123

Figure 3.4.3 Titration of proteome incubated with N-ethylmaleimide (NEM) with $ZnCl_2$ in the presence of FluoZin-3 126

Figure 3.4.4 Titration of proteome incubated with N-ethylmaleimide (NEM) with $ZnCl_2$ in the presence of Newport Green (NPG) 129

Figure 3.4.5 Titration of proteome incubated with 5,5-dithio-bis-(2-nitrobenzoic acid) (DTNB) with $ZnCl_2$ in the presence of FluoZin-3 131

Figure 3.5.1 Fluorescence micrograph images of cellular Zn^{2+} observed after exposure to the Zn^{2+} fluorophore TSQ 133

Figure 3.5.2 Reaction of TSQ and CCRF-CEM cells blocked at G1 phase by thymidine 136

Figure 3.5.3 Fluorescence spectra of the cell lysate collected from CCRF-CEM cells (TSQ) 137

Figure 3.5.4 Reaction of Zinquin (ZQ) and CCRF-CEM cells blocked at G1 phase by thymidine 140

Figure 3.5.5 Fluorescence spectra of the cell lysate collected from CCRF-CEM cells (ZQ) 141

Figure 3.5.6 Reaction of TSQ and proteome isolated from CCRF-CEM cells blocked at G1 phase by thymidine 144

Figure 3.5.7 Reaction of Zinquin (ZQ) and proteome isolated from CCRF-CEM cells blocked at G1 phase by thymidine 148

Figure 3.5.6 Reaction of TSQ and proteome isolated from CCRF-CEM cells blocked at G2/M phase by nocodazole 152

Figure 3.5.7 Reaction of Zinquin (ZQ) and proteome isolated from CCRF-CEM cells blocked at G2/M phase by nocodazole 156

LIST OF TABLES

Table 3.5.1: Comparison of the normalized fluorescence intensities from TSQ reaction and zinc contents of proteome isolated from control (untreated) CCRE-CEM cells and thymidine blocked cells 145

Table 3.5.2: Comparison of the normalized fluorescence intensities from Zinquin reaction and zinc contents of proteome isolated from control (untreated) CCRE-CEM cells and thymidine blocked cells 149

Table 3.5.3: Comparison of the normalized fluorescence intensities from TSQ reaction and zinc contents of proteome isolated from control (untreated) CCRE-CEM cells and nocodazole blocked cells 153

Table 3.5.4: Comparison of the normalized fluorescence intensities from Zinquin reaction and zinc contents of proteome isolated from control (untreated) CCRE-CEM cells and thymidine blocked cells 157

ACKNOWLEDGEMENTS

I am thankful to my advisor, Dr. David H. Petering, for his incessant advice and cooperation all along my graduate program.

Furthermore, I am grateful to my thesis committee members for helping me with various ideas regarding the experimentation, and their comments on the thesis. Dr. Michael Laiosa, associate professor of School of Public Health, UWM, deserves gratitude for his help with flow cytometry.

I would also like to thank my family members, especially my parents and wife, and friends for their support and inspiration.

1. INTRODUCTION

Living organisms require a number of metal ions to serve both as structural constituents and catalytic cofactors in a wide range of proteins.[1, 2] Among these biological metal ions, Zn^{2+} ranks the second in terms of abundance, immediately following iron.[3] Because of having a fully occupied d-orbital ($3d^{10}$), zinc does not participate in redox chemistry. Nevertheless, it has been identified as an integral component in about 3,000 Zn-proteins, collectively known as Zn-proteome, which make up about 10% of the eukaryotic proteome.[4, 5] Examples of proteins in which Zn^{2+} serves as an important structural component include the most prevalent eukaryotic transcription factors – the Zn-finger proteins, which bind DNA and in turn, regulate gene expression.[4, 6] Some of the well-known instances of enzymes containing Zn^{2+} as a catalytic cofactor are carbonic anhydrase, alcohol dehydrogenase, alkaline phosphatase, and so on. In these enzymes, Zn^{2+} can either act as a Lewis acid or help in holding the enzyme-substrate complex together, and thus assists in catalytic conversion of the substrate into product.[7, 8] Typically, the thiolate, carboxylate and/or imidazole ligands from cysteine, aspartate and histidine, respectively, bind Zn^{2+} occupying three coordination sites and thus leaving the fourth binding site for the substrate or other molecules, including water.[9] However, other possible coordination numbers of Zn^{2+} in Zn-proteins have also been reported.[4, 5, 10-12]

Eukaryotic cells contain several hundred micromolar of Zn^{2+}.[13, 14] Almost all of this is bound to proteins to make thousands of Zn-proteins.[15] The concentration of steady-state cellular free or labile Zn^{2+} falls in the range of picomolar to nanomolar.[3, 13, 14, 16] Despite the extensive research that has been carried out to understand the function of these thousands of Zn-proteins and the

role of Zn^{2+} in them, the mechanisms of Zn^{2+} trafficking that results in the generation of the native Zn-proteins are still not well understood. Copper, another cellular trace metal ion, is shuttled by different copper chaperon proteins to its target proteins.[17-19] Copper trafficking pathways may suggest that zinc is also transported by various not yet discovered zinc chaperon proteins to find the target proteins. However, the important difference between copper and zinc proteins is that there is only a handful of copper proteins in the cell, as opposed to ca. 3000 zinc proteins. To utilize the similar chaperone mediated pathway, Zn^{2+} will require perhaps hundreds to thousands of chaperone proteins, which seems to be unlikely.

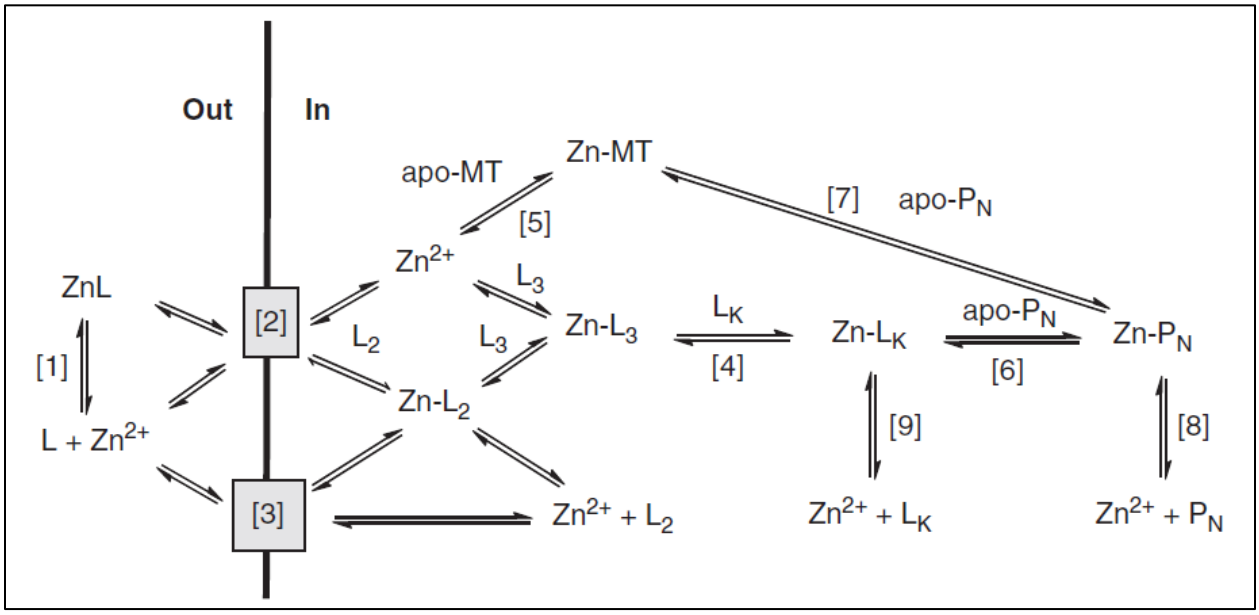

Figure 1.1 Hypothetical trafficking pathways of Zn^{2+} between and within cellular compartments.

Figure 1.1 portrays a general model for Zn^{2+} trafficking pathways between the extracellular medium and the cytosol or among the cellular compartments.[20] One possible trafficking pathway involves the binding of intracellular Zn^{2+} to apo-metallothionein, following the

transportation of Zn^{2+} - free or albumin bound (Zn-L) - into the cytosol from outside by membrane Zn^{2+} transporters of the ZIP family, to form Zn-Metallothionein, which then serves as a Zn^{2+} donor to apo Zn-proteins to generate specific Zn-proteins.[20] An important cellular Zn-protein, metallothionein (MT) can bind up to seven Zn^{2+} with high stability constants of $10^{11\text{-}12}$ per Zn^{2+} in two Zn-thiolate clusters.[21-24] The fully saturated metallothionein, Zn_7-MT displays ligand substitution reactivity with apo-Zn-proteins such as carbonic anhydrase, which have large stability constants for Zn^{2+} (log K = 11-12).[24-26] This reactivity suggests that $Zn_{n\ (1\text{-}7)}$-MT can serve as an intermediate along the way to form specific Zn-proteins (reactions 1 and 2).[23, 24, 27, 28]

$$n\ Zn^{2+} + \text{apo-MT} \rightleftharpoons Zn_n\text{-MT} \qquad (1)$$

$$Zn_n\text{-MT} + n\ \text{apo-}P_N \rightleftharpoons n\ \text{Zn-}P_N + \text{apo-MT} \qquad (2)$$

An alternative possible pathway is that Zn^{2+} transported into cytosol non-specifically binds to proteins containing potential Zn^{2+} binding sites (Zn-L_2 or Zn-L_3), and through ligand substitution is distributed randomly among different proteins of the proteome and small molecules such as glutathione.[20] Finally, as Zn-L_k encounters apo-Zn-protein (apo-P_N), Zn^{2+} is transferred to generate native Zn-proteins (Zn-P_N) (reaction 3). Proteome's non-specifically zinc binding capacity has been reported in some recent studies.[13, 29-33]

$$Zn^{2+} + L_2 \rightleftharpoons Zn\text{-}L_2; \qquad Zn\text{-}L_2 + L_3 \rightleftharpoons Zn\text{-}L_3 + L_2;$$
$$Zn\text{-}L_3 + L_K \rightleftharpoons Zn\text{-}L_K + L_3; \qquad Zn\text{-}L_K + P_N \rightleftharpoons Zn\text{-}P_N + L_K \qquad (3)$$

Moreover, the free Zn^{2+} pool resulting from the equilibrium between the randomly bound Zn^{2+} ($Zn\text{-}L_K$) and the unbound Zn^{2+} can bind to apo-Zn-protein (P_N) to generate specific Zn-proteins ($Zn\text{-}P_N$) (reaction 4).[20] This free Zn^{2+} pool may also participate in cellular Zn^{2+} signaling.

$$Zn\text{-}L_K \rightleftharpoons L_K + Zn^{2+}; \quad Zn^{2+} + P_N \rightleftharpoons Zn\text{-}P_N \qquad (4)$$

Apart from the roles of important structural and catalytic components in Zn-proteins, Zn^{2+} also serves as an intracellular regulatory signal. The best studied example of Zn^{2+}'s role as a regulatory signal in eukaryotic cells is the increased synthesis of metallothionein when the intracellular concentration of Zn^{2+} is elevated.[34, 35] The elevated concentration of intracellular Zn^{2+} binds to apo-Zn-fingers of the metal response element (MRE) – binding transcription factor 1 (MTF-1), and thus changes its conformation such that it can bind the MRE sequences of the promoter region of metallothionein and ZnT1 transporter genes (reaction 5).[36-39] This association, in turn, stimulates the synthesis of metallothionein and ZnT1 transporter mRNAs, which then translate into apo-metallothionein and ZnT1 transporter proteins. Apo-metallothionein binds the cell's increased level of Zn^{2+} and ZnT1 transporters efflux Zn^{2+} out of the cell and thus, maintain the cellular zinc homeostasis.[40]

$$\text{MTF-1}_{\text{inactive}} + n\ Zn^{2+} \rightleftharpoons Zn_{n\ (1\text{-}6)}\text{-MTF-1}_{\text{active}}$$
$$Zn_n\text{-MTF-1} + \text{MRE} \rightleftharpoons Zn_n\text{-MTF-1}\bullet\text{MRE} \qquad (5)$$

Moreover, various studies have reported the participation of Zn^{2+} in dyanamic cellular signaling processes such as synaptic chemical transmission and endocrine signaling.[41, 42] Abundant in synaptic vesicles of glutamatergic neurons, Zn^{2+} is released into the synaptic cleft following

neuronal stimulation.[43-45] However, the exact mechanism of how it serves as a signaling agent is yet to understand.

The cellular roles of Zn^{2+} as a regulatory signal and a chemical messenger in neuronal synapses clearly suggest that it is not only bound to fixed binding sites in various Zn-proteins as structural and catalytic constituents. Rather, cells have a transient concentration of mobile or free Zn^{2+} generated by some stimulus, which in turn participates in cellular signaling.[46] The generation of this dyanamic Zn^{2+} pool can be shown by the following equation:

$$Zn\text{-}L + \text{stimulus} \rightleftharpoons Zn^{2+} + L \qquad (6)$$

L represents Zn^{2+} binding ligands, including Zn-protein and small molecules such as glutathione.

Following the revelation of the transient mobile Zn^{2+} pool and its function in cellular signaling, the biochemical studies of Zn^{2+} metabolism has gained a new momentum. This required the discovery of some analytical tool to study the cellular functions of this dynamic Zn^{2+} pool. As yet, zinc fluorescent sensors have been considered the best analytical tool for this purpose. Over the past couple of decades, a number of fluorescent sensors with a wide variety of structures, stability constants ranging from micromolar to nanomolar, excitation wavelength (350 – 550 nm) and emission wavelength (450 – 600 nm) have been designed and synthesized to image the mobile Zn^{2+} pool of the cells.[1, 2, 47-49] The structures of these fluorescent sensors contain a fluorophore reporter linked with the Zn^{2+} chelating ligand. Upon Zn^{2+} binding, sensors display an enhancement of fluorescence through photo-induced electron transfer (PET) quenching mechanism.[1, 2] According to this mechanism, in the absence of Zn^{2+} ion, the electron rich receptor (chelating ligand) quenches the fluorescence of the fluorophore. As Zn^{2+} binds to

the receptor and thus prevents its interference in fluorescence emission, an enhancement of emission is followed.[1, 2]

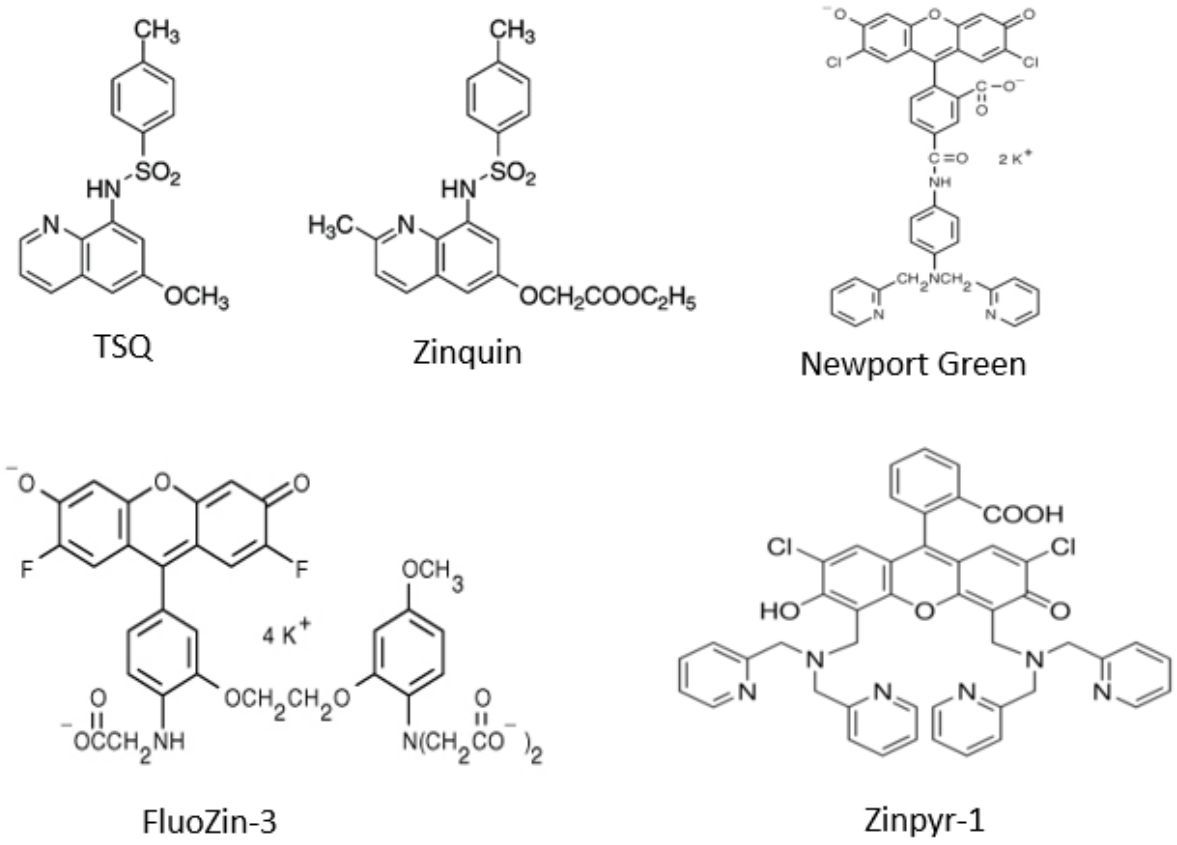

Figure 1.2 Examples of some commonly used fluorescent sensors to image cellular Zn^{2+}.

In typical experiments aimed at studying the dynamic cellular Zn^{2+} using fluorescent sensors, cells are incubated with the cell-permeable ester form of the sensor molecule (e.g. Zinquin, Newport Green, FluoZin-3 etc.), which following its entry into the cell gets cleaved by cellular esterases into its negatively charged acid form and thus becomes trapped inside the cell.[50]

However, some sensors (e.g. TSQ, Zinpyr-1) are charge neutral and can permeate the cell membrane, and thus their ester forms are not required for cellular use. Upon influx into the cell, the fluorescence enhancement and its reversal by the introduction of a cell permeable strong Zn^{2+} chelator, typically N, N, N', N'-tetrakis (2-pyridylmethyl) ethane-1, 2-diamine (TPEN-structure in Figure 1.2), are attributed to the imaging of free or labile Zn^{2+}.[46] The sensing of free Zn^{2+} pool generated by the equation (6) by the fluorescent sensor and its chelation by TPEN can be displayed by the following equations:

$$Zn^{2+} + \text{Sensor} \rightleftharpoons \text{Zn-Sensor} \qquad (7)$$

$$\text{Zn-Sensor} + \text{TPEN} \rightleftharpoons \text{Zn-TPEN} + \text{Sensor} \qquad (8)$$

The discovery of these fluorescent sensors has boosted the biochemical research of zinc metabolism, which, in turn, has revealed further evidence of the role of Zn^{2+} as a regulatory signal and secondary messenger. For example, an enhancement of a Zn^{2+} sensor fluorescence in brain injury models has led to the conclusion that labile or chelatable Zn^{2+} plays a crucial role in neurodegenerative diseases.[51-53] In another study, pulmonary endothelial cells were exposed to nitric oxide or lipopolysaccharide in the presence of a zinc sensor that resulted in an increase of zinc sensor fluorescence signal, which suggested that Zn^{2+} participates in cellular signaling pathways that result in airway constriction.[54-56]

Although the *in vitro* application of these fluorescent sensors to bind free Zn^{2+} is simple, their cellular use to image labile Zn^{2+} pool might be complicated due to a number of factors. Firstly, for quantitative measurement of free or competitively bound Zn^{2+} using these sensors, the stability constant of the sensor must be within the range of cellular free Zn^{2+} concentration or

similar to that of competing ligands for bound Zn^{2+}. Moreover, in case of sensors with relatively high stability constants compared with cellular Zn^{2+} pools (ZnL_k, Fig. 1.1) or with large intracellular concentration, the sensor might itself react with the bound Zn^{2+} pool of the cell and therefore, disturb the equilibrium between the Zn^{2+} bound to different ligands and free Zn^{2+} (reaction 5). Another possible unwanted reaction is that the sensor might directly chelate Zn^{2+} out of native Zn^{2+} binding sites (proteins or small molecules) (reaction 9). Both cases give rise to fluorescence enhancement, which may confuse the researchers with the fluorescence due to imaging of mobile Zn^{2+}.

$$\text{Zn-Ligand} + \text{Sensor} \rightleftharpoons \text{Ligand} + \text{Zn-Sensor} \qquad (9)$$

A significant number of studies have been done over the past two decades that used these fluorescent sensors to detect the mobile Zn^{2+} in cells.[49, 57-63] However, the key drawback of most of these studies is that they relied mostly on fluorescent micrographs obtained following the incubation of cells with the sensor using a fluorescence microscope to draw their conclusions. Not much of the chemistry that occurs between the sensor and the cellular constituents has been investigated. The sole dependence on the fluorescence observation through a microscope, therefore, may often give misleading results. For example, 6-methoxy-8-p-toluenesulfonamido-quinoline (TSQ) and its derivative Zinquin (ZQ) are two quinolone-based fluorophores commonly used by the researchers to image cellular free or labile Zn^{2+} pool.[49, 57, 61, 64] These fluorophores use their bidentate ligands comprised of quinoline and sulfonamide nitrogens to bind Zn^{2+} in a 2:1 stoichiometry (Figure 1.2).[50, 65] Although structurally similar to TSQ, the presence of a methyl group at the 2 position enhances Zinquin's affinity for Zn^{2+}

(Figure 1.2), and therefore it can sense smaller intracellular Zn^{2+} concentration than TSQ.[50] The fluorescence increase upon their treatment with cells has naively been attributed to their binding of Zn^{2+} to from fluorescent species $Zn(TSQ)_2$ or $Zn(ZQ)_2$. However, Meeusen *et al.* and Nowakowski *et al*. have shown that when used in cells, both TSQ and Zinquin actually image a subset of Zn-proteins, not free Zn^{2+} as various studies claimed, through the formation of the ternary adduct, TSQ-Zn-Protein or Zinquin-Zn-Protein.[50, 65, 66] This subset of Zn-proteins imaged by TSQ or ZQ represents about 15-20% of the Zn-proteome. The generation of this ternary adduct species is quite evident from its different spectral properties. $Zn(TSQ/ZQ)_2$ complex displays an emission maximum of 490 nm when excited at 370 nm, whereas (TSQ/ZQ)-Zn-Protein ternary adduct gives a blue-shifted 470 nm emission. As Zinquin binds Zn^{2+} with higher affinity than TSQ, along with ZQ-Zn-Protein ternary adduct formation, it also may react with Zn-proteome to generate $Zn(ZQ)_2$ complex.[50] Like of $Zn(TSQ/ZQ)_2$, the fluorescence of (TSQ/ZQ)-Zn-Protein ternary adduct is also readily reversed by the reaction with the strong Zn^{2+} chelator TPEN. Meeusen *et al.* have also demonstrated that other than chelating Zn^{2+} out of the ternary adduct as Zn-TPEN, TPEN, itself can also form ternary adduct TPEN-Zn-Protein by replacing the sensor.[67]

$$2\ Zn^{2+} + TSQ/ZQ \rightleftharpoons Zn(TSQ/ZQ)_2 \qquad (\lambda_{emission,\ max} \sim 490\ nm) \qquad (10)$$

$$TSQ/ZQ + Zn\text{-}Protein \rightleftharpoons (TSQ/ZQ)\text{-}Zn\text{-}Protein \qquad (\lambda_{emission,\ max} \sim 470\ nm) \qquad (11)$$

$$2\ ZQ + Zn\text{-}Protein \rightleftharpoons Zn(ZQ)_2 + apo\text{-}Protein \qquad (12)$$

$$(TSQ/ZQ)\text{-}Zn\text{-}Protein + TPEN \rightleftharpoons Zn\text{-}TPEN + TSQ/ZQ + apo\text{-}Protein \qquad (13)$$

$$(TSQ/ZQ)\text{-}Zn\text{-}Protein + TPEN \rightleftharpoons TPEN\text{-}Zn\text{-}Protein + TSQ/ZQ \qquad (14)$$

This finding further deepens the question of what various sensors actually image at the cellular level. The present study has examined the chemical and biological properties of Newport Green, a fluorescent Zn^{2+} sensor with modest binding constant ($K_d \sim 10^{-5} – 10^{-6}$ M) and its efficiency as a zinc sensor within the cellular framework. To compare with Newport Green results, a relatively higher affinity sensor, Zinpyr-1, with the binding constant of 0.7 nM has also been studied. Furthermore, having found that TSQ and Zinquin bind Zn-proteins to form ternary adducts (TSQ/Zinquin)-Zn-Protein, this study has investigated how TSQ, Zinquin and FluoZin-3 interact with proteome incubated with diethylamine NONOate (DEA-NO). This nitric oxide (NO) donor spontaneously releases NO at physiological pH, which in turn reacts with proteomic sulfhydryl groups to induce the liberation of Zn^{2+} from native Zn-proteins. One of the key findings of these studies was that aside from the native Zn^{2+} binding sites of Zn-proteins, proteome possesses a good number of high affinity Zn^{2+} binding sites. Therefore, we next examined the proteomic components involved in these high affinity Zn^{2+} binding. Finally, the hypothesis that cells synthesize varied concentration of Zn-proteome at different phases of the cell cycle, which can explain the asymmetric distribution of fluorescence among neighboring LLC-PK_1 cells observed by Meeusen et al. following the incubation of cells with TSQ, was investigated.

2. MATERIALS AND METHODS

2.1 Chemicals and Reagents

The zinc fluorescent sensors Newport Green, DCF diacetate (NPG_E) and Newport Green dipotassium salt (NPG_A) were purchased from Invitrogen, TSQ from AnaSpec, Inc., Zinquin – both acid and ethyl ester - from Enzo Life Sciences, FluoZin-3 from Molecular Probes, and Zinpyr-1 (ZP1) from Santa Cruz Biotechnology. All these zinc sensors were dissolved in DMSO and stored in the dark at -20^0 C in small aliquots. Diethylamine NONOate (DEA-NO) was obtained from Cayman Chemical. DEA-NO was dissolved in 0.01 M NaOH and stored in aliquots at -80^0 C until use. N-ethylmaleimide (NEM), nocodazole and thymidine were bought from Sigma. All the other chemicals and reagents were purchased from either Fisher Scientific or Sigma-Aldrich at the highest grade available.

The model zinc proteins alcohol dehydrogenase and carbonic anhydrase were obtained from Sigma in the form of lyophilized powder. The powders were dissolved in degassed 20 mM Tris adjusted to pH 7.4 and stored at -80^0 C. The antibiotics penicillin G and streptomycin sulfate for cell culture were purchased from Fisher Scientific and Sigma, respectively. Fetal calf serum (FCS) was also bought from Fisher Scientific and stored at -80^0 C until use.

2.2 Cell Culture

2.2.1. Preparation of medium and solutions

Both LLC-PK_1 (pig kidney cells) cell line (adherent cell line) and CCRF-CEM human lymphocytic leukemia cells (suspension cell line) were purchased from ATCC and were grown in Medium 199 with HEPES modification and RPMI 1640 medium, respectively. Medium powder from the bottle was dissolved in 1L MilliQ water. 2.2 g (for Medium 199) or 2.0 g (for RPMI 1640) sodium bicarbonate ($NaHCO_3$) was added to the medium solution and the pH of the solution was adjusted to 7.2. The medium was then supplemented with 50 mg/L penicillin G and 50 mg/L streptomycin sulfate, and sterile filtered before use.

Confluent LLC-PK_1 cells were released from the culture flask by 10X trypsin-EDTA treatment. To prepare 200 mL 10X trypsin-EDTA solution, 1.0 g trypsin, 0.4 g EDTA tetrasodium salt and 1.8 g sodium chloride (NaCl) were dissolved in MilliQ water. The solution was sterile filtered and stored in 10 mL-aliquot at -20^0 C.

2.2.2. Cell culture

LLC-PK_1 cells were grown in Medium 199 with HEPES modification supplemented with 2.2 g/L $NaHCO_3$, 50 mg/L penicillin G, 50 mg/L streptomycin and 4% fetal calf serum (FCS) (from Fischer Scientific). Each flask of cells contained 15 mL of media mix. The cells were incubated at 37^0 C in the presence of 5% CO_2. The media was changed every 2-3 days until confluence. At the point of confluence, old media was discarded completely and cells were released by 10X trypsin-EDTA solution for 10-15 min in the incubator. Once the cells were released, 0.1-0.2 mL cell

suspension was used to make new culture flask and the remaining cells were used for growing cells in 100-mm culture plates. Each plate contained 10 mL of media mix and 0.4 mL of FCS along with cells.

CCRF-CEM human lymphocytic leukemia cells were cultured in suspension (0.5×10^6 to 1.0×10^6 cells per mL) in RPMI 1640 medium supplemented with 10% FCS. Once the cell density reached to 0.5 – 1.0 x 10^6 cells per mL, cells were subdivided by dilution in new media (CCRF-CEM).

2.3 Synchronization of CCRF-CEM cells at G1 and G2/M phases

To synchronize CCRF-CEM cells at G1 phase, cells were grown in RPMI medium supplemented with 2.0 g/L $NaHCO_3$, 50 mg/mL penicillin, 50 mg/L streptomycin and 10% fetal calf serum (FCS). When the cell density reached about 5.0 x 10^5 cells per mL, 2.0 mM thymidine was added to each plate of cells. Prior use, thymidine was dissolved in purified MilliQ water and the solution was then sterile filtered. The cells were incubated with 2.0 mM thymidine for 24 hours. Following the incubation, the cell synchronization at G1 phase was confirmed using Flow Cytometry.

To block CCRF-CEM cells at G2/M phase, each plate of cells was incubated with 100 ng/mL nocodazole after the cell density reached 5.0 x 10^5 cells per mL. Following 24 hours of incubation, cells were sorted using a flow cytometer to confirm the synchronization at G2/M phase.

2.4 Cell counting

LLC-PK_1 and CCRF-CEM cells were counted using a hemacytometer. In case of LLC-PK_1 cells, the culture medium from one plate of confluent of cells (ca. 10^7 cells) was discarded and the cells were then incubated with 450 µL of 10X trypsin-EDTA solution for 10-15 min at 37^0 C. 1 mL of DPBS was added to the released cells following trypsin-EDTA incubation. Cells were then transferred to a centrifuge tube containing 550 µL horse serum to make the final volume of 2 mL (450 µL trypsin-EDTA + 1 mL DPBS + 550 µL horse serum) and mixed very well. 10 µL of cells was then transferred to an eppendorf tube and diluted to 100 µL using DPBS. 10 µL from the final cell suspension was placed onto a hemacytometer and the cells were counted. The counted number was finally multiplied by the dilution factor and the actual number of cells determined.

For counting CCRF-CEM cells, cells suspended in RPMI media from one plate were transferred to a centrifuge tube and mixed very well by inverting the tube. 10 µL of cell suspension was then placed onto a hemacytometer and the cells were counted.

2.5 Cell viability assay (Trypan blue exclusion assay)

2.5.1 Cell viability of LLC-PK_1 cells incubated with Newport Green ester (NPG_E)

The culture medium of one plate of LLC-PK1 cells containing 10^7 cells was completely drained off and the cells were incubated with 1 mL of 10X trypsin-EDTA solution for 10-15 min. The released cells were collected in a centrifuge tube and washed three times with fresh DPBS and

finally resuspended in DPBS. Cells were then incubated with 10 µM NPG_E for an hour at 25 ^{0}C. One hour later, 10^4 cells were reacted with 0.4% Trypan Blue solution in 1:1 ratio and viable cells were counted immediately using a hemacytometer. Trypan blue is a dye which can penetrate the compromised cell membrane of a dead cell and the cell will in turn look blue under the hemacytometer, while the living cells will appear colorless as Trypan blue is not able to permeate through the cell membrane of an intact cell.[68-70] The cell viability assay was also used with LLC-PK_1 cells suspended in culture medium.

2.5.2 Cell viability assay of CCRF-CEM cells blocked at G1 and G2/M phases

Following 24 hours of incubation of CCRF-CEM cells with 2 mM thymidine or 100 ng/mL nocodazole, 10 µL cell suspension was taken in an Eppendorf tube and was mixed with 10 µL 0.4% Trypan Blue solution. The viable cells were counted immediately using a hemacytometer. Trypan blue exclusion assay was also performed for control cells, which were treated with neither thymidine nor nocodazole.

2.6 Flow cytometry of CCRF-CEM cells blocked at G1 and G2/M phases

CCRF-CEM cells were incubated with 2 mM thymidine or 100 ng/mL nocodazole for 24 hours. Following incubation, synchronized and control (untreated) cells were transferred to centrifuge tubes, spun down and the extracellular medium was discarded. Cells were then washed twice with Flow Cytometry staining buffer (FACS buffer) prepared by mixing Dulbecco's phosphate

buffered saline (DPBS), 5% fetal calf serum (FCS) and 0.1% sodium azide. Cells were resuspended in 70% ethanol while vortexing tube and stored at -20^0 C. On the day of run, stored cells were pelleted for 10 min at 3400 rpm, washed twice with FACS buffer and resuspended in 500 µL FACS buffer. In order to eliminate the staining of double stranded RNA (dsRNA), 500 µg/mL RNase A was added to the cells. Cells were then incubated for 20 min at room temperature. After incubation, cells were again pelleted and resuspended in 500 µL FACS buffer. Prior to running cells on flow cytometer, 10 µL of 4',6'-diamidino-2-phenylindole (DAPI) from 1 mg/mL stock solution (in DMF) was added to both control and synchronized cells. Flow cytometry of the cells was performed on a BD FACSAria III, DIVA version 6.1.3.

2.7 Fluorescence Spectroscopy of LLC-PK$_1$ Cells

2.7.1 Fluorescence spectroscopy of LLC-PK$_1$ cells incubated with Newport Green ester (NPG$_E$)

Cultured cells were grown in 100-mm culture plates until confluence was attained. Culture media was discarded and the plates washed three times with cold cholate buffer, prepared by dissolving 2.47 g Na_2HPO_4, 0.53 g NaH_2PO_4, 17.0 g NaCl and 13.33 g choline chloride in 2 L MilliQ water. Cells were then gently scraped from the plates with a rubber cell scraper and pooled in Dulbecco's phosphate buffered saline (DPBS) (0.1 g/L $MgCl_2.6H_2O$, 0.2 g/L KCl, 0.2 g/L KH_2PO_4, 8.0 g/L NaCl, 1.15 g/L anhydrous Na_2HPO_4). Cells were collected by centrifugation at 680 g for 5 min and resuspended in 10 mL DPBS. The cell suspension was then transferred to a cuvette and treated with 10 µM Newport Green ester (NPG$_E$) and incubated in the dark for one hour at 25 ^{0}C. For comparison, experiments were also conducted at 37^o C. Then, over a 45 min

period and using an excitation wavelength of 505 nm, emission spectra were recorded between 515 nm and 600 nm with a Hitachi F-4500 fluorescence spectrophotometer. Afterwards, 10 μM N,N,N',N'-tetrakis(2-pyridylmethyl)ethane-1,2-diamine (TPEN) was added and the fluorescence spectrum monitored for another 15 min. Finally, the reaction mixture was centrifuged using a microcentrifuge for about 1 min at 290 g to separate the extracellular medium and the cells, followed by resuspension of the cells in 1 mL DPBS.

2.7.2 Fluorescence spectroscopy of LLC-PK_1 cells incubated with Zinpyr-1 (ZP1)

Harvested LLC-PK_1 cells were suspended in DPBS and an aliquot of 1 mL cell suspension (ca. 10^7 cells) was transferred to a cuvette. Cells were then incubated with 10 μM ZP1 for 15 min. Using an excitation wavelength of 515 nm, emission spectra were recorded between 520 nm and 600 nm. Subsequently, 30 μM TPEN was added for 15 min and fluorescence spectrum observed. In a separate experiment, 30 μM ethylenediaminetetraacetate (EDTA) was added to cells for 15 min following incubation with 10 μM ZP1 for 15 min.

2.7.3 Fluorescence spectroscopy of LLC-PK_1 cells incubated with Zinquin or TSQ followed by diethylamine NONOate (DEA-NO)

LLC-PK_1 cells were harvested and resuspended in DPBS. An aliquot of 1 mL cell suspension (ca. 10^7 cells) was placed in a cuvette and treated with 20 μM Zinquin ethyl ester or TSQ and incubated for 30 min at 25 ^{0}C followed by 500 μM DEA-NO for another 25 min. Using an excitation wavelength of 370 nm, emission spectra were recorded between 400 nm and 600

nm. Afterwards, 10 μM TPEN was added and the fluorescence spectrum monitored for another 10 min.

2.7.4 Fluorescence spectroscopy of CCRF-CEM cells synchronized in G1 phase incubated with TSQ or Zinquin

Cultured CCRF-CEM cells were grown in 100-mm culture plates. When the cell density reached about 5.0 x 10^5 cells per mL, 2 mM thymidine was added to each plate. Following 24 hours of incubation, cells suspended in RPMI medium were transferred from culture plates to a 50-mL centrifuge tube. Cells were then spun down and the medium discarded. Cells were washed twice with DPBS and finally resuspended in fresh DPBS. An aliquot of 1 mL cell suspension (ca. 1-2 x 10^7 cells) was placed in a cuvette and treated with 20 μM TSQ or Zinquin for 20-25 min at 25^0 C. Using an excitation wavelength of 370 nm, emission spectra of the cell suspension were recorded between 400 nm and 600 nm. The protocol was repeated for the control experiment, namely, fluorescence spectroscopy of untreated cells with TSQ or Zinquin.

2.8 Isolation of cell lysate following incubation of cells with sensor (and DEA-NO) and its fractionation using gel filtration column or Centricon filtration

2.8.1 Preparation of Sephadex G-75 gel filtration column

Sephadex G-75 beads (4-5 g per gel filtration column) purchased from GE Healthcare were soaked in 20 mM Tris buffer (pH 7.4) for 24 hours. Following on, soaked beads were degassed for an hour and then slowly packed in glass columns to make 0.7 cm x 80 cm Sephadex G-75 gel

filtration columns. Columns were washed with degassed 20 mM Tris buffer (pH 7.4) each time before use.

2.8.2 Isolation of cell lysate following incubation of cells with sensor (and DEA-NO)

Following incubation of LLC-PK_1 or CCRF-CEM (control or synchronized) cells with NPG_E or ZP1 or ZQ/TSQ $\pm$ DEA-NO, cell suspensions were centrifuged at 640 g to separate the pellet from the extracellular medium and to remove extracellular sensors. Cells were further washed twice with fresh DPBS to get rid of any residual extracellular sensors. The last cell pellet was resuspended in 1 mL of cold MilliQ water. Cells were then lysed by sonication and centrifuged at 47,000 g for 20 min at 4^o C to collect the cell supernatant or cell lysate.

2.8.3 Fractionation of the cell lysate using Sephadex G-75 gel filtration column or Centricon filtration

The cell lysate collected as above was either loaded onto an 80 cm $\times$ 0.75 cm gel filtration column of Sephadex G-75 (GE Healthcare) equilibrated with 20 mM Tris buffer (pH 7.4) at room temperature or filtered through a Millipore Centricon Centrifuge filter (3K MW cut off) at 4^o C by centrifugation at 13000 rpm for 30 min to separate the high and low molecular weight fractions. During gel-filtration chromatography, the column was eluted with degassed 20 mM Tris-Cl (pH 7.4) and ninety (for NPG_E incubated cells) or sixty (for ZP1 or TSQ or ZQ incubated cells) fractions were collected. Emission spectra of all fractions were obtained as described above. The zinc content in each fraction was also detected by flame atomic absorption spectroscopy (AAS).

2.9 Isolation of Proteome Using Sephadex G-75 Chromatography

LLC-PK_1 or CCRF-CEM cells were harvested as described above and finally resuspended in 1 mL cold MilliQ water. Cells were then lysed by sonication and centrifuged at 47,000 g for 20 min to collect the cell supernatant, which was then loaded onto a Sephadex G-75 column equilibrated with degassed 20 mM Tris buffer (pH 7.4). The supernatant was eluted with degassed 20 mM Tris-Cl (pH 7.4) and 1 mL fractions were collected. Fractions within the high molecular weight region having absorbance at 280 nm were pooled. These pooled fractions were referred to as the proteome. Proteome was stored in 1 mL aliquots at -80^0 C until use. On the day of experiment, proteome was slow ice-thawed.

2.10 Reaction of isolated proteome with fluorescent sensors

Frozen proteome was ice-thawed and transferred to a cuvette. Proteome was then incubated with the fluorescent sensor (NPG, ZP1, TSQ, Zinquin, FluoZin-3) for a certain time depending on the type of sensor. The progress of the reaction was monitored by recording emission spectrum at a certain time interval. Upon completion of the reaction, the final reaction mixture was fractionated using either Sephadex G-75 gel filtration column or Centricon filtration in order to determine the location of the fluorescent species. In case of Sephadex G-75 gel filtration, the sample was eluted with degassed 20 mM Tris buffer (pH 7.4) and sixty fractions were collected. All the fractions were analyzed for both fluorescence, and zinc content using flame atomic absorption spectrophotometry.

2.11 BioRad DC Protein Assay

The protein concentration was measured using a BioRad DC Protein Assay kit; 2.0 mg/mL bovine serum albumin (BSA) served as the standard. Prior to the measurement of the sample protein concentration, a calibration curve was made using six standard protein concentrations ranging from 2.0 mg/mL to 0.0625 mg/mL prepared by serial dilution. 25 µL of each of the standards and a blank (Tris buffer only) were mixed with 125 µL alkaline copper tartarate and 1 mL dilute Folin reagent.[71, 72] Upon mixing, the solutions were then incubated for 15 min at room temperature. Following incubation, the absorbance at 750 nm of each of the standards and blank was recorded using a UV-Visible spectrophotometer. The absorbance at 750 nm was plotted against the concentrations of the standards to make the calibration curve. To measure the concentration of the protein sample, the above mentioned protocol was followed and the recorded absorbance was compared with the calibration curve.

2.12 Isolation of subcellular proteomes from LLC-PK_1 cells

Subcellular proteomes were isolated as described with modifications.[73] LLC-PK_1 cells were collected and resuspended in 4 mL of pre-chilled homogenation buffer (0.25 M sucrose, 15 mM KCl, 1.5 mM $MgSO_4$, and 10 mM Tris-Cl pH 7.4). The cell suspension was then homogenized using a pestle and centrifuged at 1,000 g for 10 min at 4^o C. The pellet was saved as the nominal membrane-nuclear fraction. Supernatant was then centrifuged at 10,000 g for 15 min at 4^o C. The pellet was retained as the mitochondrial fraction. Supernatant was centrifuged again at 100,000 g at 4^o C and the resultant supernatant was designated the cytosolic

proteome. The membrane-nuclear and mitochondrial fractions were sonicated and centrifuged at 47,000 g for 20 min at 4 ^{0}C and the resultant supernatants were labelled as 'membrane/nuclear and mitochondrial proteomes, respectively. The protein concentrations of all three fractions were measured using BioRad DC protein assay. Subcellular proteome samples were stored at -80^{0} C, if not used immediately after isolation. On the day of experiment, the frozen samples were slowly ice-thawed.

2.13 Reaction of LLC-PK$_1$ cells with Zn(pyrithione)$_2$ in the presence of Newport Green (NPG$_E$)

Harvested and washed LLC-PK$_1$ cells were resuspended in 1 mL DPBS and transferred to a cuvette. Cells were then incubated with 10 µM NPG$_E$ for 30 min while monitoring the progress of the reaction by recording the emission spectrum. 30 min later, the cell suspension was centrifuged at 640 g for 5 min and the supernatant was discarded. The cell pellet was washed twice with DPBS to remove any residual extracellular NPG and resuspended in 1 mL DPBS. Following wash, the emission spectrum of the cell suspension was recorded for another 10 min. Cells were then reacted with a pre-incubated mixture of 10 µM $ZnCl_2$ and 2 µM pyrithione for 20 min. Change of fluorescence was recorded upon addition of Zn(pyrithione)$_2$. Subsequently, 10 µM EDTA was added for 10 min followed by 10 µM TPEN for another 10 min.

2.14 Reaction of model Zn-proteins (alcohol dehydrogenase, carbonic anhydrase) with Newport Green or Zinpyr-1

The solutions of the model Zn-proteins, such as alcohol dehydrogenase and carbonic anhydrase, were prepared by dissolving the lyophilized powder of the Zn-proteins in degassed 20 mM Tris buffer (pH 7.4). The zinc concentration of the protein solutions were measured using flame AAS. Zn-protein solutions were incubated with Newport Green (acid or ester) or Znpyr-1 and the progress of the reaction was monitored by recording emission spectrum. To identify the fluorescent species, the final reaction mixture was fractionated using either Sephadex G-75 gel filtration column or Centricon filtration. For Sephadex G-75 gel filtration, the sample was eluted with degassed 20 mM Tris buffer (pH 7.4) and 50-60 fractions were collected. All the fractions were analyzed for both fluorescence, and zinc content using flame atomic absorption spectrophotometry.

2.15 Quantification of Zn^{2+} by Atomic Absorption Spectrophotometry

The concentration of Zn^{2+} in solutions was determined by flame Atomic Absorption Spectrophotometry (AAS). A GBC model 904 instrument employed an acetylene torch to atomize samples using an 80:20 mixture of compressed air and acetylene. Zinc measurements were made with deuterium background correction. The instrument was calibrated before each run using three standard Zn^{2+} solutions of 0.5 ppm, 1.0 ppm and 2.0 ppm. The calibration curve was not considered acceptable until the maximum error was 0.2 µM or less.

2.16 Quantification of sulfhydryl groups in proteome

The concentration of sulfhydryl groups was determined with Ellman's Reagent or 5, 5'-dithiobis-2-nitrobenzoic acid (DTNB).[74] To prepare a 10 mM DTNB stock solution, 25 mL MilliQ water was added to 0.1 g DTNB solid. The mixture was gently stirred. Because DTNB is insoluble at acid pH but oxidizes immediately at pH greater than 8.0, the pH of the solution was monitored while being stirred. Since the pH was around 3.0 to start out and little DTNB powder was in solution, a few crystals of Trizma (Tris) base was added until the pH was between 6.5 and 7.0. The solution was then filtered to remove the residual amount of undissolved DTNB. The filtered DTNB solution was kept into a small brown bottle and stored in dark. The color of the solution was pale yellow.

For measurement of sulfhydryl concentrations of proteome samples, 60 µL of proteome sample was diluted with 540 µL 20 mM Tris-Cl, pH 7.4. 60 µL of 10 mM DTNB was then added to the sample and vortexed immediately. The solution was incubated in dark for 30-60 min before the absorbance at 412 nm was obtained. An extinction coefficient of 13,600 $cm^{-1}M^{-1}$ was used to determine the concentration of reactive thiol groups in the samples.

3. RESULTS

3.1 Chemical Biology of Newport Green (NPG)

Newport Green (NPG) is a fluorescent zinc sensor with relatively low stability constant for Zn^{2+} ($K_d \sim 10^{-5} – 10^{-6}$ M).[1, 46] A number of studies have used this sensor to image intracellular mobile Zn^{2+} and revealed various physiological roles of Zn^{2+} based on the spectral properties of Newport Green.[75-80] Upon binding Zn^{2+}, NPG displays an enhancement of fluorescence at 530 nm. Typically, the fluorescence enhancement following the incubation of cells with NPG is linked with the intracellular Zn-NPG formation (reaction 3.1). However, the possibilities of other reactions of NPG with the cellular constituents are often ignored. For example, like TSQ and Zinquin, NPG may react with cellular Zn-proteins to generate ternary adduct species NPG-Zn-Protein (reaction 3.2).[23, 65]

$$Zn^{2+} + NPG \rightleftharpoons Zn\text{-}NPG \qquad (3.1)$$

$$Zn\text{-}Protein + NPG \rightleftharpoons NPG\text{-}Zn\text{-}Protein \qquad (3.2)$$

Moreover, due to its low stability constant for Zn^{2+}, NPG may have to compete with other potential cellular ligands for Zn^{2+}, including proteome and small molecules. Therefore, its ability to effectively image intracellular Zn^{2+} will depend on the stability of Zn-NPG in the presence of other cellular competitors of Zn^{2+}. This present work examines how effectively NPG can serve as an intracellular zinc sensor.

3.1.1. Spectral properties of NPG and Zn-NPG

The ester form of Newport Green, NPG_E, does not fluoresce but gains its fluorescent property upon conversion to its acid form, NPG_A, catalyzed by cellular esterase. With excitation at 505 nm, NPG_A emitted fluorescence with a wavelength maximum at 530 nm. However, the fluorescence of NPG_A and Zn-NPG_A were not linearly dependent on their concentration (**Figure 3.1.1**). With increasing concentration, their fluorescence intensity increased non-linearly until a maximum value after which it declined. Moreover, the emission wavelength maximum changed with concentration. The declining fluorescence intensity of NPG_A and Zn-NPG_A at higher concentration might be due to the stacking of fluorescein, the reporter part of NPG. Regardless of the cause, this property of NPG_A makes it difficult to quantify the actual Zn^{2+} concentration simply from the observation of its fluorescence response. When titrated with Zn^{2+}, NPG_A formed a 1:1 complex with its emission wavelength maximum unaltered and about twice the intensity of the free ligand (**Figure 3.1.2** and **3.1.3**). The product rapidly reacted with TPEN, a cell permeant, high affinity chelator of Zn^{2+}, returning the fluorescence to that of NPG_A (**Figure 3.1.3**).

3.1.2. Cell viability

As the cellular experiments in this study were performed in DPBS buffer at 25 ^{0}C for an hour or so, the cell viability was determined under such conditions using the Trypan Blue exclusion assay. Cell viability under experimental conditions was calculated to be 90%, whereas cells kept in complete culture medium were found to be almost 100% viable.

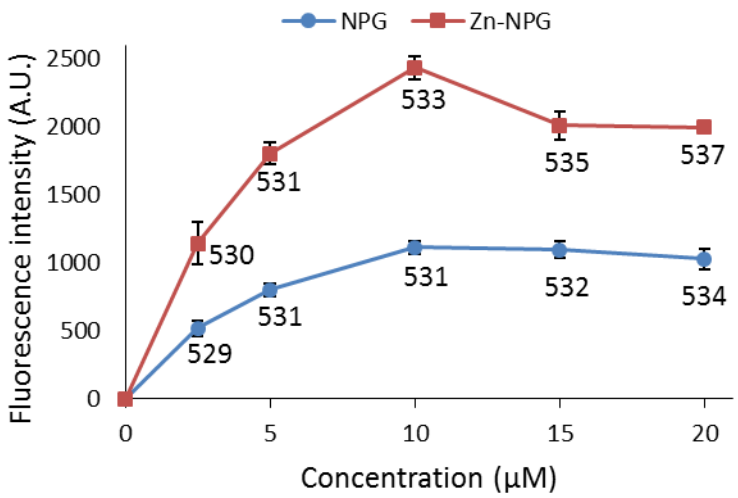

***Figure 3.1.1 Change of fluorescence intensity and emission wavelength maximum of NPG_A and Zn-NPG_A with increasing concentration*:** Equivalent amounts of NPG_A and $ZnCl_2$ were mixed to make Zn-NPG complex. The numbers under each data point indicate the emission wavelength maximum of each spectrum in nanometers.

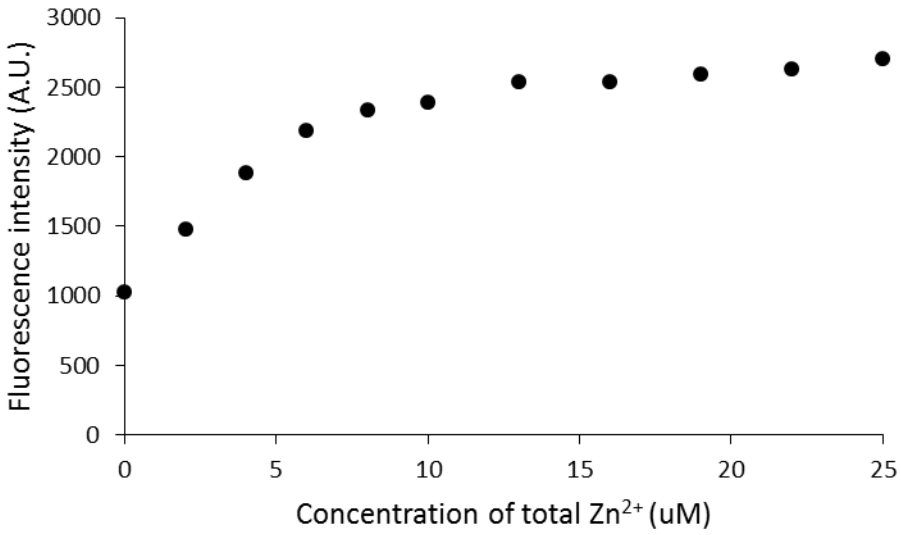

Figure 3.1.2 Titration of NPG with Zn^{2+}: 10 µM NPG_A in 20 mM Tris (pH 7.4) was titrated with the increasing concentration of $ZnCl_2$ at 25° C. Following each addition of $ZnCl_2$, the sample was excited at 505 nm and fluorescence spectrum was read in the range of 515 – 600 nm. The maximum fluorescence intensity of each titration point was plotted against the total concentration of the added Zn^{2+}.

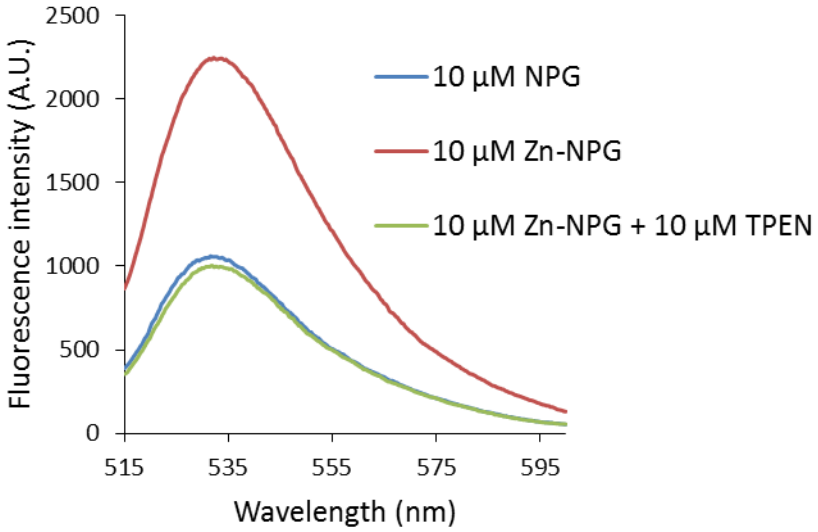

Figure 3.1.3 Fluorescence spectra of NPG, Zn-NPG and the quenching by TPEN: 10 µM NPG_A in 20 mM Tris (pH 7.4) was incubated with 10 µM $ZnCl_2$ at 25° C. Subsequently, 10 µM TPEN was added to the solution. The sample was excited at 505 nm and the fluorescence spectra were read in the range of 515 – 600 nm.

3.1.3 Reaction of NPG_E with LLC-PK_1 cells

As a basis for addressing the question of what NPG images in cells, the reaction of NPG_E with 10^7 LLC-PK_1 cells in DPBS buffer was monitored by spectrofluorimetry at 25° and 37° C. At 25°C, fluorescence intensity increased slowly at 530 nm, reaching a maximum after 40 min, indicative at least of the conversion of some NPG_E to NPG_A catalyzed by cellular esterases (**Figure 3.1.4**). The background fluorescence of media and cells was insignificant in comparison with the fluorescence contributed by the formation of NPG_A (**Figure 3.1.5B**). Considering the initial extracellular concentration of NPG_E, complete hydrolysis of the sensor would result in an intensity of about 5000 arbitrary units. Since the observed, maximal fluorescence was only about 1200 units, at most about 25% of NPG_E had undergone reaction during this period. At that point, TPEN was added to quench the fluorescence of any Zn-NPG_A that had formed. No reduction in fluorescence emission was observed over a period of 20 min, leading to the conclusion that detectable Zn-NPG_A had not been produced in these cells. Since TPEN forms ternary adducts with Zn-proteins, the results also suggested that NPG_A had not formed NPG-Zn-protein species that could be converted to TPEN-Zn-proteins.[67]

The reaction of NPG_E with 10^7 LLC-PK_1 cells at 37 °C was qualitatively similar to the one at 25° C though as expected it proceeded at a faster rate (**Figure 3.1.4**). Moreover, treatment of cells with TPEN prior to addition of NPG_E failed to modify the reaction, confirming the lack of interaction of NPG with intracellular Zn^{2+}. Although the formation of Zn-NPG_A was not supported at either temperature, it remained possible that ternary adducts of NPG_A-Zn-proteins accounted for some of the fluorescence increase, and were unreactive with TPEN.

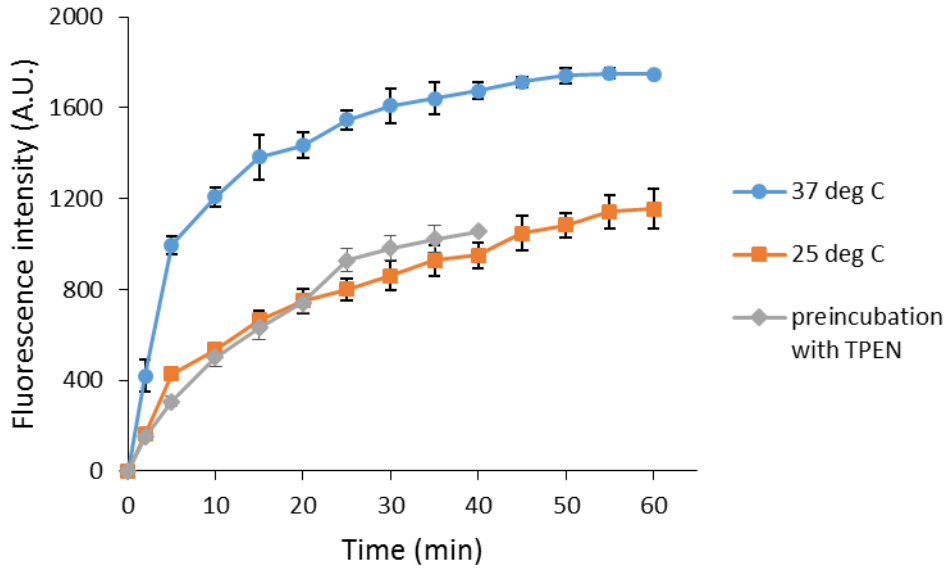

Figure 3.1.4 Reaction of LLC-PK$_1$ cells with NPG$_E$. 10^7 LLC-PK$_1$ cells suspended in 1 mL DPBS were treated with 10 µM NPG$_E$ for 40 min at 25°C. Subsequently, 10 µM TPEN was added for another 20 min. The reaction was repeated at 37°C. In the third case, 10^7 LLC-PK$_1$ cells were pre-incubated 10 µM TPEN for 20 min at 25°C followed by the treatment with 10 µM NPG$_E$ for another 40 min.

After the reaction, the cell suspension was centrifuged to separate the extracellular medium and cells, which were then resuspended in DPBS. Surprisingly, most of the fluorescence (about 70%) was found in the external medium (**Figure 3.1.5A**), and it could not be quenched by the addition of 10 μM TPEN for 5 min (**Figure 3.1.6**). To investigate this surprising result, 2.7×10^7 cells/mL were incubated with 10 μM NPG_E in DPBS at 25 ^oC for 40 min followed by fluorescence emission analysis. The suspension (1) was centrifuged to produce extracellular supernatant (a), and the cells (2) were then resuspended in 1 mL of NPG_E-free medium for 20 min. After a fluorescence measurement, supernatant (b) was isolated. The relative fluorescence emission properties of both suspensions and supernatants were determined. According to **Figure 3.1.7**, most of the fluorescence was found in the extracellular part of the first cell suspension (a) and a significant fraction of the external medium of the second cell suspension (b). Since cell suspension 2 began its incubation with only intracellular NPG_A and perhaps some NPG_E, the fact that fluorescence made its way into the external medium demonstrated that NPG_A underwent efflux from the cells during the 20 min period.

We considered the possibility that during the initial isolation of cells *via* scraping some cells were damaged resulting in progressive release of intracellular esterase activity and/or NPG into the external medium. However, we repeated this experiment with CCRF-CEM cells, a cell line that grows in suspension culture, and did not require scraping and obtained the same result (**Figure 3.1.8**), ruling out the possibility that scraping had resulted in the appearance of NPG_A in the extracellular medium.

These findings are consistent with two hypotheses, either (i) NPG_E is accumulated by cells and undergoes internal esterase hydrolysis to NPG_A which is then transported out of the cells or (ii)

NPG_E both moves into cells and is hydrolyzed on the extracellular surface of the cell. In the absence of extracellular NPG_E, the ester leaves the cell and undergoes ester hydrolysis. In either case, the interaction of NPG with cells is considerably more complicated than anticipated and results in most of the detectable sensor (NPG_A) residing in the external medium.

A.

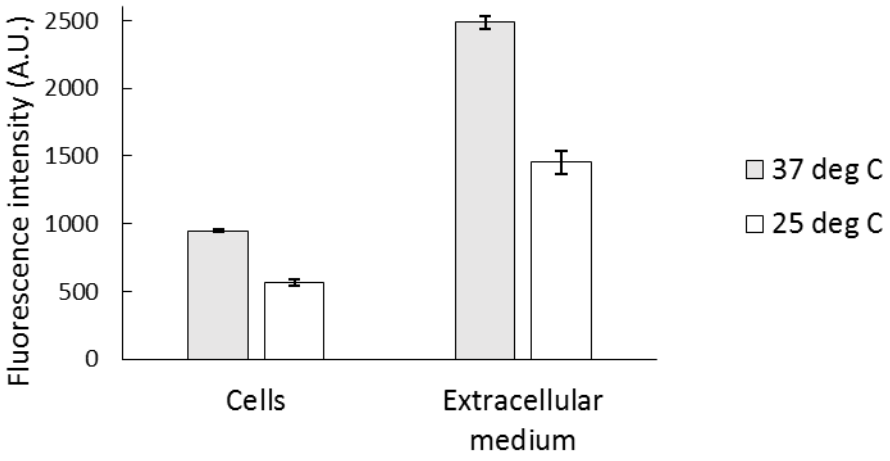

B.

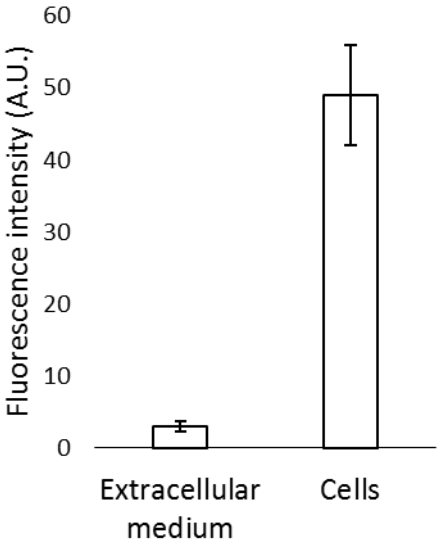

Figure 3.1.5 Reaction of LLC-PK$_1$ cells with NPG$_E$. (A) 10^7 LLC-PK$_1$ cells suspended in 1 mL DPBS were treated with 10 µM NPG$_E$ for 40 min at 25^{o}C. Subsequently, 10 µM TPEN was added for another 20 min. The reaction mixture, after 1 h, was centrifuged at 290 g and the extracellular

medium separated from the cells. The cells were resuspended in 1 mL DPBS. Error bar represents standard error for three measurements. (B) Background fluorescence of extracellular medium (DPBS), and 10^7 LLC-PK_1 cells suspended in DPBS at 25^o C.

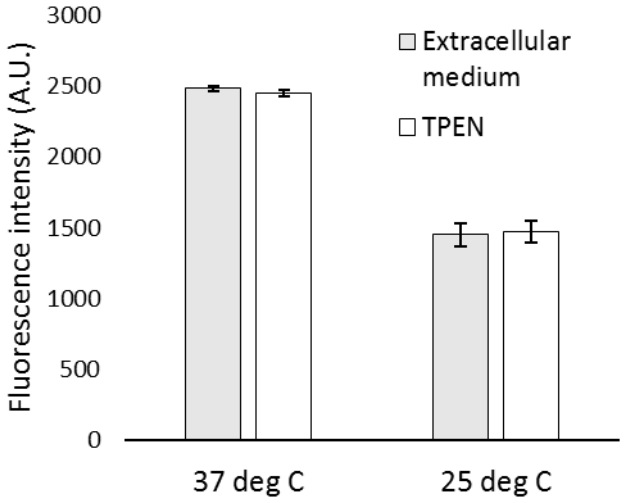

Figure 3.1.6 TPEN effect to the extracellular fluorescence: Reaction of TPEN with the extracellular medium separated from the reaction of 10^7 LLC-PK_1 cells with 10 µM NPG_E for an hour at 25^o C. 10 µM TPEN incubated for 5 min.

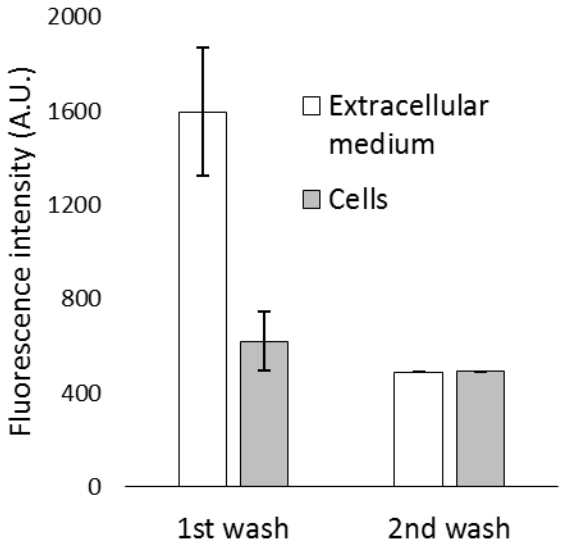

Figure 3.1.7 Efflux of NPG_A from cells. 2.7×10^7 LLC-PK_1 cells were reacted with 10 µM NPG_E for 40 min. The reaction mixture was centrifuged to separate the extracellular medium and cells. The cells resuspended in 1 mL DPBS were incubated for another 20 min and then centrifuged again to separate the extracellular medium and cells, which were then resuspended in 1 mL DPBS.

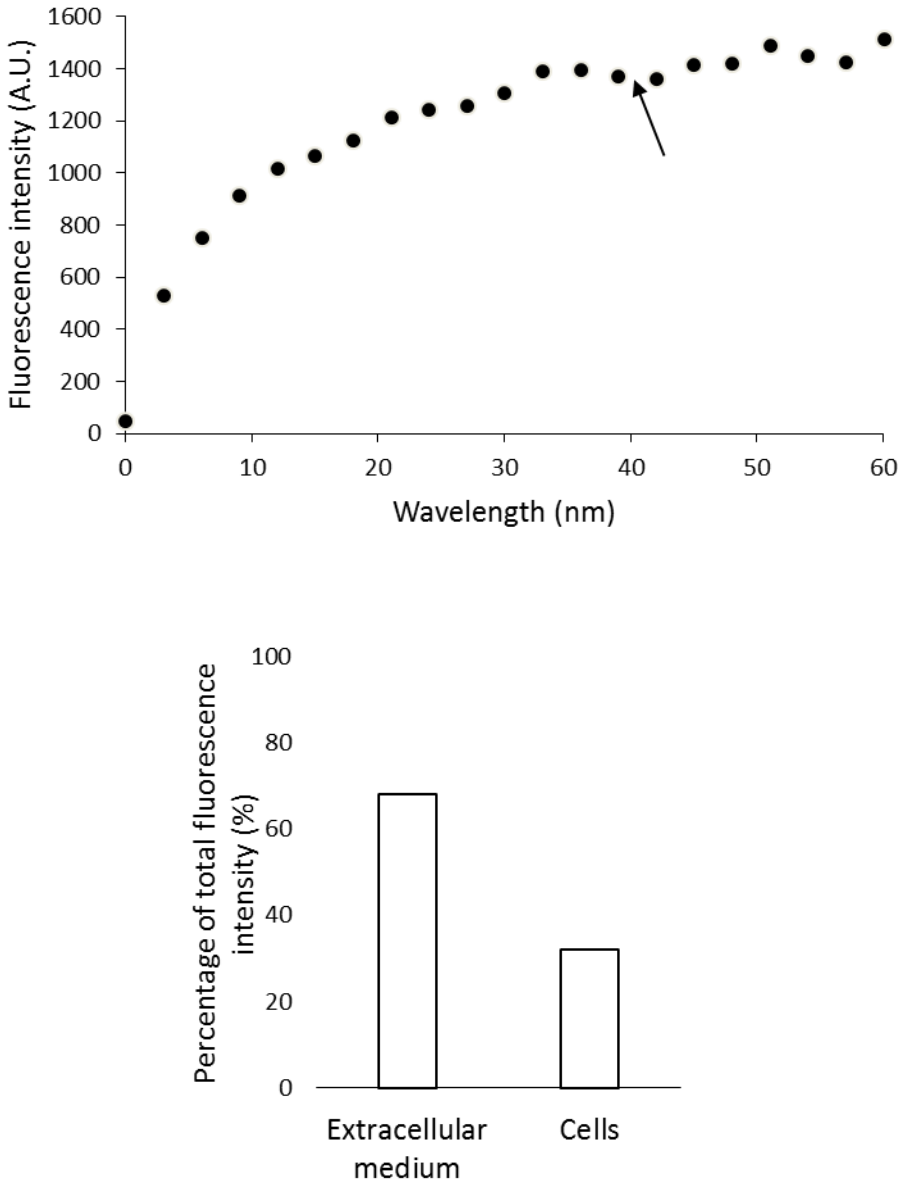

Figure 3.1.8 Reaction of CCRF-CEM cells and NPG_E: (A) Reaction of 2 x 10^7 CCRF-CEM cells suspended in DPBS at 25° C and 10 µM NPG_E for about 40 min followed by the addition of 10 µM TPEN for another 20 min (arrow). (B) After one hour, the final reaction mixture was centrifuged to separate extracellular medium and cell pellet. Cell pellet was subsequently resuspended in 1 mL DPBS.

3.1.4 Location of NPG_A among cell constituents.

To characterize the intracellular properties of NPG_A, cells isolated after one hour incubation with NPG_E were lysed and the supernatant subjected to Sephadex G-75 chromatography. Proteome and low molecular weight fractions were assayed for Zn^{2+} and fluorescence. Zn^{2+} was associated with the high molecular weight proteome fractions, whereas fluorescent NPG_A emerged from the column without bound Zn^{2+} well beyond the total volume of the column indicative of a favorable interaction between the Sephadex beads and NPG_A (**Figure 3.1.9**). Possibly, the chromatographic separation altered the original supernatant distribution. To investigate this possibility, proteome and low molecular weight species were separated using the Centricon filtration system and a 3 kDa cut-off filter. The majority of NPG_A (about 85% of total fluorescence intensity) was retained by the filter during centrifugation along with the proteome (**Figure 3.1.10**). Thus, NPG_A was weakly associated with protein in the supernatant but was dissociated from the proteome during Sephadex chromatography.

3.1.5 Reaction of NPG_E and NPG_A with isolated proteome.

In order to gain a more detailed understanding of the reaction of NPG with cells, an analogous set of experiments was conducted using isolated supernatant or proteome in place of whole cells. NPG_E was slowly hydrolyzed to NPG_A by supernatant or proteome, indicative of the presence of proteomic esterases that catalyze this conversion (**Figure 3.1.11**). As in cells, much of the NPG_A (84% of total fluorescence intensity) that was generated became associated with the proteome as shown by centrifugal filtration. The addition of TPEN failed to quench the

proteome-associated fluorescence (**Figure 3.1.12**), consistent with the conclusion that NPG_A-Zn-proteins did not form during the enhancement of fluorescence.

$$NPG_E \rightarrow NPG_A$$

$$Proteome + NPG_A \leftrightarrows Proteome \bullet NPG_A$$

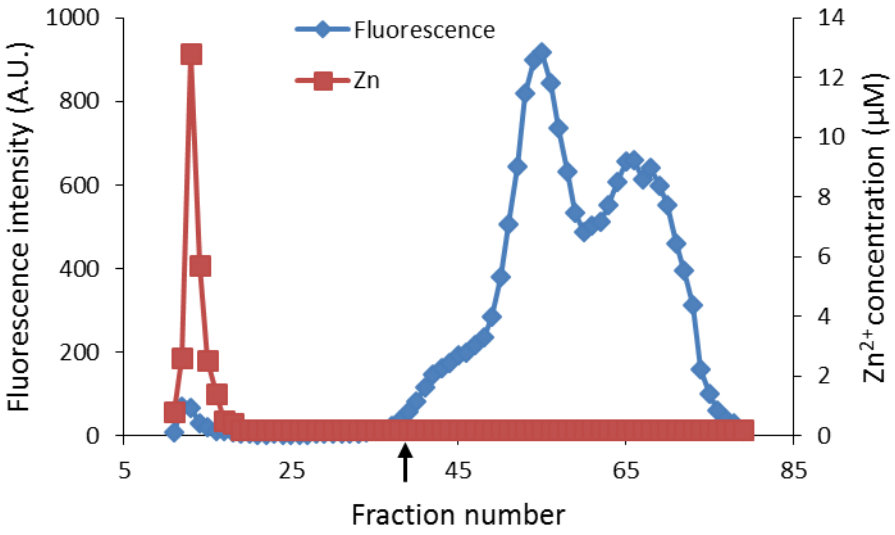

Figure 3.1.9 Interaction of NPG_A with Sephadex beads: Proteome (10 µM Zn^{2+}) in 20 mM Tris (pH 7.4) was reacted with 10 µM NPG_A for 15 min at 25° C followed by Sephadex G-75 filtration of the final reaction mixture. The eluted fractions were analyzed for both fluorescence and zinc. Arrow shows total volume of the column.

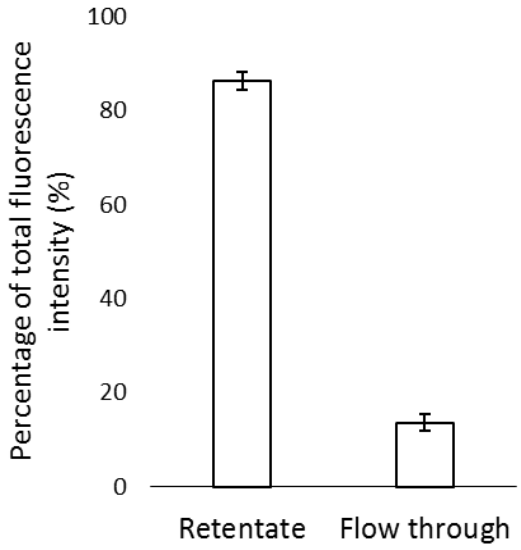

Figure 3.1.10 Centricon filtration of the reaction mixture of proteome and NPG_A: 2.5×10^8 LLC-PK_1 cells suspended in DPBS were reacted with 10 µM NPG_E for an hour in the dark. The cells were then washed three times to remove the extracellular NPG and resuspended in MilliQ water. Following sonication and centrifugation, the cell lysate was filtered using the Centricon filtration system and a 3kDa cut-off filter to separate high molecular weight (retentate) and low molecular weight (flow through) components.

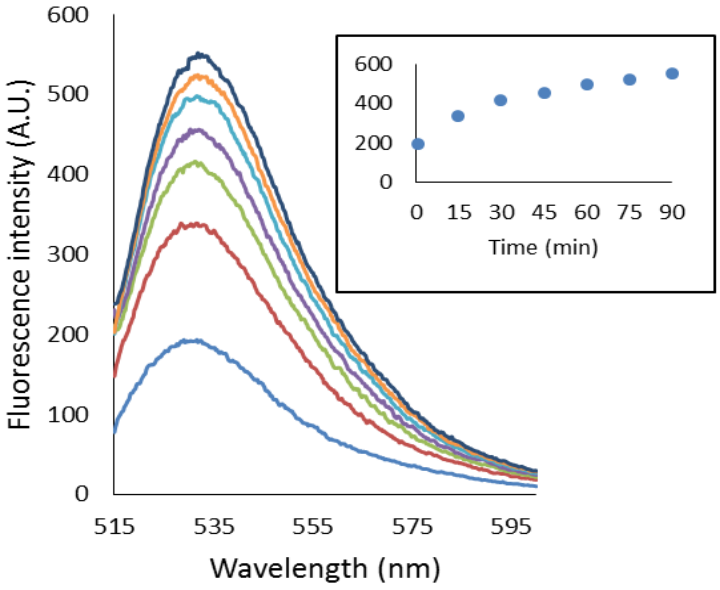

Figure 3.1.11 Reaction of proteome with NPG_E. 4.2 mg/mL proteome in 20 mM Tris pH 7.4 containing 7 µM Zn^{2+} was incubated with 10 µM NPG_E at ambient temperature (ca. 23^{o} C) for 90 min. Fluorescence spectra were read every 15 min. The inset shows the progress of reaction with time.

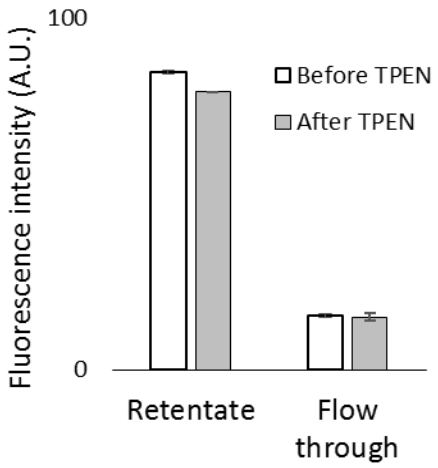

Figure 3.1.12 Centricon filtration of the reaction mixture of proteome and NPG_E. 4.2 mg/mL proteome in 20 mM Tris pH 7.4 containing 7 µM Zn^{2+} was incubated with 10 µM NPG_E at ambient temperature (ca. 23^{o} C) for 90 min. The final reaction mixture was separated by Centricon filtration using 3K cut-off filter into the high molecular weight retentate and the low molecular weight filtrate. 10 µM TPEN was added for 5 min to both retentate and flow through fractions.

3.1.6 Reactions of NPG with model Zn-proteins (alcohol dehydrogenase, carbonic anhydrase).

The cellular and proteomic experiments with NPG indicate that the sensor does not successfully compete for native, proteomic Zn^{2+}. But they do not exclude the possibility that NPG may form ternary adducts with Zn-proteins that are insensitive to the presence of TPEN. To address this issue, NPG_E was reacted with two model Zn-proteins, alcohol dehydrogenase and carbonic anhydrase, that are known to form TPEN-sensitive ternary adducts with the Zn^{2+} sensors, TSQ and/or Zinquin (ZQ).[50, 65] Upon incubation of NPG_E with Zn-ADH, the fluorescence gradually increased with time (**Figure 3.1.13 A**). However, TPEN was unable to quench the fluorescence. Therefore, the fluorescence increase was indicative of the capacity of ADH to act upon NPG_E as an esterase not the ability of NPG to associate with one of ADH's bound Zn^{2+} ions. ZQ removes 1 Zn^{2+} from this protein as $Zn(ZQ)_2$ and binds to the other to form a fluorescent adduct.[50] Both are quenched by TPEN as it acquires Zn^{2+} from $Zn(ZQ)_2$ and displaces ZQ from ZQ-Zn-ADH to form TPEN-Zn-ADH.[50] Together with this information, the current result strongly implies that NPG neither binds to nor extracts Zn^{2+} from this protein. Similar results were obtained with Zn-CA; the protein has NPG_E esterase activity but is otherwise unreactive with NPG (**Figure 3.1.14 A**). Nevertheless, the majority of NPG_A did associate with Zn_2-ADH and Zn-CA according to Centricon filtration analysis (**Figure 3.1.13 B and 3.1.14 B**).

A.

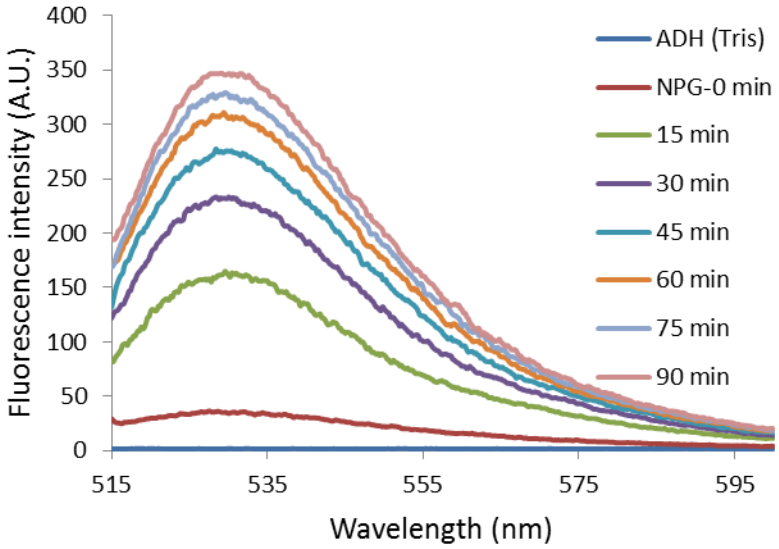

B.

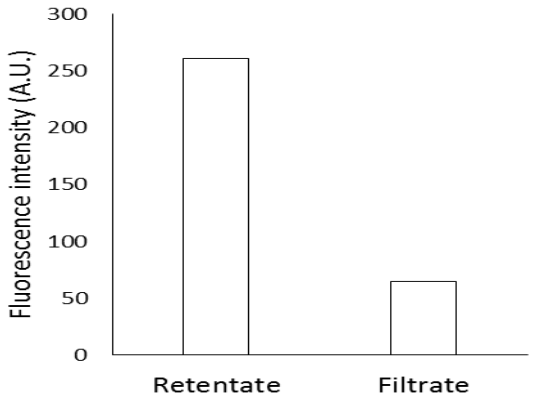

Figure 3.1.13 Reaction of alcohol dehydrogenase (ADH) with NPG_E. (A) 2 µM alcohol dehydrogenase was incubated with 10 µM NPG_E at ambient temperature (ca. 23^{o} C) for 90 min. (B) Separation of the final reaction mixture by Centricon filtration using 3K cut-off filter.

A.

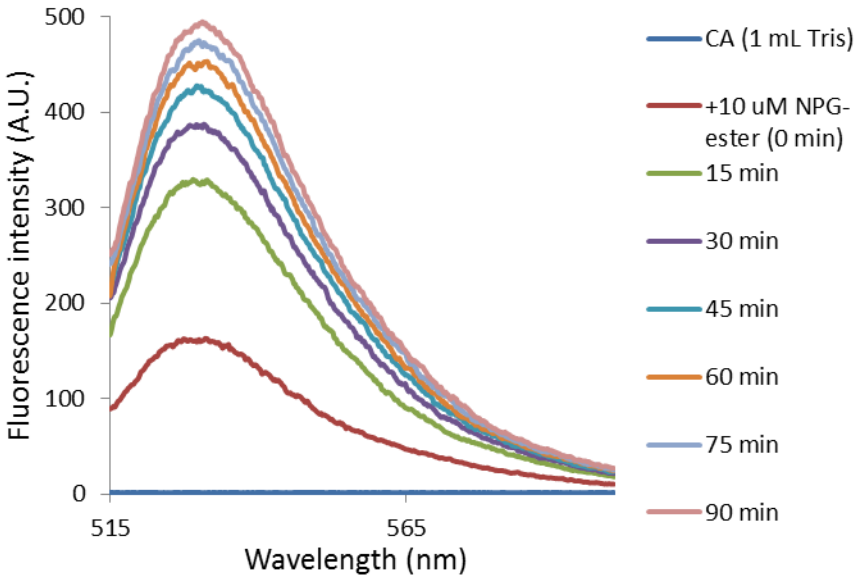

B.

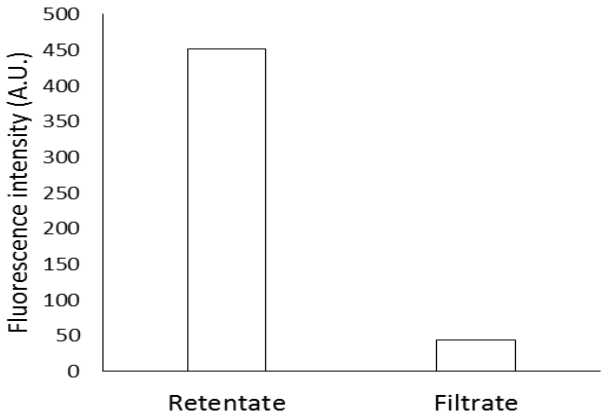

Figure 3.1.14 Reaction of carbonic anhydrase (CA) with NPG_E. (A) 10 µM carbonic anhydrase was incubated with 10 µM NPG_E at ambient temperature (ca. 23° C) for 90 min. (B) Separation of the final reaction mixture by Centricon filtration using 3K cut-off filter.

3.1.7 Stability of Zn-NPG_A with proteome.

It was evident that NPG_A cannot compete with native, protein bound Zn^{2+} to form Zn-NPG_A. We then inquired whether it can compete for adventitiously bound Zn^{2+} that might be produced under certain physiological or pathological conditions. Initially, 10 μM Zn-NPG_A was titrated with proteome to test whether this species exhibits stability in the presence of protein competitors for Zn^{2+}. **Figure 3.1.15** shows that addition of proteome up to about 50 μg protein/mL (0-170 nM Zn^{2+} bound as Zn-protein) reduced the starting fluorescence intensity of Zn-NPG_A to that of an equivalent concentration of NPG_A. Thus, NPG_A does not compete favorably with proteome for Zn^{2+}.

$$\text{Zn-NPG}_A + \text{Proteome} \leftrightarrows \text{Proteome} \bullet \text{Zn} + \text{NPG}_A$$

The capability of NPG_A to compete with proteome for Zn^{2+} was probed another way: 4.2 mg/mL proteome containing 7 μM Zn-proteins was mixed with 10 μM NPG_A initially in 20 mM Tris (pH 7.4) and then titrated with Zn^{2+} (**Figure 3.1.16**). NPG_A fluorescence did not increase until Zn^{2+} reached 30-35 μM or about 5x the total proteomic concentration of Zn^{2+}. At higher concentrations of Zn^{2+}, fluorescence emission at 535 nm increased; but even at 100 μM Zn^{2+}, stoichiometric Zn-NPG_A had not been generated, showing that proteomic sites continued to partially sequester Zn^{2+} even at these large concentrations. Both experiments demonstrated that under the described conditions, NPG_A has little, if any, capacity to compete with native proteome for Zn^{2+} that might be liberated from cellular binding sites during physiological or pathological processes.

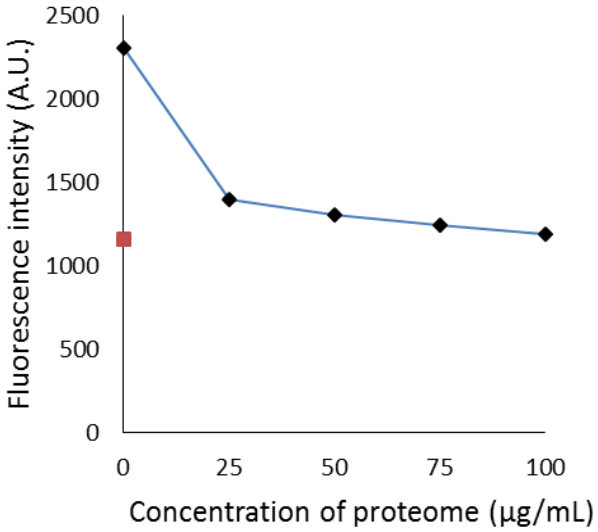

Figure 3.1.15 Stability of Zn-NPG$_A$ in the presence of proteome. 10 µM Zn-NPG$_A$ complex was titrated with the increasing concentration of proteome isolated from LLC-PK$_1$ cells. Following each addition of proteome, the fluorescence spectrum was recorded. The maximum fluorescence intensity was plotted against the total concentration of proteome. The dilution of the sample by 100 µg/mL proteome was only 2% and was ignored. The red square indicates the baseline fluorescence of 10 µM NPG$_A$.

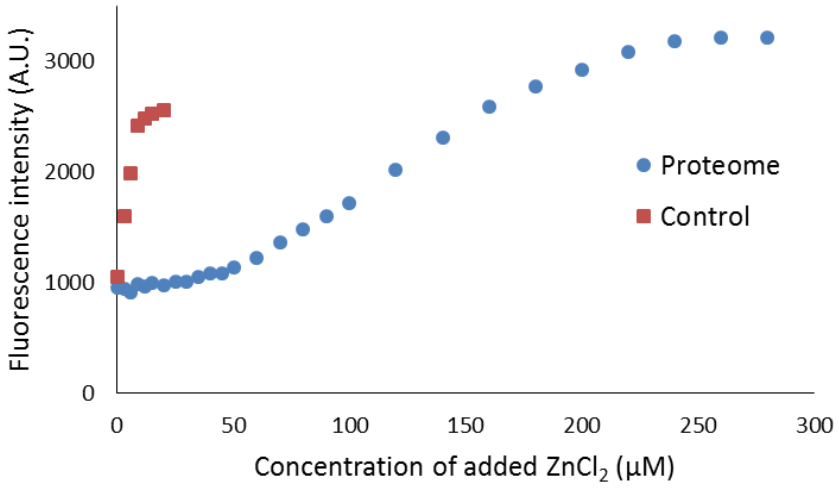

Figure 3.1.16 Titration of proteome with $ZnCl_2$ in the presence of NPG_A. 4.2 mg/mL proteome (7 µM Zn^{2+} content) isolated from LLC-PK_1 cells was titrated with $ZnCl_2$ in the presence of 10 µM NPG_A. The reaction was performed in 20 mM Tris buffer at pH 7.4. Following each addition of $ZnCl_2$, the fluorescence spectrum was recorded, and the maximum fluorescence intensity was plotted against the total concentration of the added $ZnCl_2$. Control: 10 µM NPG_A in 20 mM Tris buffer at pH 7.4 was titrated with $ZnCl_2$.

We considered the possibility that proteins with substantial zinc buffering capacity might be distributed among some organelles and not able to interfere with NPG_A's ability to image free or loosely bound Zn^{2+} in other compartments. To investigate this possibility, 1.7 mg/mL of cytosolic proteome (ca. 2.8 μM Zn^{2+}), isolated by gentle homogenization of cells followed by centrifugation at 100,000 x g, was mixed with 10 μM NPG_A and subsequently titrated with Zn^{2+} (**Figure 3.1.17**). A detectable increase of fluorescence was not observed until the added Zn^{2+} reached about 10 μM. Beyond that, NPG_A partially competed with cytosolic proteome for additional Zn^{2+}. This result was in qualitative agreement with the findings with whole proteome in the previous experiment and indicated that a subset of proteins within the cytosolic proteome possesses substantially higher affinity for free or loosely bound Zn^{2+} than does NPG_A. Similar results were obtained with membrane/nuclear and mitochondrial proteomes (**Figure 3.1.17**). All of the compartments displayed substantial Zn^{2+} buffering capacity.

3.1.8 Stability of Zn-NPG_A with Glutathione.

The stability of Zn-NPG_A was also studied in the presence of glutathione (GSH). GSH exists in the cells in mM concentration and displays modest affinity for Zn^{2+} ($10^{4.2}$. pH 7.2, 25° C).[81] As little as 30 μM of GSH decreased the fluorescence intensity of 10 μM Zn-NPG_A by almost 80% (**Figure 3.1.18**). The competition of glutathione for Zn^{2+} with NPG_A was also confirmed by the titration of NPG_A with Zn^{2+} in the presence of glutathione (**Figure 3.1.19**).

$$\text{Zn-NPG}_A + \text{Glutathione} \leftrightarrows \text{Glutathione - Zn} + \text{NPG}_A$$

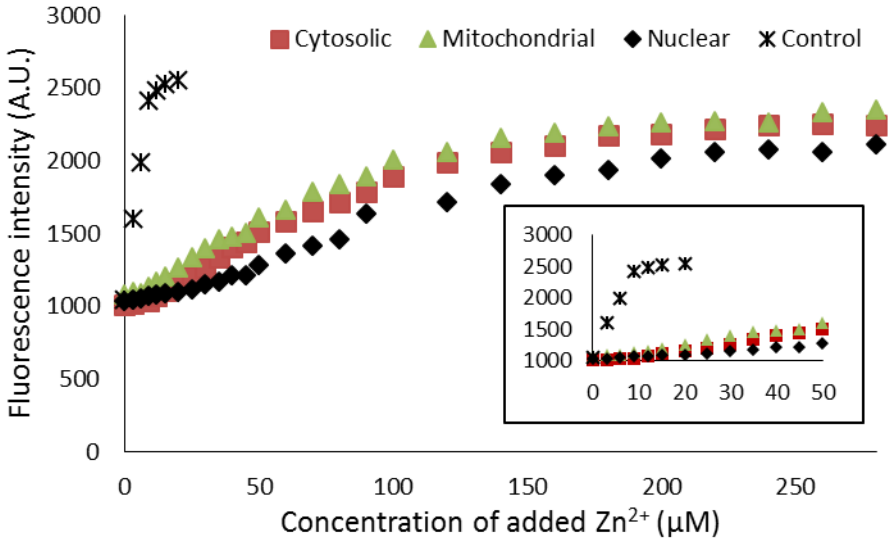

Figure 3.1.17 Stability of Zn-NPG$_A$ with sub-cellular proteome. 1.7 mg/mL cytosolic proteome, 1.6 mg/mL mitochondrial proteome and 1.6 mg/mL nuclear proteome were titrated with $ZnCl_2$ in the presence of 10 µM NPG_A. Initially, subcellular proteome was incubated with NPG_A for 15 min. The incubation period of NPG_A with the subcellular fractions after each addition of Zn^{2+} was 5 min. The inset highlights the initial buffering region.

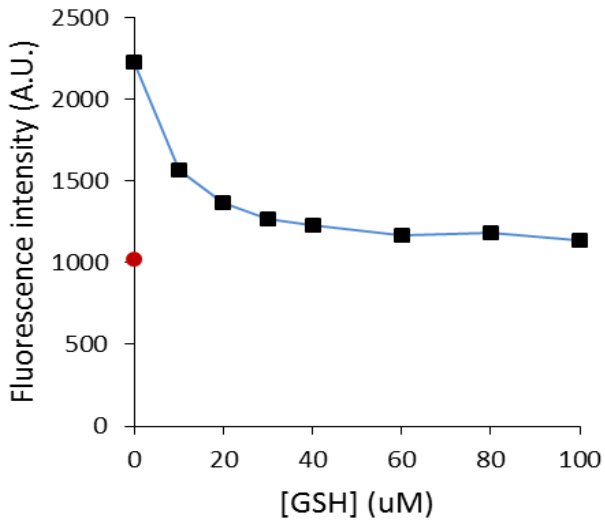

Figure 3.1.18 Stability of Zn-NPG$_A$ in the presence of glutathione (GSH). 10 µM Zn-NPG$_A$ complex in 20 mM Tris buffer at pH 7.4 was titrated with the increasing concentration of glutathione (GSH). The incubation period after each addition was 5 min. Following each addition, the fluorescence spectrum was recorded, and the maximum fluorescence intensity was plotted against the glutathione concentration. The dilution of the sample by 40 µM GSH was 2%. The red circle indicates the baseline fluorescence of 10 µM NPG$_A$.

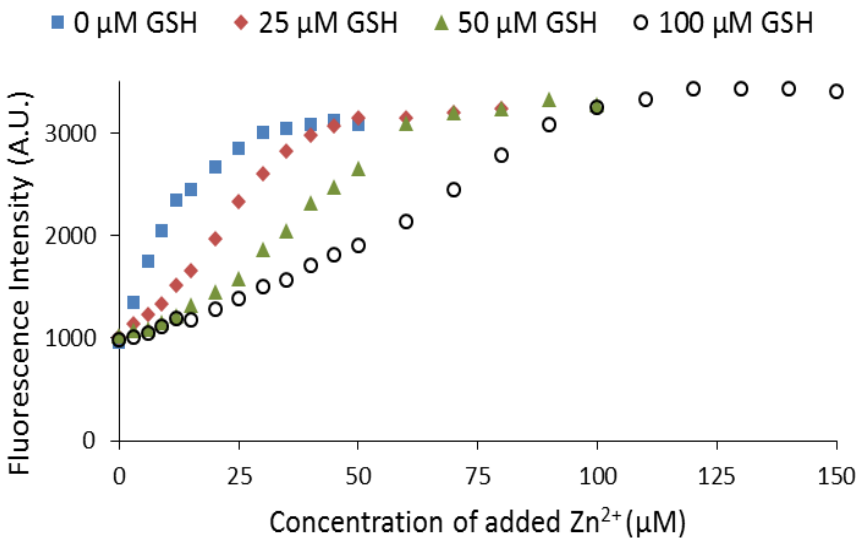

Figure 3.1.19 Titration of NPG_A with $ZnCl_2$ in the presence of glutathione (GSH). 10 µM NPG_A in 20 mM Tris buffer at pH 7.4 was titrated with $ZnCl_2$ in the absence or presence of various concentrations of glutathione. Following each addition of ZnCl2, the fluorescence spectrum was recorded, and the maximum fluorescence intensity was plotted against the total concentration of added $ZnCl_2$. Initially, NPG_A was mixed with GSH and for 5 min after each addition of Zn^{2+}.

3.1.7 Reaction of NPG and Zn-NPG with bovine serum albumin (BSA)

As albumin has a potential zinc binding site,[82] 10 µM Zn-NPG_A was reacted with bovine serum albumin (BSA) to test its stability in the presence of BSA. As a control, 10 µM NPG_A was reacted with 10 µM BSA. Figure **3.1.20 A** shows that in control reaction, fluorescence increased by two fold and the emission maximum of NPG_A shifted significantly from 532 nm to 538 nm suggesting the non-specific interaction of NPG_A with BSA. BSA also reacted with Zn-NPG_A with an enhancement of fluorescence and wavelength shift from 532 nm to 538 nm indicative of either specific interaction of Zn-NPG_A with BSA (BSA-Zn-NPG_A) through its zinc binding site or non-specific interaction (BSA-NPG_A-Zn). Regardless of the mode of interaction, this finding further complicates the use of NPG as a cellular sensor, since it may undergo non-specific interaction with cellular components. Following Centricon filtration of the final reaction mixture using 3K cut-off filter, all the fluorescence was found in the retentate, which confirmed the interaction of NPG_A with BSA (**Figure 3.1.20 B**). To extend the understanding of the reaction between Zn-NPG_A and BSA, 10 µM Zn-NPG_A was titrated with the increasing concentration of BSA (**Figure 3.1.21**). Interestingly, fluorescence of Zn-NPG_A initially decreased until a minimum was reached and increased again at higher concentrations of BSA. In addition, the emission maximum changed from Zn-NPG's 532 nm to final 538 nm. This suggested that at lower concentration of BSA, Zn^{2+} was extracted from Zn-NPG_A by BSA, hence the reduction of fluorescence was observed. However, at higher concentration of BSA, NPG binds BSA with an enhancement of fluorescence and a wavelength shift.

$$\text{Zn-NPG} + \text{BSA} \leftrightarrows \text{Zn-BSA} + \text{NPG (at lower concentration of BSA)}$$

$$\text{BSA} + \text{NPG} \leftrightarrows \text{BSA-NPG (at higher concentration of BSA)}$$

A.

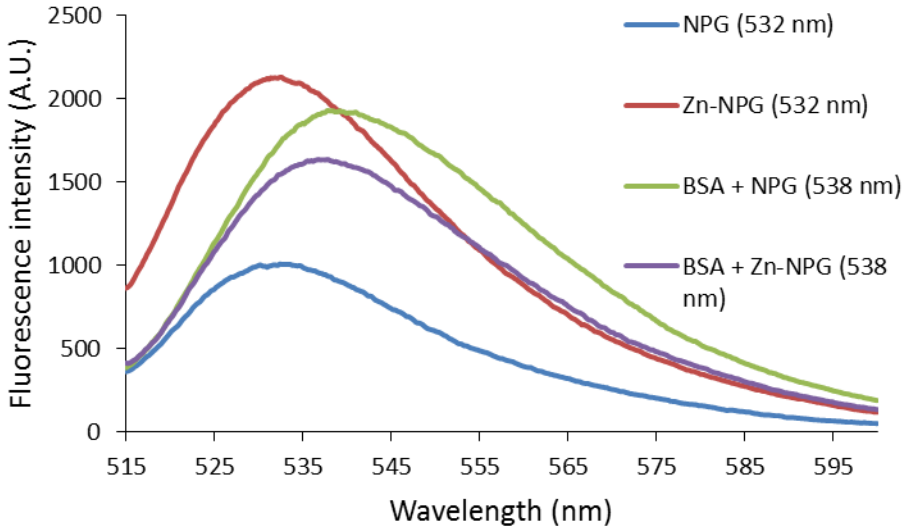

B.

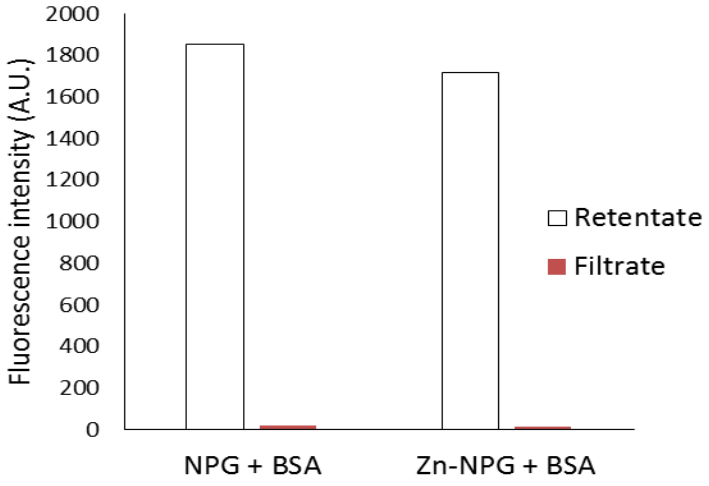

Figure 3.1.20 Reaction of NPGA and Zn-NPGA with bovine serum albumin (BSA). (A) 10 µM NPG or Zn-NPG in 20 mM Tris buffer at pH 7.4 was reacted with 10 µM BSA for 15 min. (B) Centricon filtration of the final reaction mixtures using 3K cut-off filter.

A.

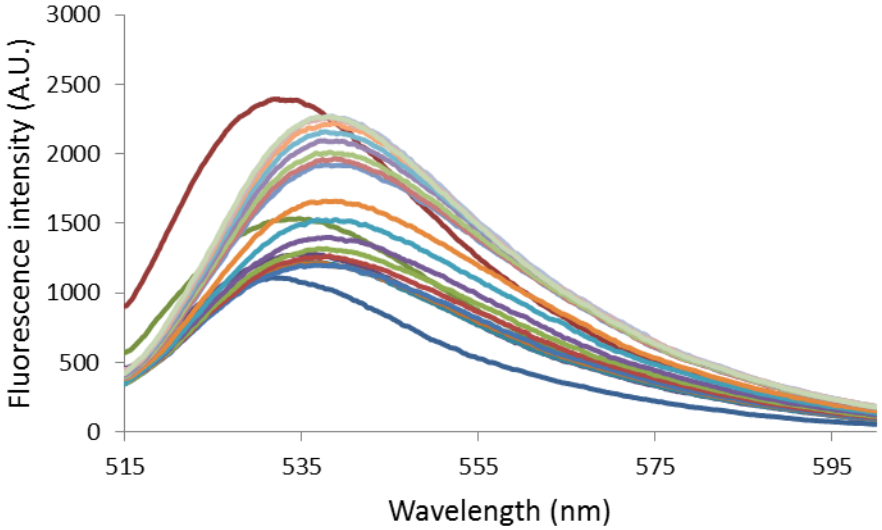

B.

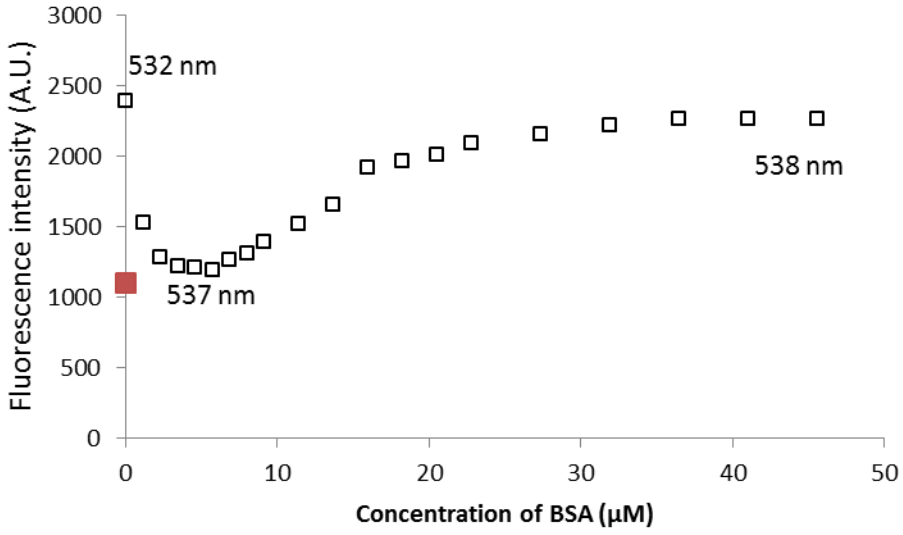

Figure 3.1.21 Titration of Zn-NPG$_A$ with BSA: (A) 10 µM Zn-NPG$_A$ in 20 mM Tris (pH 7.4) was titrated with the increasing concentration of BSA. (B) Change of maximum fluorescence intensity and emission maximum with increasing concentration of BSA.

3.1.9 Response of intracellular NPG_A to added Zn^{2+}.

The stability of Zn-NPG_A within the cellular environment was also investigated. To do so, 1.5 x 10^7 LLC-PK_1 cells were reacted with 10 µM NPG_E for 30 min followed by washing to remove any remaining extracellular medium. The cells resuspended in DPBS were subsequently treated for 20 min with a pre-incubated mixture of 10 µM $ZnCl_2$ and 2 µM pyrithione, which served as an ionophore to conduct Zn^{2+} into cells. During this time the internal concentration of Zn^{2+} increased from 1.8 nmoles/10^7 cells to 2.6 nmoles/10^7 cells, representing 15% of the added Zn^{2+}. An increase of fluorescence (173% of control) was observed after the addition of Zn-pyrithione (**Figure 3.1.22**). However, 10 µM EDTA rapidly reversed the fluorescence to 104% of control suggesting that the elevation in fluorescence was mostly due to the binding of extracellular Zn^{2+} to NPG_A that had diffused out of the cells. The inability of 10 µM TPEN to quench the remaining fluorescence ruled out the possibility that the residual 4% increase in fluorescence originated from binding of added Zn^{2+} to intracellular NPG_A. Instead, it probably arose from the continuing hydrolysis of intracellular non-fluorescent NPG_E to fluorescent NPG_A. Thus, although the intracellular Zn^{2+} concentration had increased almost 50%, no Zn-NPG_A was observed in the cells. Therefore, the results indicated that the intracellular NPG_A did not compete for adventitious Zn^{2+} within the cellular environment.

$$Zn_{out} \leftrightarrows Zn_{in}$$

$$Zn_{in} + Proteome + NPG_{A,in} \leftrightarrows Proteome \bullet Zn_{in} + NPG_{A,in}$$

$$NPG_{A,in} \leftrightarrows NPG_{A,out}$$

$$NPG_{A,out} + Zn\text{-}pyr_{out} \leftrightarrows Zn\text{-}NPG_{A,out} + pyr_{out}$$

$$Zn\text{-}NPG_{A,out} + EDTA \rightarrow Zn\text{-}EDTA + NPG_{A,out}$$

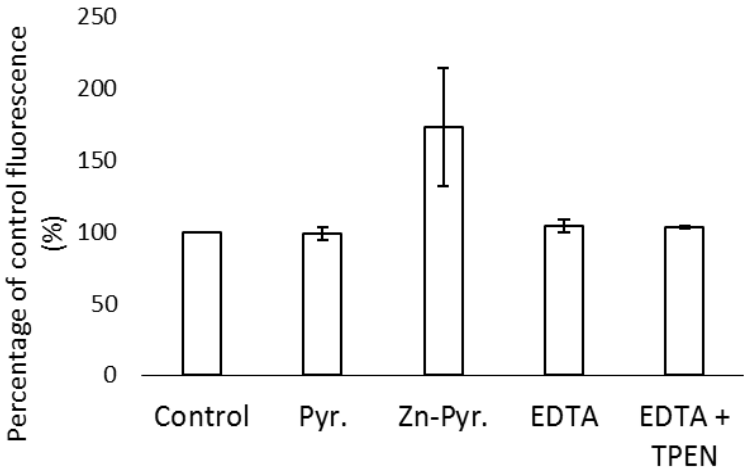

Figure 3.1.22 Reaction of NPG_E incubated LLC-PK_1 cells with Zn-pyrithione. $1.5x10^7$ cells were treated with 10 µM NPG_E for 30 min, washed twice and resuspended in DPBS (control). A pre-incubated mixture of 10 µM $ZnCl_2$ and 2 µM pyrithione was then added for 20 min. Pyr. indicates pyrithione. Subsequently, 10 µM EDTA was introduced for 10 min followed by 10 µM TPEN for another 10 min. Error bar represents standard error for three measurements.

3.1.10 Reaction of proteome with thiol reactive agents NO and NEM in the presence of NPG_A

To further examine if NPG_A can image Zn^{2+} released from Zn-proteins, 3.6 mg/mL proteome containing 12 μM Zn-proteins was reacted with 200 μM of the nitric oxide donor, diethylamine NONOate (DEA-NO) in the presence of 10 μM NPG_A. The NO produced from the breakdown of DEA-NO can react with sulfhydryl groups in the Zn binding sites of the Zn-proteins resulting in the release of Zn^{2+}.[27] A 17% increase of fluorescence upon addition of DEA-NO was observed, which initially pointed to the release of Zn^{2+} and the subsequent formation of Zn-NPG_A (**Figure 3.1.23**). However, the observation that TPEN did not reduce the fluorescence undermined this possibility. As a control, NPG_A was reacted with DEA-NO to see if the sensor, itself, underwent reaction with DEA-NO. A 50% increase of fluorescence was observed upon its reaction with DEA-NO for 2 hours (**Figure 3.1.23**). Apparently, NPG_A directly reacts with NO released from DEA-NO, resulting in an enhancement of fluorescence.

NPG_A's weak ability to image adventitious Zn^{2+} released from the Zn-proteome was further verified with the use of another thiol binding reagent, N-ethylmaleimide (NEM). 5.14 mg/mL proteome containing 17 μM Zn-proteins was reacted with NEM. A total of 500 μM NEM reduced the proteomic thiol concentration by almost 64% (from 352 μM to 125 μM) and caused about a 12% increase of fluorescence of 10 μM NPG_A, maximally equivalent to the formation of about 1 μM Zn-NPG_A (**Figure 3.1.24**). The addition of 30 μM TPEN for 30 min reduced the fluorescence to 109% of control. Thus, no more than 0.3 μM Zn-NPG_A had actually formed. In contrast, substituting 20 μM Zinquin for NPG_A, the higher affinity zinc sensor displayed a 47% increase of fluorescence after addition of only 100 μM NEM to the proteome. In the process,

25% of the proteomic zinc (4.2 µM) was labilized by NEM, much of it becoming bound to Zinquin.[83]

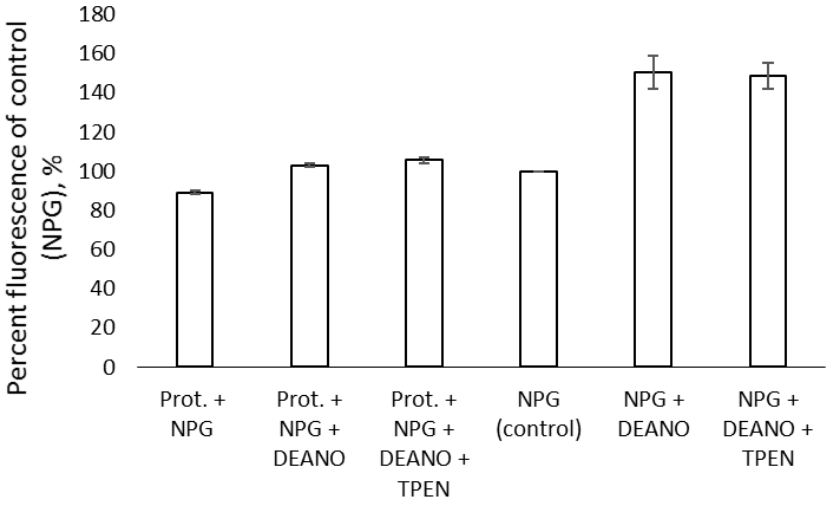

Figure 3.1.23 Reaction of proteome with diethylamine NONOate (DEA-NO) in the presence of NPG_A. Proteome (10 µM Zn^{2+}) isolated from LLC-PK_1 cells was reacted with with 200 µM DEA-NO for 90 min in the presence of 10 µM NPG_A followed by the treatment with 10 µM TPEN for 30 min. The fluorescence was recorded continuously. 10 µM NPG_A in Tris was reacted with 200 µM DEA-NO for 2 hours as a control. Prot. indicates proteome.

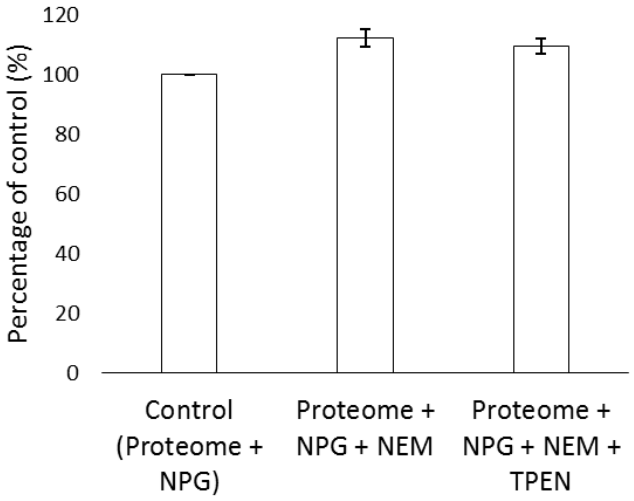

Figure 3.1.24 Reaction of proteome with N-ethylmaleimide (NEM) in the presence of NPG_A. Proteome (17 µM Zn^{2+}) was reacted with 500 µM NEM in the presence of 10 µM NPG_A for 30 min. Subsequently, 30 µM TPEN was added for another 30 min. Error bar represents standard error for three measurements.

3.2 Chemical Biology of Zinpyr-1 (ZP1)

Having found that Newport Green, a low affinity zinc senor, is unable to form intracellular Zn-NPG complex by outcompeting proteome's non-specific Zn^{2+} binding sites, for comparison, the chemical-biological properties of a relatively higher affinity sensor, Zinpyr-1 (ZP1), were studied. ZP1 has a dichlorofluorescein as the fluorophore and two appended di-2-picolylamine (DPA) moieties as Zn^{2+} binding ligands (**Figure 1.2**). Of these two binding sites, one is of higher affinity (K_d 0.7 nM) than the second one (K_d 85 μM).[1] Various articles have reported the intracellular imaging of Zn^{2+} by ZP1.[84-89] However, due to its high affinity Zn^{2+} binding site, it may undergo other possible reactions. For example, ZP1 may directly react with the native Zn-proteins and thus perturb the equilibrium between the bound and the free Zn^{2+} (reaction 3.2.1).

$$\Sigma \text{ Zn-protein} + \text{ZP1} \rightleftharpoons \Sigma \text{ apo-protein} + \text{ZP1(Zn)}_2 \quad (3.2.1)$$

Moreover, like Zinquin (ZQ) which also has nanomolar stability constant, ZP1 can form ternary adduct with specific Zn-proteins and generate ZP1-Zn-Protein ternary adduct (reaction 3.2.2).

$$\Sigma \text{ Zn-protein} + \text{ZP1} \rightleftharpoons \Sigma \text{ ZP1-Zn-Protein} \quad (3.2.2)$$

From Newport Green study, we have seen that proteome possesses a zinc buffering capacity. So, ZP1 can also interact with Zn^{2+} adventitiously bound to various non-specific proteomic sites (reaction 3.2.3).

$$\text{Proteome} + Zn^{2+} + \text{ZP1} \rightleftharpoons \text{Proteome}\bullet\text{Zn-ZP1} \quad (3.2.3)$$

This study investigated all these possible reactions of ZP1 both *in vitro* and *in vivo*.

3.2.1 Reaction of ZP1 with $ZnCl_2$

To investigate the spectral properties of ZP1, 10 μM ZP1 in 20 mM Tris (pH 7.4) was titrated with the increasing concentration of $ZnCl_2$ (**Figure 3.2.1 A**). When excited at 515 nm, the solution of ZP1 (pink in color) in Tris shows very little fluorescence centered at 535 nm. As $ZnCl_2$ is added, it expectedly first binds the higher affinity site of ZP1 with a very small enhancement of fluorescence and the emission maximum stays at 535 nm as of ZP1 solution itself. Once the higher affinity Zn^{2+} binding is occupied and half-saturated ZP1-Zn forms, added Zn^{2+} starts binding to the lower affinity site with much higher increase of fluorescence and a wavelength shift from 535 nm to 525 nm to generate the fully saturated $ZP1(Zn)_2$ complex. As fully saturated $ZP1(Zn)_2$ forms, the color of the solution changes from pink to green.

$$ZP1 + Zn^{2+} \leftrightarrows ZP1\text{-}Zn \text{ (535 nm, pink, weakly fluorescent)}$$

$$ZP1\text{-}Zn + Zn^{2+} \leftrightarrows ZP1(Zn)_2 \text{ (525 nm, green, strongly fluorescent)}$$

The first Zn^{2+} binding to ZP1 with weak fluorescence and the second with strong fluorescence gives the titration curve a sigmoidal shape (**Figure 3.2.1 B**). Since the binding of Zn^{2+} to the stronger site results in very weak fluorescence, the use of ZP1 as a cellular sensor becomes complicated.

A.

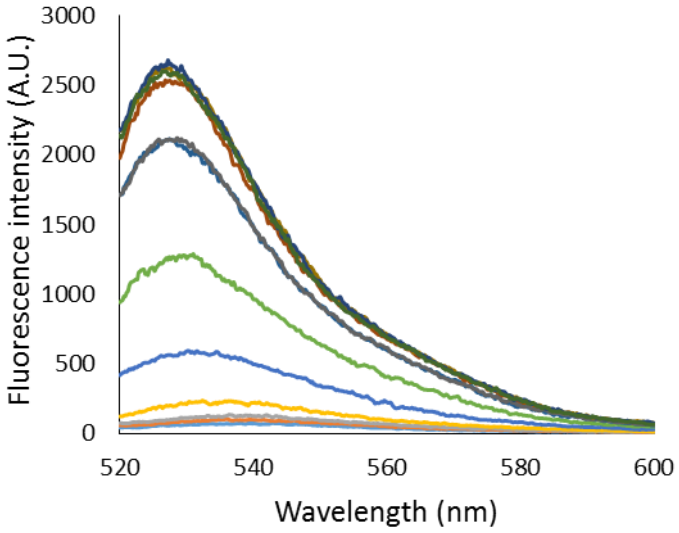

B.

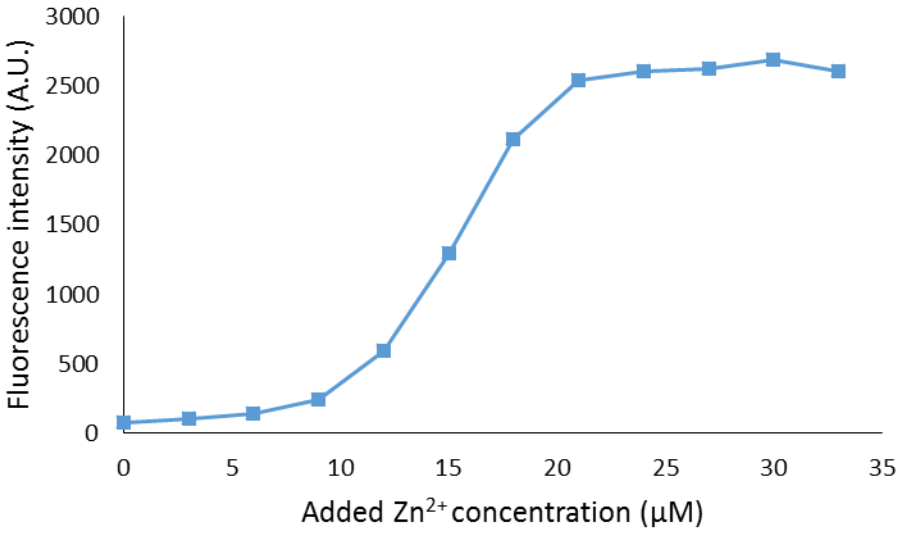

Figure 3.2.1 Titration of ZP1 with Zn^{2+}: (A) 10 µM ZP1 in 20 mM Tris (pH 7.4) was titrated with increasing concentration of $ZnCl_2$. (B) Change of fluorescence of ZP1 as it binds Zn^{2+}.

3.2.2 Reaction of LLC-PK_1 cells with ZP1

As 10^7 LLC-PK_1 cells were incubated with 10 µM ZP1 for 15 min, very small fluorescence centered at 535 nm was observed that did not change over time (**Figure 3.2.2 A**). Since ZP1-Zn fluoresces with an emission maximum of 525 nm, the λmax of 535 nm in this reaction indicates either no reaction of ZP1 with the native Zn-proteome, as ZP1 solution itself shows very weak fluorescence at 535 nm, or some reaction other than the formation of ZP1-Zn. However, 30 µM TPEN, a very strong, intracellular zinc chelator, could not reverse the fluorescence that resulted from the reaction of LLC-PK_1 cells and ZP1 (**Figure 3.2.2 B**), suggesting no involvement of native Zn^{2+} in the observed fluorescence. Nevertheless, it is difficult to draw any conclusion from this experiment, as we have seen from previous experiment (titration of ZP1 with Zn^{2+}) that the intital zinc binding gives very weak fluorescence. Therefore, even if there may be some reactions of ZP1 with the native configuration of Zn^{2+}, it's unlikely to be observed and any effect of TPEN is also not expected. To test whether the observed fluorescence has originated due to the binding of extracellular Zn^{2+}, 30 µM EDTA (ethylenediaminetetraacetic acid), a cell impermeable Zn^{2+} chelator, was introduced to the reaction of LLC-PK_1 cells and ZP1. Like TPEN, EDTA couldn't affect the fluorescence either ruling out the possibility of the involvement of any extracellular Zn^{2+} (**Figure 3.2.2 B**).

To further investigate the source of this fluorescence, 2 x 10^8 LLC-PK_1 cells in DPBS were incubated with 10 µM ZP1 for 15 min. Subsequently, the cell suspension was centrifuged and washed with fresh DPBS to remove any extracellular ZP1. The washed cell suspension resuspended in 1 mL MilliQ water was sonicated, centrifuged and the resultant cell lysate was fractionated using Sephadex G-75 gel filtration column. Following the elution of the fractions

with degassed 20 mM Tris (pH 7.4), all the collected fractions were analyzed for both fluorescence and zinc content. As **figure 3.2.3** shows that the majority of the fluorescence resided in the high molecular weight fractions and nicely aligned with Zn^{2+} concentration in those fractions. The fluorescence in the high molecular weight fractions may suggest the formation of ternary adduct, ZP1-Zn-Protein from the reaction between Zn-Protein and ZP1.

$$\text{Zn-Protein} + \text{ZP1} \leftrightarrows \text{ZP1-Zn-Protein}$$

Moreover, a small band of fluorescence in low molecular weight region also appeared, although no zinc was associated with this fluorescence indicating the low molecular weight fluorescence resulted from unbound ZP1.

A.

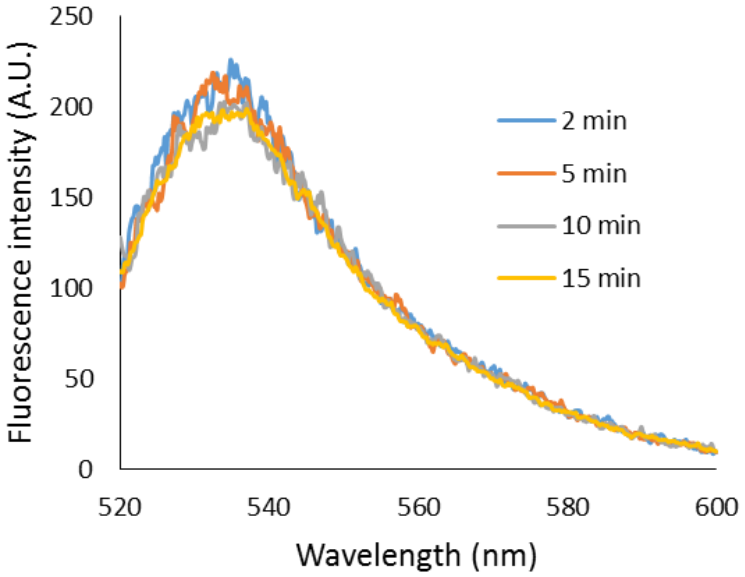

B.

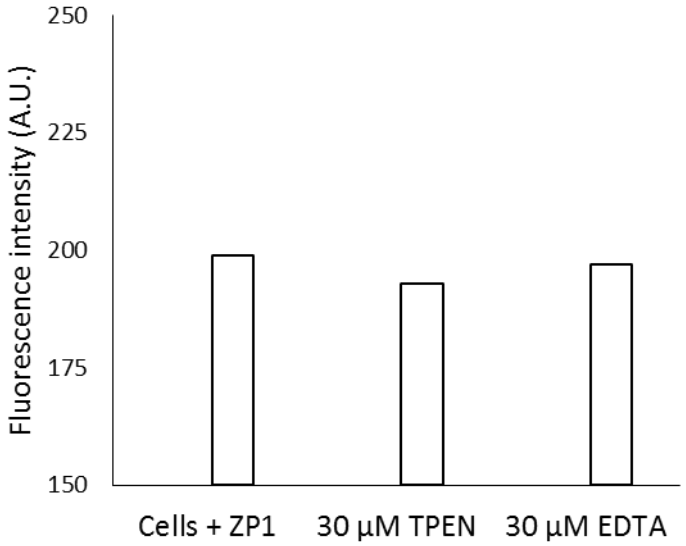

Figure 3.2.2 Reaction of LLC-PK$_1$ cells with ZP1. (A) 10^7 LLC-PK$_1$ cells in DPBS were reacted with 10 µM ZP1 for 15 min. (B) Effect of 30 µM TPEN and 30 µM EDTA on the fluorescence resulted from the reaction of LLC-PK$_1$ cells and 10 µM ZP1.

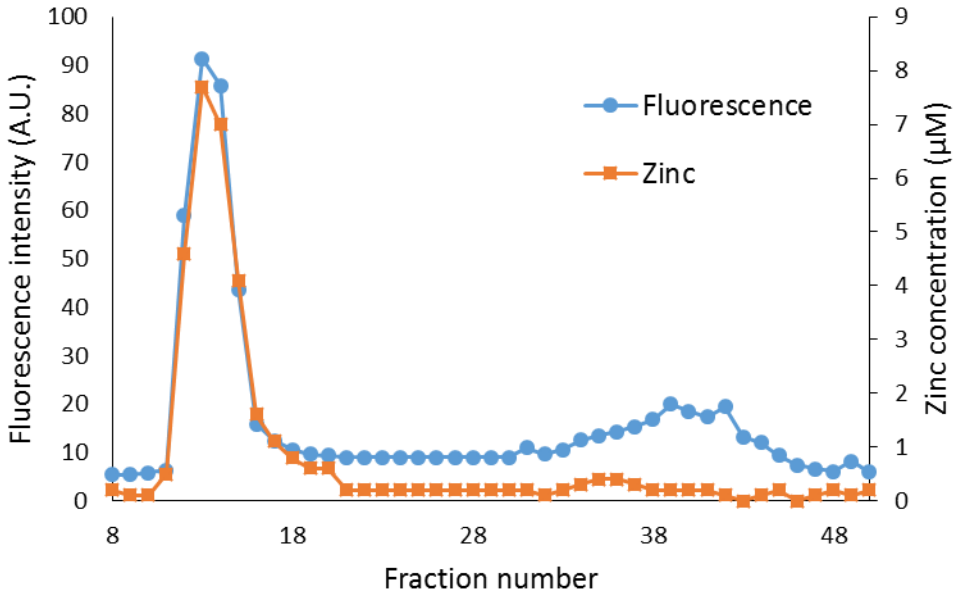

Figure 3.2.3 Locating fluorescent species in the reaction of LLC-PK$_1$ cells and ZP1. 2 x 10^8 LLC-PK1 cells suspended in DPBS were incubated with 10 μM ZP1 for 15 min. The cell suspension was then centrifuged and resuspended in fresh DPBS, and this was repeated two more times. Finally the cells were resuspended in MilliQ water, sonicated, centrifuged, and the resultant cell lysate was loaded onto a Sephadex G-75 gel filtration column. The fractions eluted with degassed 20 mM Tris buffer (pH 7.4) were analyzed for fluorescence and zinc content.

3.2.3 Reaction of ZP1 with isolated proteome

Isolated proteome (9 µM Zn^{2+}) from LLC-PK_1 cells was reacted with 10 µM ZP1. A significant increase of fluorescence compared to blank (ZP1 solution in Tris buffer) was observed and the emission maximum was found to be about 540 nm (**Figure 3.2.4**). 20 µM TPEN reduced the enhancement by about 44% (Figure 3.2.4B) indicating the participation of Zn^{2+} in the increment of fluorescence and the formation of ZP1-Zn-Proteome ternary adduct.

To acquire a better insight into this reaction, the final reaction mixture following the incubation of isolated proteome (10 µM Zn^{2+}) with 10 µM ZP1 for 15 min was fractionated using a Sephadex G-75 gel filtration column. When the fractions eluted with 20 mM Tris (pH 7.4) were analyzed for fluorescence, most of the fluorescence was found in the high molecular weight region (**Figure 3.2.5 A**). This again suggested that ZP1 formed ternary adduct, ZP1-Zn-Proteome, with Zn-Proteome. A small low molecular weight pool of fluorescence also appeared, that might possibly be attributed to the unbound ZP1. As the high molecular weight fractions were reacted with 10 µM TPEN, the integrated fluorescence intensity was brought down by about 25% considering that ZP1 itself shows some fluorescence (**Figure 3.2.5 B**). TPEN effect further confirms the formation of ZP1-Zn-Proteome ternary adduct, in which TPEN may either removes Zn^{2+} from the adduct to form Zn-TPEN complex or replaces ZP1 to form TPEN-Zn-proteome.

$$\text{ZP1-Zn-Proteome + TPEN} \leftrightarrows \text{Zn-TPEN + ZP1 + apo-Proteome}$$

$$\text{ZP1-Zn-Proteome + TPEN} \leftrightarrows \text{TPEN-Zn-Proteome + ZP1}$$

A.

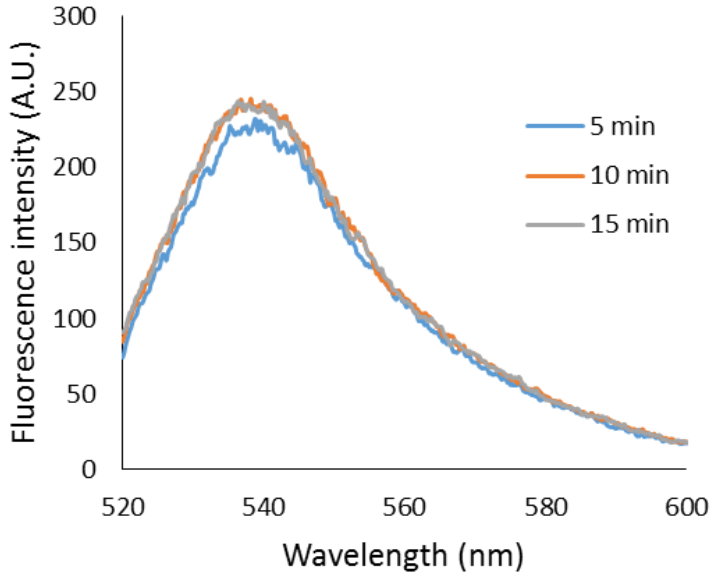

B.

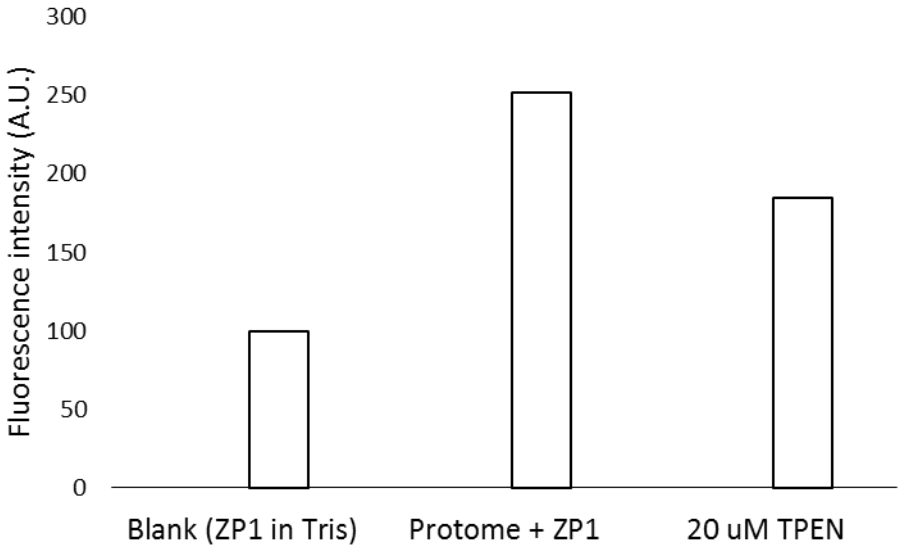

Figure 3.2.4 Reaction of ZP1 with isolated proteome. (A) Isolated proteome containing 9 µM Zn^{2+} in 20 mM Tris buffer (pH 7.4) was reacted with 10 µM ZP1. (B) Effect of 20 µM TPEN on the fluorescence.

A.

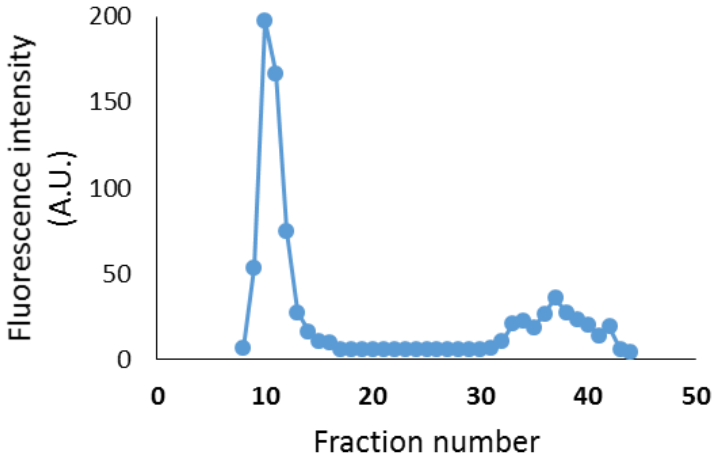

B.

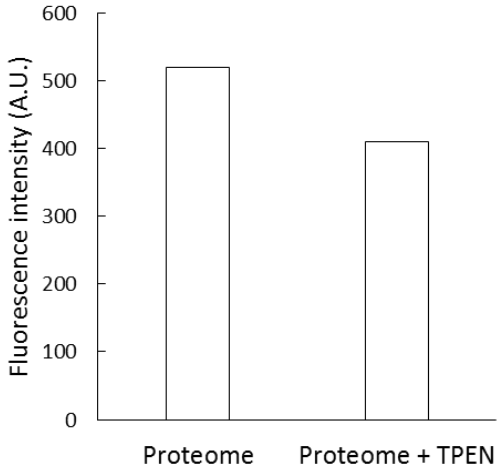

Figure 3.2.5 Sephadex G-75 gel filtration of the reaction mixture of isolated proteome (10 µM Zn^{2+}) and ZP1. (A) Isolated proteome (10 µM Zn^{2+}) in 20 mM Tris buffer (pH 7.4) was reacted with 10 µM ZP1. The final reaction mixture was then passed through a Sephadex G-75 gel filtration column and was eluted with 20 mM Tris (pH 7.4) buffer. The eluted fractions were analyzed for fluorescence. (B) Effect of 10 µM TPEN on the integrated fluorescence intensity of high molecular weight (HMW) fractions.

3.2.4 Titration of proteome with Zn^{2+} in the presence of ZP1

As fluorescent sensors are used to image Zn^{2+} liberated from various cellular zinc binding sites or Zn^{2+} released from different cellular zinc stores, e.g. endoplasmic reticulum, ZP1 was probed to determine if it forms ternary adduct, Proteome-Zn-ZP1, with proteome and added Zn^{2+}. In doing so, isolated proteome containing 9 µM Zn^{2+} was incubated with 10 µM ZP1 for 15 min. The resultant fluorescence intensity with an emission maximum of 540 nm suggested the formation of ternary adduct, ZP1-Zn-Protein, from the reaction of ZP1 and native Zn-Protein.

$$\text{ZP1} + \text{Zn-Protein} \leftrightarrows \text{ZP-Zn-Protein}$$

Following the incubation of proteome and ZP1 for 15 min, the final reaction mixture was titrated with the increasing concentration of Zn^{2+} (**Figure 3.2.6 A and B**). As Zn^{2+} was added, fluorescence intensity immediately increased. This immediate change of fluorescence indicated that this was not just simple titration of ZP1 with Zn^{2+}, in which the initial strong binding gives little fluorescence. Thus, the fluorescence increase in this titration is not due to the formation of ZP1-Zn complex. Moreover, as the fluorescence intensity further increased with the addition of more zinc, the emission maximum stayed unchanged at 535-540 nm. This differs from the titration of ZP1 with Zn^{2+}, where initially the emission maximum is 540 nm at low concentration of Zn^{2+} and low fluorescence intensity, but shifts to 525 nm as the concentration of Zn^{2+} increases with higher fluorescence intensity. All these differences from the titration of ZP1 and Zn^{2+} suggested the formation of Proteome•Zn-ZP1 ternary adduct, where the added Zn^{2+} binds various adventitious zinc binding sites of proteome which in turn binds ZP1.

$$\text{Proteome} + \text{ZP1} + Zn^{2+} \leftrightarrows \text{Proteome.Zn-ZP1}$$

To confirm the notion of Proteome•Zn-ZP1 ternary adduction generation, the final reaction mixture following the titration of proteome with Zn^{2+} in the presence of ZP1 was fractionated using a Sephadex G-75 gel filtration column. As the fractions eluted with 20 mM Tris buffer (pH 7.4) were analyzed for both fluorescence and zinc content, most of the fluorescence was found associated with the high molecular weight fractions (**Figure 3.2.6 C**). The emission maximum of the fluorescence spectrum in these fractions was found to be 535 nm. Moreover, the fluorescence intensities in high molecular weight fractions were very consistent with the zinc concentrations in those fractions (**Figure 3.2.7 A**). The residence of the majority of the fluorescence in the high molecular weight fractions further points to the formation of Proteome•Zn-ZP1 ternary adduct. However, a small low molecular weight fluorescence pool also emerged. The absence of measurable zinc in those low molecular weight fractions indicated that the unbound ZP1 might be attributed to this small pool of fluorescence. The effect of 10 μM TPEN on the fluorescence intensities of the high molecular weight fractions further validates the claim of the generation of ternary adduct, Proteome•Zn-ZP1 in this reaction. TPEN quenched the integrated fluorescence intensity of the high molecular weight proteomic fractions almost by 50% (**Figure 3.2.7 B**).

Proteome•Zn-ZP1 + TPEN ⇆ Proteome + Zn-TPEN + ZP1

Proteome•Zn-ZP1 + TPEN ⇆ Proteome•Zn-TPEN + ZP1

A.

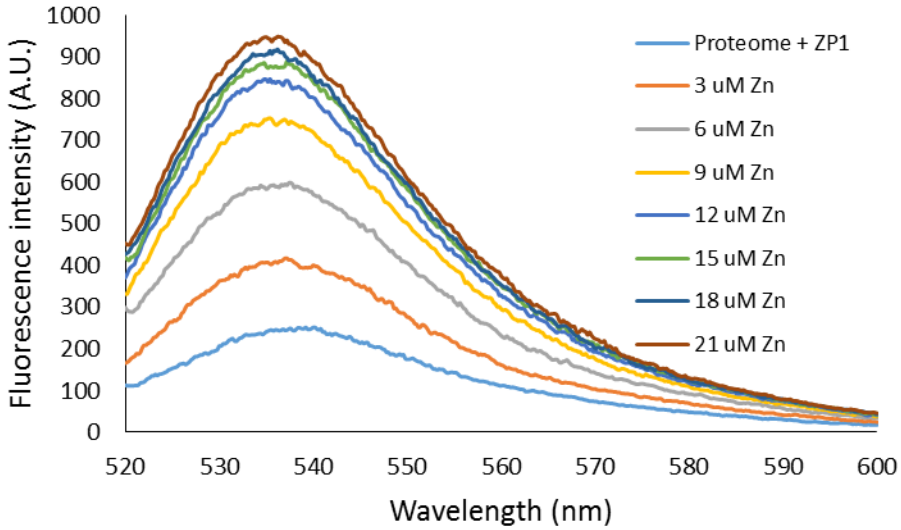

B.

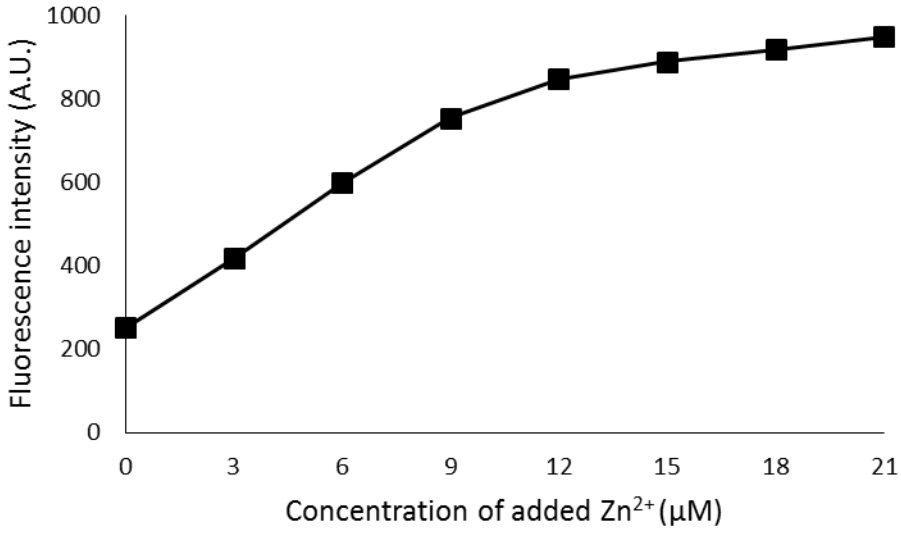

Figure 3.2.6 Titration of proteome with Zn^{2+} in the presence of ZP1. (A) Proteome containing 9 µM Zn^{2+} was reacted with the increasing concentration of Zn^{2+}. (B) Change of fluorescence with the increasing concentration of Zn^{2+}.

A.

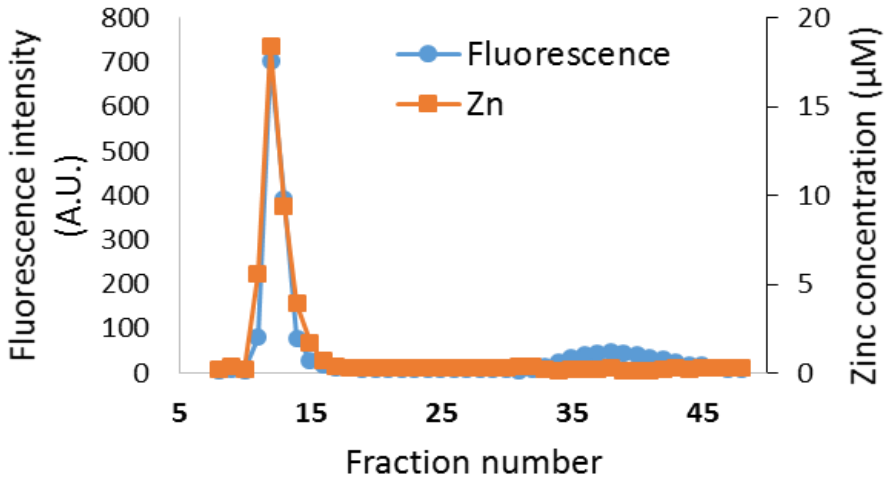

B.

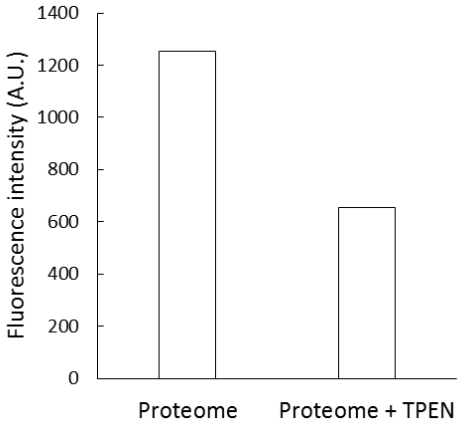

Figure 3.2.7 Sephadex gel filtration of the proteome titrated with $ZnCl_2$ in the presence of ZP1.

(A) Proteome (9 µM Zn^{2+}) was reacted with the increasing concentration of Zn^{2+}.The final reaction mixture was fractionated using a Sephadex G-75 gel filtration column and the fractions eluted with 20 mM Tris (pH 7.4) were analyzed for both fluorescence and zinc content. (B) Effect of 10 µM TPEN on the integrated fluorescence intensity of high molecular weight fractions.

3.2.5 Reaction of proteome with Zn-ZP1

The formation of ternary adduct Proteome•Zn-ZP1 following the reaction of isolated proteome with ZP1 and added Zn^{2+} was investigated another way. Isolated proteome containing 9 µM Zn^{2+} was reacted with pre-mixed $ZP1(Zn)_2$. As 20 µM $ZP1(Zn)_2$ (emission maximum of 525 nm) was added to proteome, the emission maximum shifted to 540 nm indicating the production of Proteome•Zn-ZP1 ternary adduct species (**Figure 3.2.8 A**).

$$\text{Proteome} + ZP(Zn)_2 \leftrightarrows \text{Proteome•Zn-ZP1}$$

To confirm the generation of Proteome•Zn-ZP1 ternary adduction species, the final reaction mixture was fractionated using a Sephadex G-75 gel filtration column. As the fractions eluted with 20 mM Tris buffer (pH 7.4) were analyzed for both fluorescence and zinc content, most of the fluorescence (63%) was found associated with the high molecular weight fractions (**Figure 3.2.8 B**). The emission maximum of the fluorescence spectrum in these fractions was found to be 535 nm. Moreover, the fluorescence intensities in high molecular weight fractions were very consistent with the zinc concentrations in those fractions. The residence of the majority of the fluorescence in the high molecular weight fractions further points to the formation of Proteome•Zn-ZP1 ternary adduct. However, a small low molecular weight fluorescence pool also emerged. The absence of measurable zinc in those low molecular weight fractions indicated that the unbound ZP1 might generate this small pool of fluorescence. The effect of 10 µM TPEN on the fluorescence intensities of the high molecular weight fractions further validated the claim of the generation of ternary adduct, Proteome•Zn-ZP1 in this reaction.

TPEN quenched the integrated fluorescence intensity of the high molecular weight proteomic fractions almost by 82% (**Figure 3.2.8 C**).

A.

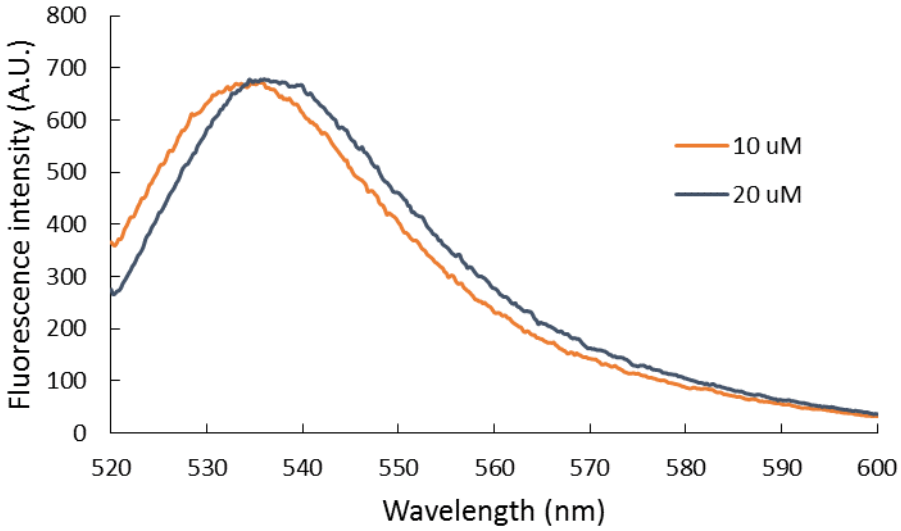

B.

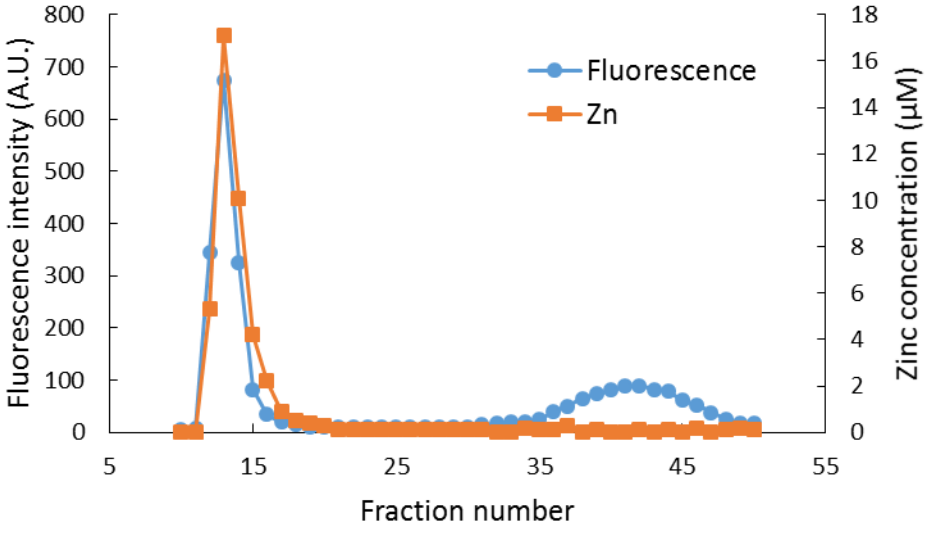

C.

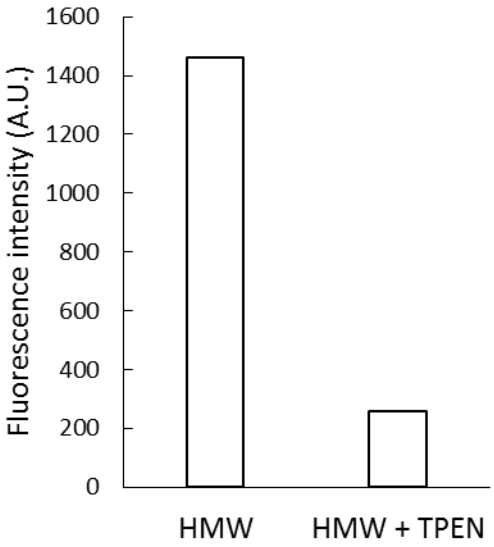

Figure 3.2.8 Reaction of proteome with ZP1(Zn)$_2$. (A) Reaction of proteome (9 µM Zn^{2+}) with 10 µM and 20 µM ZP1(Zn)$_2$. (B) The final reaction mixture was loaded onto a Sephadex G-75 gel filtration column and the fractions were eluted with 20 mM Tris buffer (pH 7.4). Both fluorescence and zinc content were determined for each of the eluted fractions. (C) Effect of 20 µM TPEN on the integrated fluorescence intensity of the high molecular weight fractions.

3.2.6 Reaction of ZP1 with TSQ-Zn-Proteome

As TSQ reacts with Zn-proteome and forms ternary adduct TSQ-Zn-Proteome, ZP1's ability to replace TSQ from this ternary adduct and, thus, to form new ternary adduct species ZP1-Zn-Proteome was probed. In doing so, isolated proteome containing 12 µM Zn^{2+} was first reacted with 20 µM TSQ for an hour. As expected, a gradual increase of fluorescence with an emission maximum of 470 nm – signature of the generation of TSQ-Zn-Proteome ternary adduct species – was observed. Afterwards, the reaction mixture was titrated with the increasing concentration of ZP1, the fluorescence intensity at 470 nm rapidly quenched and at the same time, a fluorescence peak at 535 nm, which gradually shifted to 540 nm at higher concentration of ZP1, appeared (**Figure 3.2.8 A**). The loss of fluorescence intensity at 470 nm and the emergence of fluorescence at 535-540 nm suggest the replacement of TSQ from the ternary adduct TSQ-Zn-Proteome (470 nm) and as such the creation of the new ternary adduct ZP1-Zn-Proteome (540 nm).

$$\text{Zn-Proteome} + \text{TSQ} \leftrightarrows \text{TSQ-Zn-Proteome}$$

$$\text{TSQ-Zn-Proteome} + \text{ZP1} \leftrightarrows \text{ZP1-Zn-Proteome} + \text{TSQ}$$

We also considered the possibility that the reduction of fluorescence intensity at 470 nm following the introduction of ZP1 might be attributed to the inner filter effect, i.e. ZP1 remains unreactive with TSQ-Zn-Proteome and instead, absorbs the emitted light at 470 nm and thus quenches the fluorescence. Despite the fact that the non-linear loss of fluorescence at 470 nm with the increasing concentration of ZP1 ruled out the possibility of inner filter effect (**Figure 3.2.9 B**), for further confirmation we fractionated the final reaction mixture using a Sephadex

G-75 gel filtration column and compared the fluorescence intensities of the high molecular weight fractions with those of a control experiment, in which isolated proteome containing 12 μM Zn^{2+} was reacted with 20 μM TSQ followed by the fractionation of the final reaction mixture. In the case of the ZP1 treated reaction, the fluorescence intensity at 470 nm of the high molecular weight fractions was much lower (**Figure 3.2.10 B**) compared with that of the control experiment (**Figure 3.2.10 A**). If the reduction of fluorescence at 470 nm were due to the inner filter effect of ZP1, the fluorescence intensities of high molecular weight fractions should have returned following gel filtration. In fact, the integrated fluorescence intensities at 470 nm of high molecular weight fractions turned out to be only 39% of those of the control experiment (**Figure 3.2.11 A**). All these findings cancel the possibility that the inner filter effect of ZP1 played any role in reducing the fluorescence of TSQ-Zn-Proteome ternary adduct at 470 nm. Furthermore, the quenching of the integrated fluorescence intensity of 540 nm of the high molecular weight fractions by 40-50% by 20 μM TPEN further confirms the formation of a ZP1-Zn-Proteome ternary adduct that replaces TSQ from TSQ-Zn-Proteome (**Figure 3.2.11 B**).

A.

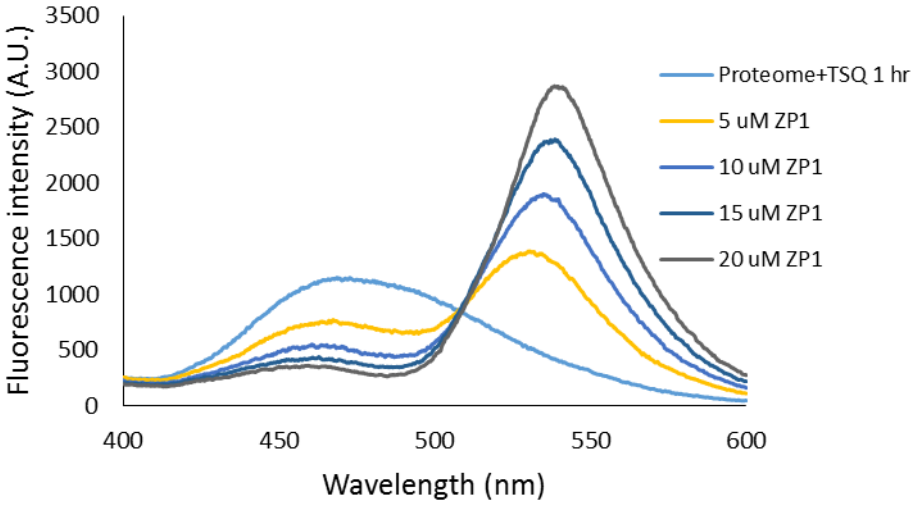

B.

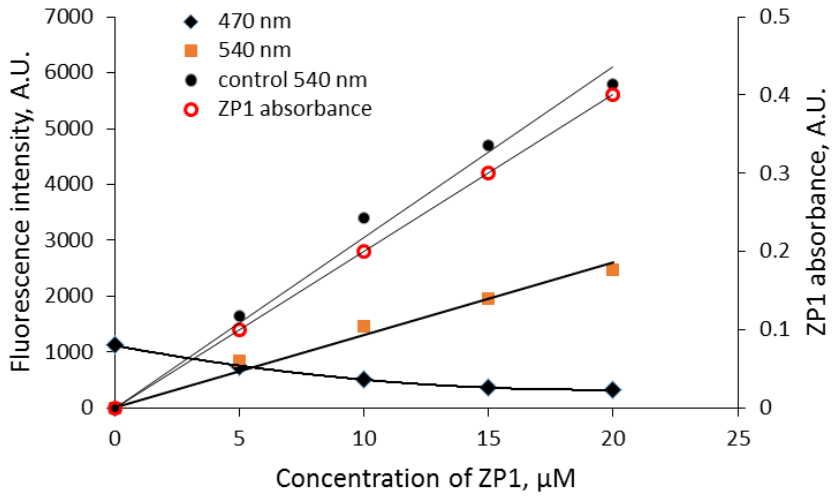

Figure 3.2.9 Reaction of ZP1 and proteome incubated with TSQ. (A) Proteome (12 µM Zn^{2+}) was reacted with 20 µM TSQ for an hour. Following on, the reaction mixture was titrated with ZP1. (B) Change of fluorescence at 470 nm, 540 nm, control 540 nm and ZP1 absorbance with the increasing concentration of ZP1.

A.

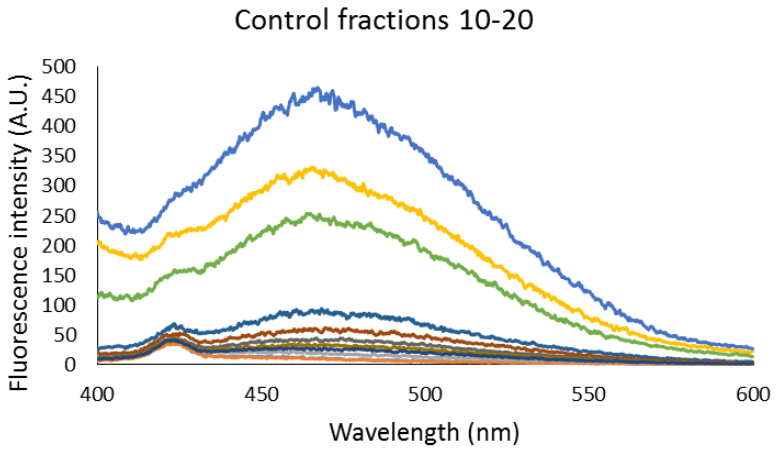

B.

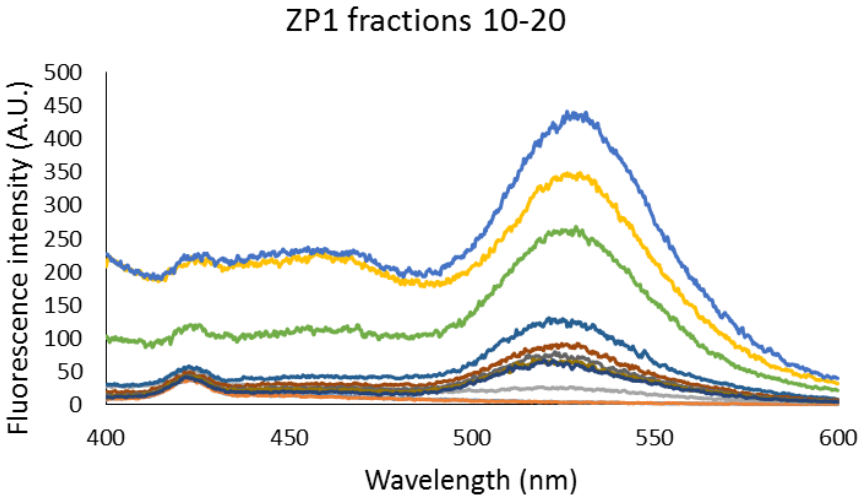

Figure 3.2.10 Sephadex gel filtration of proteome reacted with TSQ and ZP1. (A) Control: The final reaction mixture of proteome and 20 µM TSQ was fractionated using a Sephadex G-75 gel filtration column and the high molecular weight fractions eluted with 20 mM Tris buffer (pH 7.4) were analyzed for fluorescence. (B) Fluorescence spectrum of the high molecular weight fractions collected by fractionation of the final reaction mixture of proteome, TSQ and ZP1.

C.

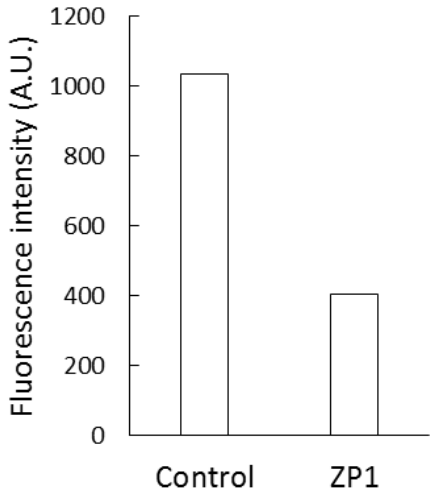

D.

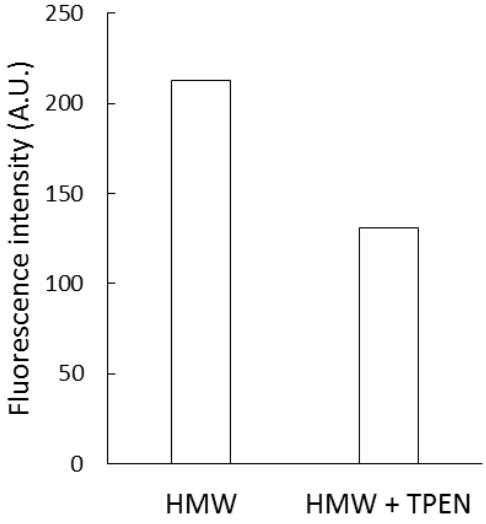

Figure 3.2.11 Integrated fluorescence of high molecular weight (HMW) fractions and TPEN effect. (A) Comparison of the integrated fluorescence intensities of the high molecular weight fractions between control and ZP1 treated reactions. (B) The effect of 20 µM TPEN on the integrated fluorescence intensity of the high molecular weight fractions of ZP1 treated reaction.

3.2.7. Reaction of ZP1 with model zinc proteins, such as alcohol dehydrogenase

ZP1 formed ternary adduct ZP-Zn-Proteome with native Zn-Proteome and Proteom.Zn-ZP1 with proteome and added Zn^{2+}. Next we wanted to investigate if ZP1 forms ternary adduct with different model Zn-proteins, such as alcohol dehydrogenase. Each alcohol dehydrogenase monomer unit has one catalytic zinc and one structural zinc.[90]

As 10 μM ZP1 in 20 mM Tris (pH 7.4) was titrated with the increasing concentration of alcohol dehydrogenase (ADH), a small but gradual enhancement of fluorescence was observed (**Figure 3.2.12 A**). The emission maximum of the fluorescence spectrum stayed at 536 nm. These observations suggested the generation of ternary adduct ZP1-Zn-ADH between ZP1 and alcohol dehydrogenase (Zn-ADH). However, even after the addition of alcohol dehydrogenase that contained 60 μM Zn^{2+}, the fluorescence intensity was still gradually increasing indicating weak interaction between ZP1 and alcohol dehydrogenase. As the final reaction mixture was reacted with 20 μM TPEN, the fluorescence intensity was almost completely reversed to the blank (ZP1 in Tris) (**Figure 3.2.12 B**). The TPEN effect further suggests the formation of ternary adduct species, ZP1-Zn-ADH and its reaction with TPEN as follows:

$$\text{ZP1} + \text{Zn-ADH} \leftrightarrows \text{ZP1-Zn-ADH}$$

$$\text{ZP1-Zn-ADH} + \text{TPEN} \leftrightarrows \text{Zn-TPEN} + \text{ZP1} + \text{ADH}$$

$$\text{ZP1-Zn-ADH} + \text{TPEN} \leftrightarrows \text{TPEN-Zn-ADH} + \text{ZP1}$$

To further confirm the formation of ternary adduct ZP1-Zn-ADH, the final reaction mixture of 10 μM ZP1 and alcohol dehydrogenase containing 60 μM Zn^{2+} was fractionated using a Sephadex G-75 gel filtration column and the fractions were eluted with 20 mM Tris buffer (pH 7.4). As the fractions were analyzed, the majority of the fluorescence was found in the low molecular weight region (**Figure 3.2.12 C**). This might be due to the weak binding of ZP1 and Zn-ADH in forming ZP1-Zn-ADH ternary adduct that was implied in the earlier experiment described by Figure 3.2.9 A and its subsequent dissociation during gel filtration.

$$\text{ZP1-Zn-ADH} \leftrightarrows \text{ZP1} + \text{Zn-ADH}$$

A.

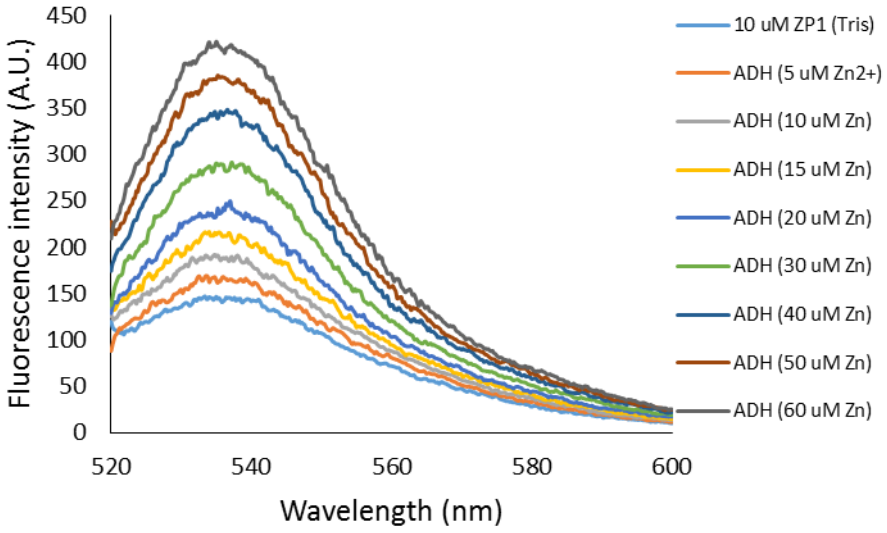
Fluorescence intensity (A.U.)
450
400
350
300
250
200
150
100
50
0
520
540
560
580
600
Wavelength (nm)
10 uM ZP1 (Tris)
ADH (5 uM Zn2+)
ADH (10 uM Zn)
ADH (15 uM Zn)
ADH (20 uM Zn)
ADH (30 uM Zn)
ADH (40 uM Zn)
ADH (50 uM Zn)
ADH (60 uM Zn)

B.

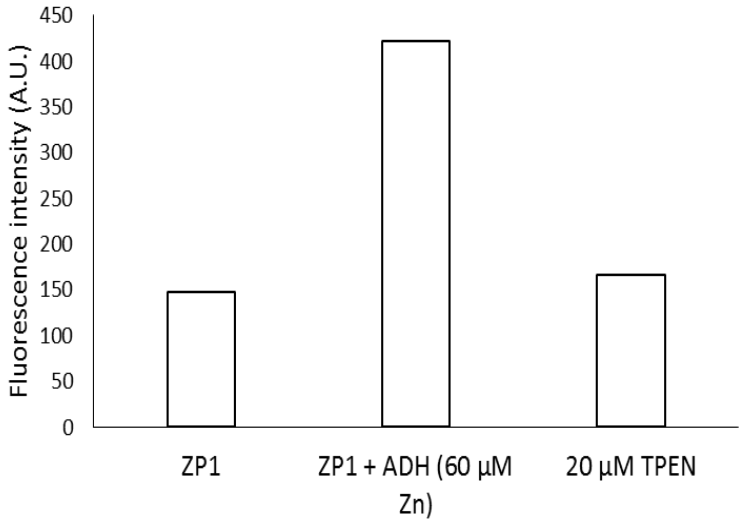
Fluorescence intensity (A.U.)
450
400
350
300
250
200
150
100
50
0
ZP1
ZP1 + ADH (60 µM Zn)
20 µM TPEN

C.

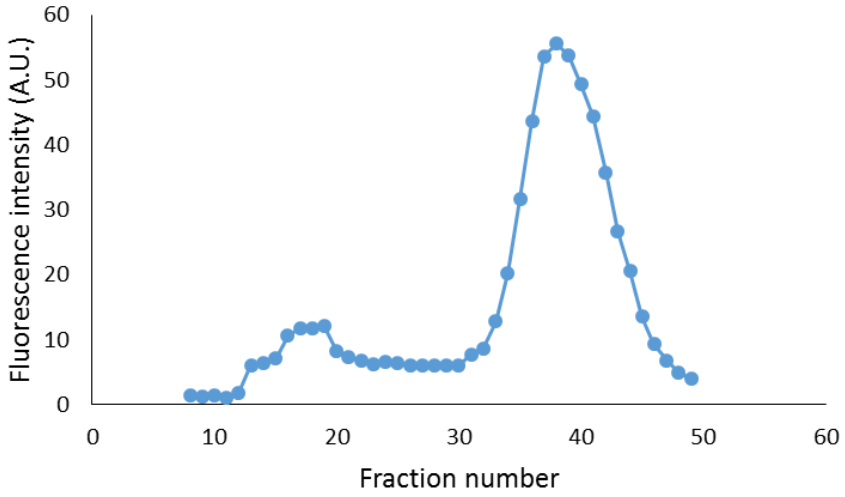

Figure 3.2.12 Reaction of ZP1 with alcohol dehydrogenase. (A) 10 µM ZP1 in 20 mM Tris (pH 7.4) was reacted with increasing concentration of alcohol dehydrogenase. (B) The effect of 20 µM TPEN on the reaction between 10 µM ZP1 and alcohol dehydrogenase containing 60 µM Zn^{2+}. (C) Fractionation of the final reaction mixture of 10 µM ZP1 and alcohol dehydrogenase containing 60 µM Zn^{2+} and the measurement of fluorescence of the fractions.

3.3 Reaction of Zn-proteome with Diethylamine NONOate (DEA-NO) in the presence of Zinquin/TSQ/FluoZin-3

The *in vitro* titration of proteome with Zn^{2+} in the presence of Newport Green (NPG) or Zinpyr-1 (ZP1) – a model of intracellular reaction of the sensor with the mobile Zn^{2+} in the presence of proteomic zinc binding ligands – has displayed two different results with two sensor with dissimilar stability constants. NPG, because of its low stability constant (10^{-5} – 10^{-6} M), could not compete with the proteome and form Zn-NPG (reaction 3.3.1), while the higher affinity sensor ZP1 (0.7 nM) generated Proteome•Zn-ZP1 ternary adduct (reaction 3.3.2). Neither could form Zn-Sensor complex.

$$\text{Proteome} + Zn^{2+} + \text{NPG} \rightleftharpoons \text{Proteome}\bullet\text{Zn} + \text{NPG} \qquad (3.3.1)$$

$$\text{Proteome} + Zn^{2+} + \text{ZP1} \rightleftharpoons \text{Proteome}\bullet\text{Zn-ZP1} \qquad (3.3.2)$$

These findings clearly show that the ability of the zinc senor to image intracellular mobile Zn^{2+} depend on its relative binding affinity compared to that of the proteomic ligands. To rationalize this finding in terms of an actual cellular process that triggers the release of Zn^{2+}, LLC-PK_1 cells were reacted with nitric oxide (NO), which reacts with the proteomic sulfhydryl groups that coordinate Zn^{2+} in specific proteins and thus causes the liberation of Zn^{2+}.[86] The sensor's ability of imaging this mobile released Zn^{2+} was studied using three different fluorescent zinc sensors – Zinquin (ZQ), TSQ and FluoZin-3.

Nitric oxide (NO) acts as a regulatory molecule, which induces the release of Zn^{2+} following its reaction with sulfhydryl groups.[91-94] However, the nitrosation of the sulfhydryl groups by nitric

oxide is not straightforward. The following reactions describe the various ways the thiol groups are nitrosated by reactive nitrogen oxide species.[95]

$$2\ {}^{\cdot}NO + O_2 \rightarrow 2\ {}^{\cdot}NO_2$$

$$2\ {}^{\cdot}NO + 2\ {}^{\cdot}NO_2 \rightarrow 2\ N_2O_3$$

$$N_2O_3 + RSH \rightarrow RSNO + NO_2^- + H^+$$

$$RSH + {}^{\cdot}NO_2 \rightarrow RS^{\cdot} + NO_2^- + H^+$$

$$RS^{\cdot} + {}^{\cdot}NO \rightarrow RSNO$$

The sulfhydryl groups can be oxidized as well following the reaction with nitric oxide.[95]

$$RS^{\cdot} + {}^{\cdot}SR \rightarrow RSSR$$

$$RS^{\cdot} + O_2 \leftrightarrows RSOO^{\cdot}$$

$$RS^{\cdot} + RS^- \leftrightarrows RSSR^{\cdot -}$$

$$RSSR^{\cdot -} + O_2 \rightarrow RSSR + O_2^{\cdot -}$$

Previous studies have reported that the primary target of NO is Zn_7-metallothionein (Zn_7-MT), which binds 7 Zn^{2+} ions in two thiolate clusters.[54, 56, 96-98] For example, Pitt *et al*. hypothesized that nitric oxide exposed to or synthesized within lung endothelial cells reacts with thiolate groups of Zn_7-MT and releases Zn^{2+}.[54] The liberation of Zn^{2+} was supported from the fluorescence enhancement of the sensors ZQ and FluoZin-3. However, other studies have found that NO is not particularly reactive with Zn_7-MT.[15] Therefore, questions arise as to the source of Zn^{2+} imaged by these sensors and the identity of the fluorescent species that causes the enhancement of fluorescence. An alternative possible source of Zn^{2+} released following NO exposure is proteomic Zn^{2+}, which is then sensed by ZQ and FluoZin-3 in the above mentioned

study. However, as ZQ and TSQ image Zn-proteins through the formation of ZQ/TSQ-Zn-Protein ternary adduct, they may also generate Proteome•Zn-ZQ/TSQ with Zn^{2+} adventitiously bound to proteome upon release.

$$\text{Zn-S-Proteome} + \text{NO} \rightleftharpoons \text{NO-S-Proteome} + Zn^{2+}$$

$$\text{Proteome} + Zn^{2+} + \text{ZQ/TSQ} \rightleftharpoons \text{Proteome•Zn-ZQ/TSQ}$$

These present experiments were undertaken to better understand the underlying chemistry of the reaction of proteome with nitric oxide (NO) monitored by the fluorescent zinc sensor Zinquin, TSQ and FluoZin-3.

3.3.1. Reactions of the LLC-PK_1 cells with DEA-NO in the absence or presence of Zinquin (ZQ).

Pig kidney LLC-PK_1 cells were used to investigate the impact of nitric oxide on the availability of intracellular Zn^{2+} to react with fluorescent zinc sensors. DEA-NO, which releases NO with a half time of about 20 min, served as the source of nitric oxide.[86] Initially, $1x10^7$ LLC-PK_1 cells were incubated with 20 μM Zinquin ethyl ester (ZQ_{ee}) for 30 min. During this time the charge neutral probe diffused into the cells and began to undergo ester hydrolysis. A fluorescence emission spectrum centered at 470 nm was observed, indicative of the formation of a ternary adduct species, ZQ-Zn-Proteome (**Figure 3.3.1 A**).[50] Based on previous estimates, the amount of protein-bound zinc participating in adduct formation represents about 10-15% of the total.[50] The introduction of 500 μM DEA-NO to the cells for another 25 min reduced the sulfhydryl concentration from 78 μM to 44 μM and caused a gradual increase of fluorescence at 470 nm, along with a noticeable shoulder at 490 nm (**Figure 3.3.1 A**). Moreover, the fluorescence ratio at 490 nm to 470 nm increased along the course of the reaction (**Figure 3.3.1 B**). Compared with the reaction of cells with ZQ_{ee}, a 25% increment in fluorescence intensity was observed (**Figure 3.3.1 C**) – consistent with the study by Pitt *et al*.[54] Subsequently, 10 μM TPEN, a cell permeable, strong zinc chelator, reversed the fluorescence to 17% of the baseline of cell background fluorescence (**Figure 3.3.1 C**), confirming that both enhancement of fluorescence followed by the treatment of ZQ_{ee} and then DEA-NO involved the participation of Zn^{2+}.

A.

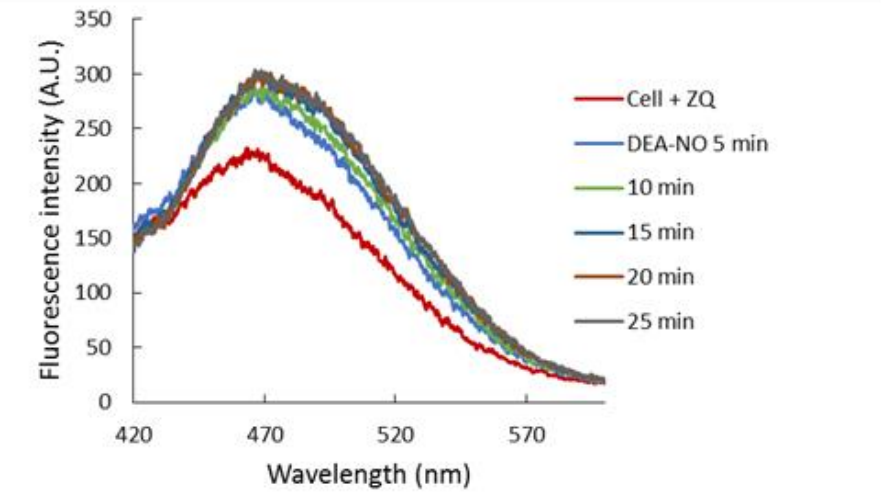
Fluorescence intensity (A.U.)
350
300
250
200
150
100
50
0
420
470
520
570
Wavelength (nm)
Cell + ZQ
DEA-NO 5 min
10 min
15 min
20 min
25 min

B.

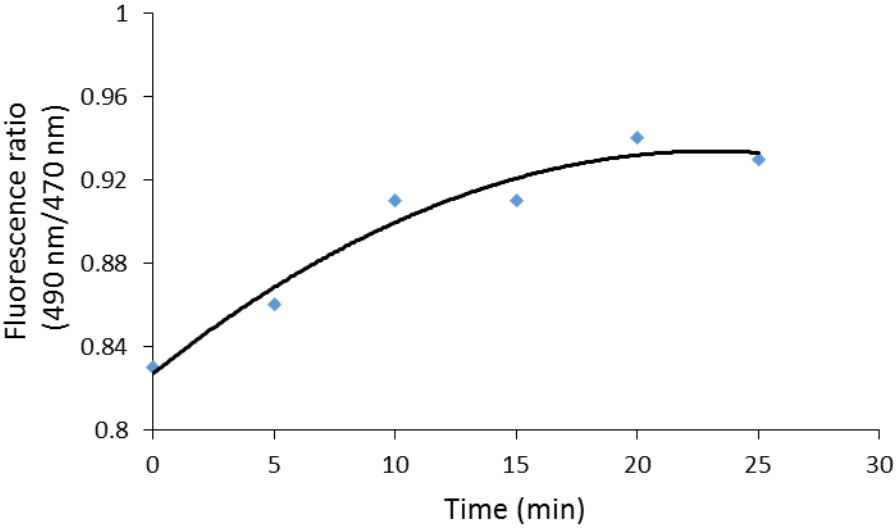
Fluorescence ratio
(490 nm/470 nm)
1
0.96
0.92
0.88
0.84
0.8
0
5
10
15
20
25
30
Time (min)

C.

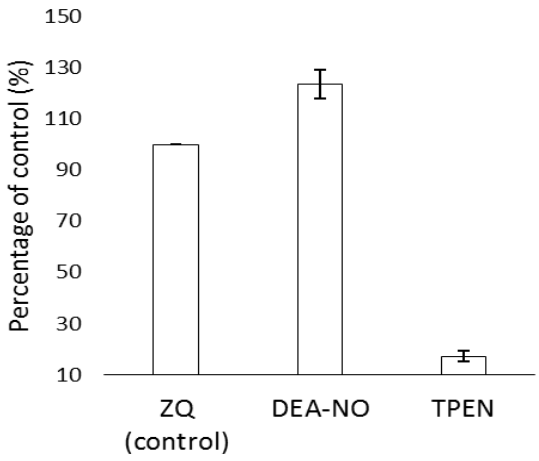

Figure 3.3.1 Reaction of LLC-PK$_1$ cells with DEA-NO in the presence of Zinquin ethyl ester: (A) Fluorescence spectra of the reaction between 10^7 LLC-PK$_1$ cells and 20 µM Zinquin ethyl ester (ZQee) for 30 min followed by the treatment with 500 µM DEA-NO for another 25 min. (B) The change of fluorescence ratio at 490 nm to 470 nm with time. (C) Percent enhancement of fluorescence upon addition of 500 µM DEA-NO and its reversal by 10 µM TPEN.

The appearance of the shoulder at 490 nm suggested the mobilization of Zn^{2+} by NO released spontaneously from DEA-NO and, in turn, the production of the $Zn(ZQ)_2$ complex (Reaction 1), which fluoresces with an emission maximum of 490 nm.[1-3] Another contributor to the fluorescence increase at 470 nm might be Zn^{2+} mobilized from Zn-proteins that non-specifically rebound to other adventitious binding sites. In turn, Zn●Proteome may bind ZQ to generate Zn-ZQ●Proteome species that fluoresce at 470 nm.

$$\text{Zn-S-Protein} + \text{NO} + 2\ \text{ZQ} \rightleftharpoons \text{NO-S-Protein} + \text{Zn(ZQ)}_2 \qquad (1)$$

To investigate further the basis for the above observations, 1.25 x 10^8 LLC-PK_1 cells were incubated with 20 μM ZQee for 30 min at room temperature before the subsequent addition of 500 μM DEA-NO for another 40 min. The cells were then lysed, centrifuged and the resultant supernatant separated by gel filtration using a Sephadex G-75 column. As the fractions were analyzed for both fluorescence and zinc content, high molecular weight (HMW) and low molecular weight (LMW) pools for both fluorescence and zinc were found for both control (reaction of cells and ZQee) and DEA-NO treated (reaction of cells and ZQee followed by DEA-NO) cells (**Figure 3.3.2A & B**). In addition, proteome associated fluorescence increased by 16% in DEA-NO treated cells compared to control. The low molecular weight fluorescence pool of control reaction constituted 19% of the total fluorescence (high molecular weight and low molecular weight), whereas that of DEA-NO treated reaction represented 32% (**Figure 3.3.2C**). The spectra of low molecular weight fractions centered around 490 nm. Consistent with the fluorescence data, the low molecular weight zinc content after DEA-NO treatment was calculated to be 13% of the total zinc, whereas that of control reaction was only 5 % (**Figure 3.3.2C**). The significant increase of both the low molecular weight zinc content and its

accompanying fluorescence emission centered at 490 nm indicated the formation of $Zn(ZQ)_2$ during the reaction of NO with cells. ZQ may have reacted with Zn^{2+} associated with or released from native Zn^{2+} binding sites that had been modified and weakened by nitric oxide. Alternatively, Zn^{2+} at such sites may have shifted to non-specific sites of binding within the proteome and reacted with ZQ to generate $Zn(ZQ)_2$ (reactions 2 and 3):

$$\text{Zn-NOS-Proteins + Proteome} \leftrightharpoons \text{NO-S-Proteins + Zn●Proteome} \quad (2)$$

$$2\ \text{ZQ + Zn●Proteome} \rightleftharpoons \text{Zn(ZQ)}_2 + \text{Proteome} \quad (3)$$

A.

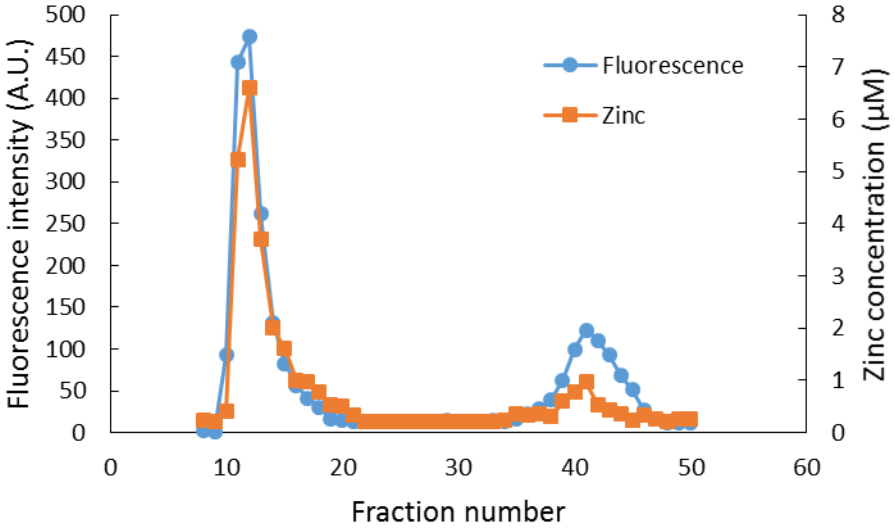
Fluorescence intensity (A.U.)
Zinc concentration (µM)
Fraction number
Fluorescence
Zinc
0
50
100
150
200
250
300
350
400
450
500
1
2
3
4
5
6
7
8
10
20
30
40
50
60

B.

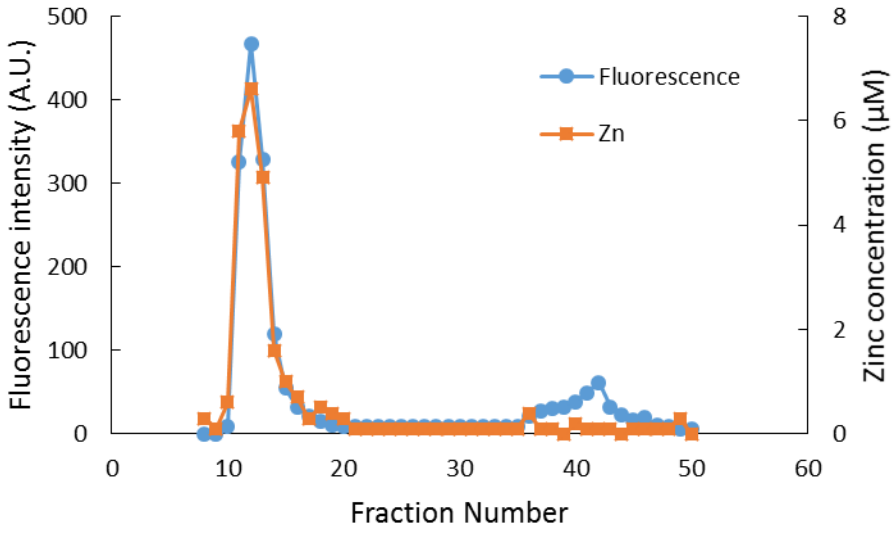
Fluorescence intensity (A.U.)
Zinc concentration (µM)
Fraction Number
Fluorescence
Zn
0
100
200
300
400
500
2
4
6
8
10
20
30
40
50
60

C.

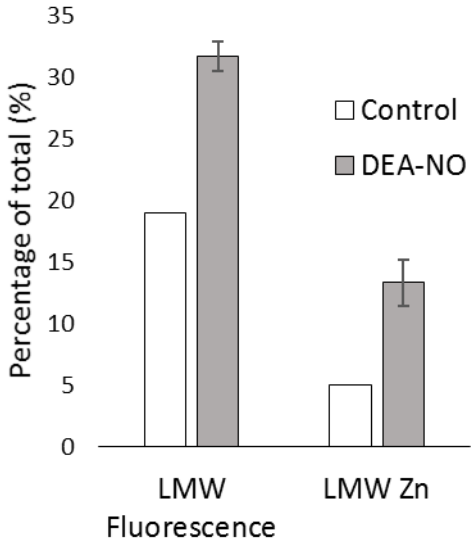

Figure 3.3.2 Sephadex G-75 filtration of LLC-PK$_1$ cells incubated with 20 µM Zinquin ethyl ester (ZQee) followed by 500 µM DEA-NO. (A) 10^8 LLC-PK$_1$ cells were reacted with 500 µM DEA-NO for 40 min following 20 µM ZQee for 30 min. The cells were lysed, centrifuged, and the supernatant was separated using a Sephadex G-75 column. The fractions were analyzed for both fluorescence and zinc. (B) Control: a parallel reaction was run at identical condition with no DEA-NO added. (C) Comparison of the low molecular weight (LMW) fluorescence and zinc content between control and DEA-NO exposed cells.

3.3.2. Reaction of isolated proteome with DEA-NO in the presence of Zinquin acid (ZQacid).

To verify the interpretation of the reaction of NO and ZQ with LLC-PK_1 cells, isolated proteome (10 µM Zn^{2+}) was first reacted with 20 µM ZQacid for 45 min at room temperature. As in whole cells, a gradual increase of fluorescence with the emission maximum of 470 nm was observed, indicative of the formation of ZQ-Zn-Protein ternary adduct. Subsequently, 500 µM DEA-NO was added for an hour. When the final reaction mixture was separated using a Sephadex G-75 column, a noticeable low molecular weight pool of fluorescence and zinc – larger than that of control – was seen (**Figure 3.3.3 A & B**). The LMW fluorescence pool (emission maximum of 490 nm) was measured to be 50% of total fluorescence, which is 40% greater than that of control (30% of total fluorescence) and displayed an emission maximum at 490 nm (**Figure 3.3.3C**). Consistently, the LMW zinc pool was found to three times greater than that of control proteome (15% of total zinc content vs. 5%). The reduction of sulfhydryl content by 41% (from 212 µM to 126 µM) following the treatment with DEA-NO (**Figure 3.3.3D**) supported the reaction between proteomic sulfhydryl groups and nitric oxide. As in whole cells, the low molecular weight fluorescence and zinc pool in the reaction of isolated proteome indicated the production of $Zn(ZQ)_2$. Moreover, proteome fluorescence intensity increased by 19% of the control suggesting the generation of new ternary adduct sites resulted from the labilization of Zn^{2+}.

A.

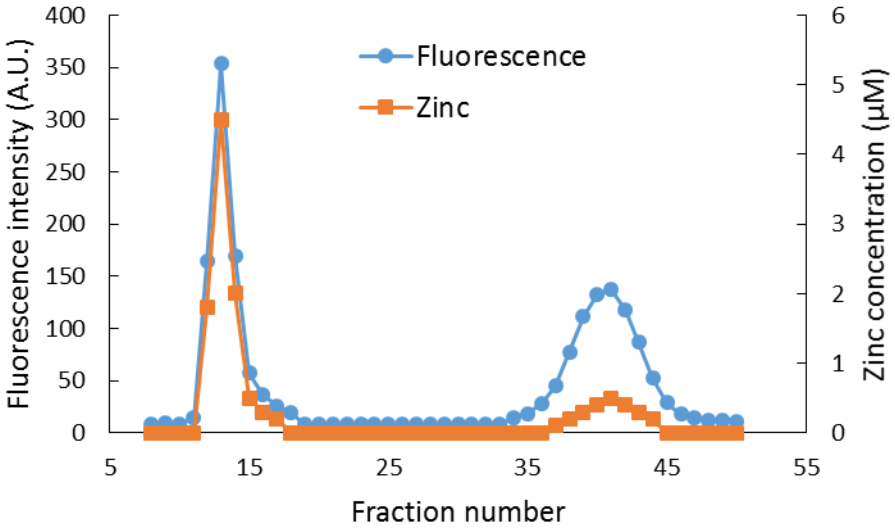
Fluorescence
Zinc
Fluorescence intensity (A.U.)
Zinc concentration (µM)
Fraction number
0
50
100
150
200
250
300
350
400
0
1
2
3
4
5
6
5
15
25
35
45
55

B.

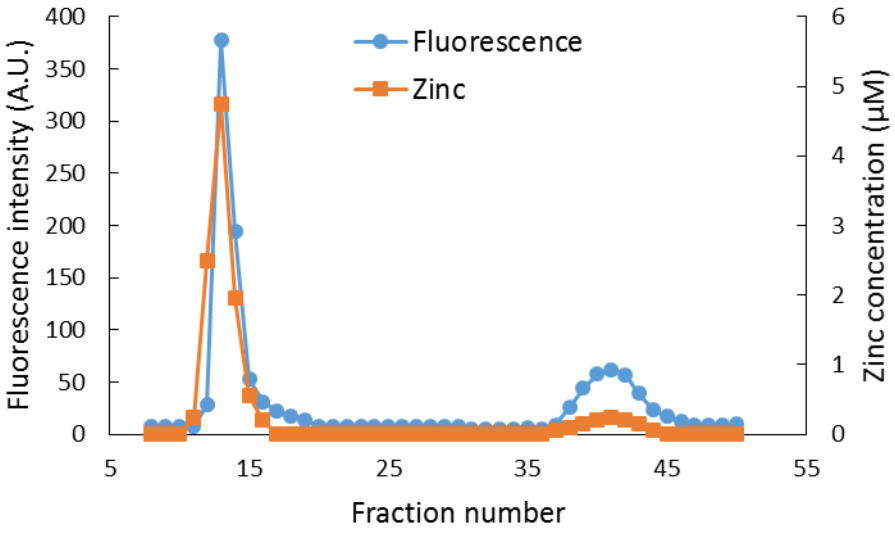
Fluorescence
Zinc
Fluorescence intensity (A.U.)
Zinc concentration (µM)
Fraction number
0
50
100
150
200
250
300
350
400
0
1
2
3
4
5
6
5
15
25
35
45
55

C.

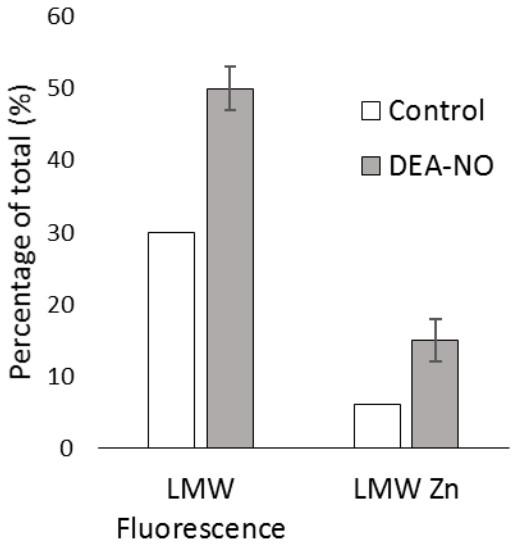

Figure 3.3.3 Sephadex G-75 filtration of isolated proteome incubated with 20 µM Zinquin acid (ZQacid) followed by 500 µM DEA-NO. (A) Isolated proteome (10 µM Zn^{2+}) was reacted with 20 µM ZQacid for 45 min followed by 500 µM DEA-NO for another 1 hour. The final reaction mixture was separated using a Sephadex G-75 column, and the fractions were analyzed for both fluorescence and zinc content. (B) Control: a parallel reaction was run at identical condition with no DEA-NO added. (C) Comparison of the low molecular weight (LMW) fluorescence and zinc content.

3.3.3. Reaction of the whole LLC-PK_1 cells with DEA-NO in the presence of TSQ.

Like Zinquin, TSQ also reacted with LLC-PK_1 cells to form TSQ-Zn-Proteome ternary adducts, as was evident from the fluorescence spectrum centered at around 470 nm. Incubation with 500 µM DEA-NO for 40 min caused a two-fold increase of fluorescence with the emission maximum shifted at 480 nm (**Figure 3.3.4 A**), substantially more than obtained with Zinquin. However, the change of fluorescence ratio at 490 nm to 470 nm was not as prominent as in the case of Zinquin (**Figure 3.3.4 B**). As with ZQ, 10 µM TPEN was able to reduce the fluorescence to 32% of the control value (100%), indicating the participation of Zn^{2+} in the enhancement of fluorescence followed by the addition of both TSQ and DEA-NO as well as the ability of TPEN to reverse much of the control fluorescence enhancement by TSQ (**Figure 3.3.4 C**). Consistent with the fluorescence enhancement, the sulfhydryl concentration reduced from 74 µM to 45 µM.

To characterize the fluorescent species, LLC-PK_1 cells were incubated with 20 µM TSQ for 40 min followed by 500 µM DEA-NO for another 45 min. Cells were then washed, lysed and centrifuged, and the resultant supernatant was fractionated using Sephadex G-75 column. Contrary to the case of Zinquin, no detectable pool of low molecular weight fluorescence and zinc as $Zn(TSQ)_2$ was found in either DEA-NO treated or control cells (**Figure 3.3.5 A & B**). Almost all the fluorescence and zinc was found in the high molecular weight proteome fractions. The integrated fluorescence intensity of the high molecular weight fractions was 50% greater than that of control (Figure 5C) and was aligned with the Zn^{2+} concentrations in the fractions. Moreover, the emission maxima of the proteomic fractions were found to be about 470 nm, indicative of TSQ-Zn-Proteome species. In contrast to the results with ZQ, these findings indicate that Zn^{2+} mobilized by incubation with DEA-NO remains bound completely

within the proteome in the presence of TSQ, forming ternary adducts instead of $Zn(TSQ)_2$. Possibly, such adducts involve Zn^{2+} previously unavailable for reaction with TSQ that is still associated with its original binding sites even after modification by NO (reaction 4). Alternatively, Zn^{2+} at such sites might be redistributed to non-specific binding sites that secondarily react with TSQ. Apparently, due to its lower affinity for Zn^{2+} relative to ZQ, TSQ cannot compete with these newly formed adducts to generate $Zn(TSQ)_2$ species.

$$\text{Zn-S-Proteins} + \text{NO} \rightleftharpoons \text{Zn-NO-S-Proteins} \qquad (4)$$

A.

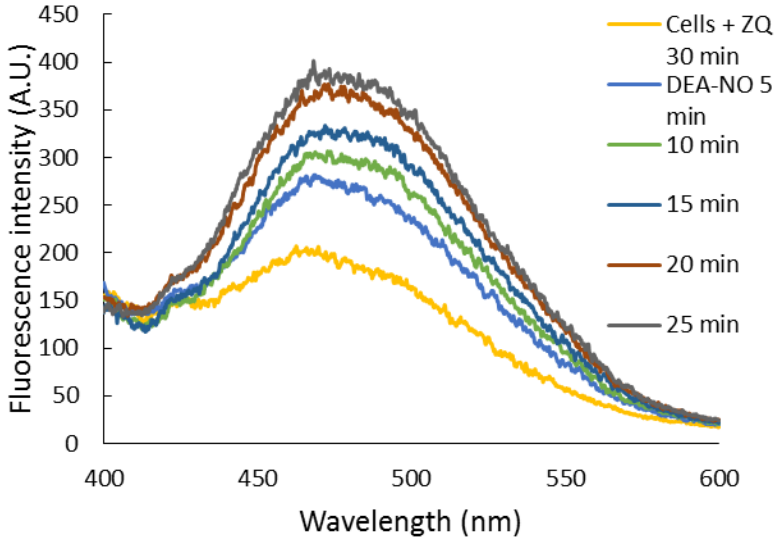
Fluorescence intensity (A.U.)
450
400
350
300
250
200
150
100
50
0
400
450
500
550
600
Wavelength (nm)
Cells + ZQ 30 min
DEA-NO 5 min
10 min
15 min
20 min
25 min

B.

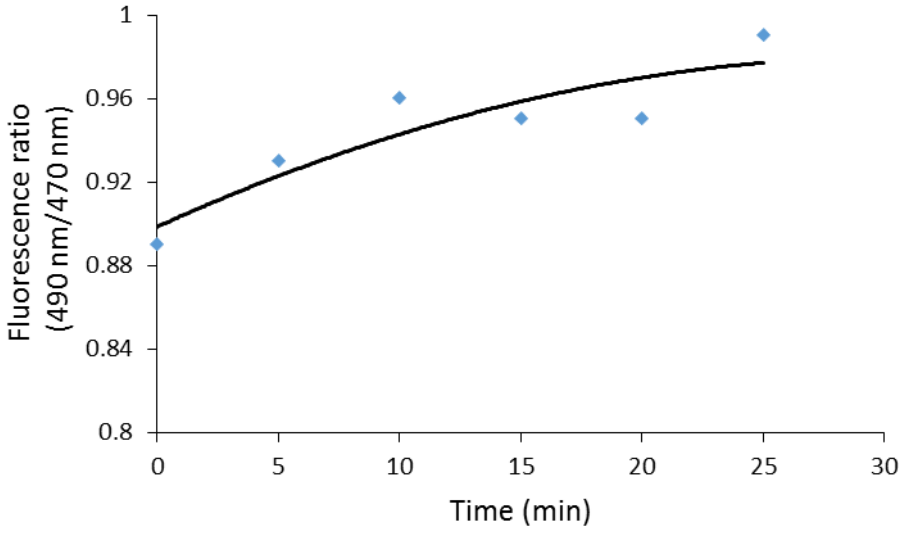
Fluorescence ratio (490 nm/470 nm)
1
0.96
0.92
0.88
0.84
0.8
0
5
10
15
20
25
30
Time (min)

C.

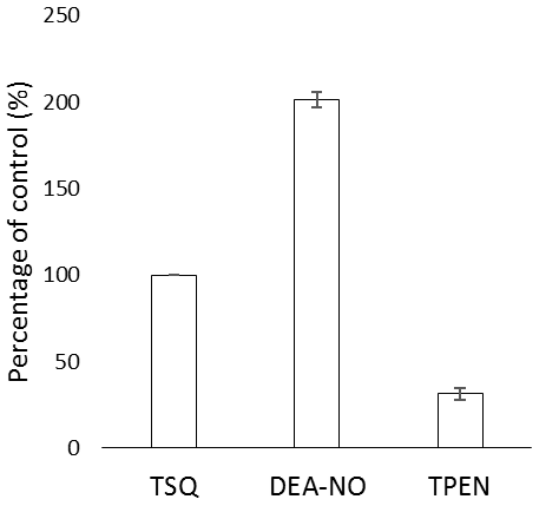

Figure 3.3.4 Reaction of LLC-PK$_1$ cells with DEA-NO in the presence of TSQ. (A) Fluorescence spectra of the reaction between 10^7 LLC-PK$_1$ cells and 20 µM TSQ for 30 min followed by the treatment with 500 µM DEA-NO for another 25 min. (B) The change of fluorescence ratio at 490 nm to 470 nm with time. (C) Percent enhancement of fluorescence upon addition of 500 µM DEA-NO and its reversal by 10 µM TPEN.

A.

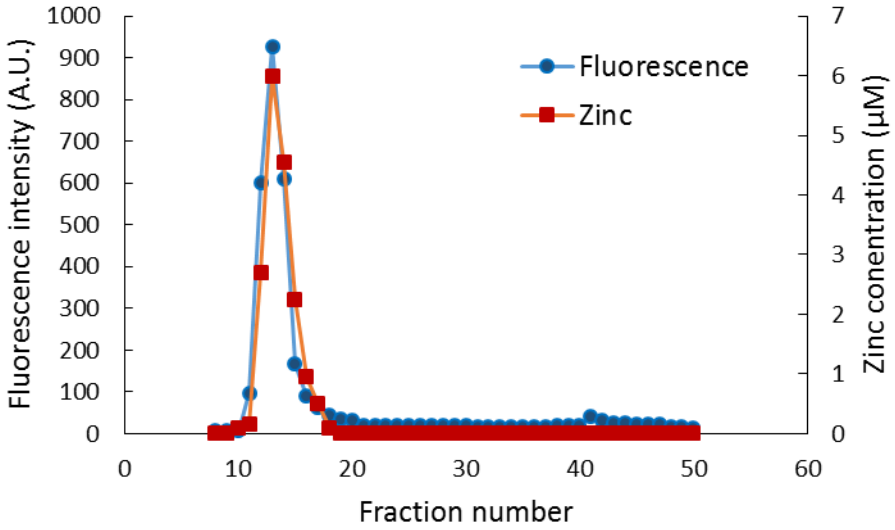
Fluorescence intensity (A.U.)
Zinc conentration (µM)
Fluorescence
Zinc
Fraction number
0
100
200
300
400
500
600
700
800
900
1000
0
1
2
3
4
5
6
7
0
10
20
30
40
50
60

B.

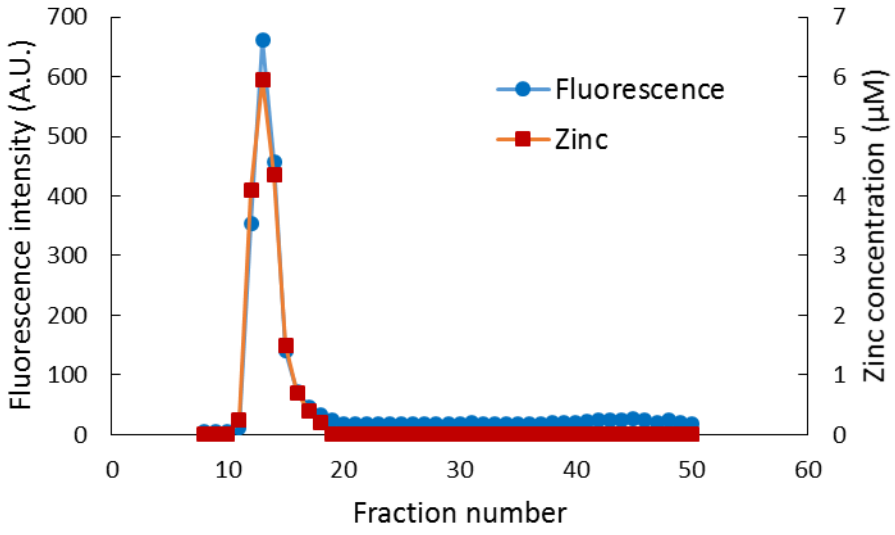
Fluorescence intensity (A.U.)
Zinc concentration (µM)
Fluorescence
Zinc
Fraction number
0
100
200
300
400
500
600
700
0
1
2
3
4
5
6
7
0
10
20
30
40
50
60

C.

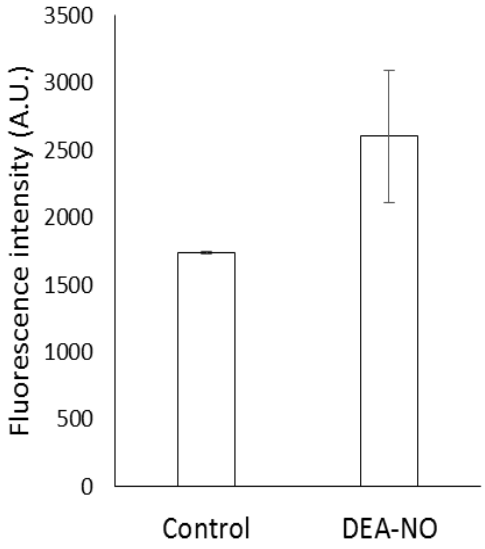

Figure 3.3.5 Sephadex G-75 filtration of LLC-PK$_1$ cells incubated with TSQ followed by 500 µM DEA-NO. (A) 10^8 LLC-PK$_1$ cells were reacted with 500 µM DEA-NO for 45 min following 20 µM TSQ for 40 min. The cells were lysed, centrifuged, and the supernatant was separated using a Sephadex G-75 column. The fractions were analyzed for both fluorescence and zinc. (B) Control: a parallel reaction was run at identical condition with no DEA-NO added. (C) Comparison of the integrated fluorescence intensity of proteome.

3.3.4. Reaction of isolated proteome with DEA-NO in the presence of TSQ.

The reaction of DEA-NO and TSQ with LLC-PK_1 cells was examined in a simpler system. Isolated proteome containing 10 µM Zn^{2+} was reacted with 20 µM TSQ for 40 min before 500 µM DEA-NO was added for another one hour. The reduction of sulfhydryl concentration by 41% (from 340 µM to 200 µM) indicated a significant extent of reaction between nitric oxide and proteomic sulfhydryl groups (**Figure 3.3.6**). Upon fractionation using gel filtration, as was observed in the reaction of whole cells, no measurable low molecular weight fluorescence or zinc was found. That is, no $Zn(TSQ)_2$ was formed in either DEA-NO treated and control reactions.

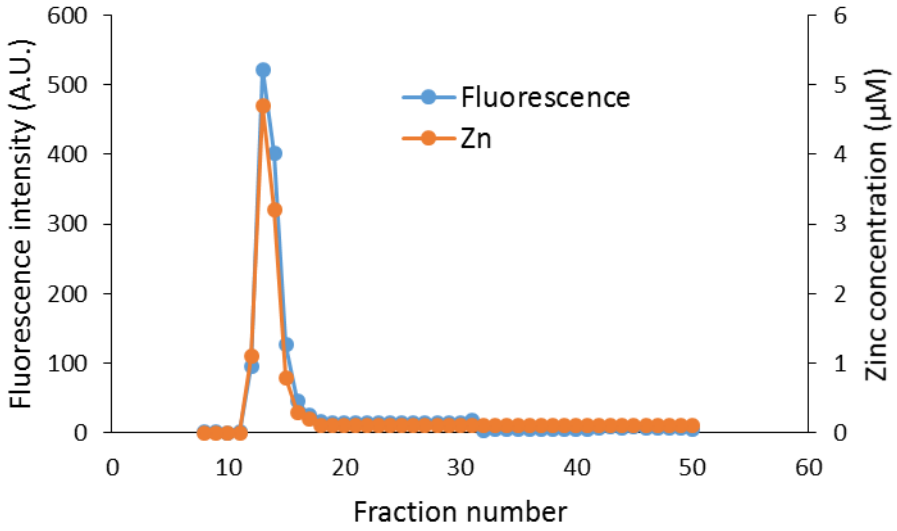

Figure 3.3.6 Reaction of isolated proteome with DEA-NO in the presence of TSQ. Isolated proteome (10 µM Zn^{2+}) was reacted with 20 µM TSQ for 40 min followed by 500 µM DEA-NO for another 1 hour. The final reaction mixture was separated using a Sephadex G-75 column, and the fractions were analyzed for both fluorescence and zinc content.

3.3.5. Reaction of isolated proteome with added Zn^{2+} in the presence of excess TSQ/ZQ.

The capacity of the proteome to bind adventitious Zn^{2+} in the absence or presence of DEA-NO and TSQ or ZQ was also investigated in order to probe the involvement of reactions 3 and 4 in the previously observed reactions of Zn-proteins with DEA-NO and these sensors. Control isolated proteome (8 μM Zn^{2+}) was titrated with Zn^{2+} in the presence of excess ZQ or TSQ. The fluorescence emission intensity centered at about 470 nm, due to the formation of ZQ/TSQ-Zn●Proteome ternary adducts, increased in parallel with the concentration of added Zn^{2+} (**Figures 3.3.7 A & 3.3.8 A**). However, in both cases, the emission maximum remained unchanged at 470 nm as Zn^{2+} was added to the proteome. Moreover, when the final reaction mixtures were fractionated by Sephadex gel filtration, no measurable low molecular weight fluorescence or zinc was detected with either fluorophore (**Figures 3.3.7 B & 3.3.8 B**). Thus, the proteome contained extensive capacity to bind Zn^{2+} and form adducts with Zn^{2+} and either sensor (reactions 5, 6).

$$\text{Zn-Proteome} + {}^{*}Zn^{2+} \leftrightharpoons \text{Zn-Proteome}\bullet{}^{*}\text{Zn} \qquad (5)$$

$$\text{Zn-Proteome}\bullet{}^{*}\text{Zn} + 2\text{TSQ/ZQ} \leftrightharpoons \text{TSQ/ZQ-Zn-Proteome}\bullet\text{Zn-TSQ/ZQ} \qquad (6)$$

Although consistent with the previous observations with TSQ in the absence or presence of DEA-NO, these results differ from the findings about the reaction of cells or proteome with DEA-NO in the presence of Zinquin. In that case, a red shifted emission maximum and a detectable low molecular weight fluorescence and zinc pool indicated that some $Zn(ZQ)_2$ are produced.

The variance in outcome related to the absence or presence of DEA-NO suggested that the behavior of ZQ depends on the existence and extent of modification of sulfhydryl groups that participate in the adventitious proteomic binding of Zn^{2+} ($*Zn^{2+}$) (reactions 7, 8) .

$$\text{Zn-S-Proteome-SH} + *Zn^{2+} \leftrightharpoons \text{Zn-S-Proteome-S-}*Zn^{2+} \qquad (7)$$

$$[RS^- + {}^{\cdot}NO \rightarrow RS^{\cdot} + NO^-$$

$$RS^{\cdot} + {}^{\cdot}NO \rightarrow RSNO]$$

$$\text{Zn-S-Proteome-S-}*Zn^{2+} + 2\ NO \leftrightharpoons \text{NO-S-Proteome-S-NO} + 2\ Zn^{2+} \qquad (8)$$

As the number of adventitious binding sites for Zn^{2+} is reduced through reaction with NO, the formation of $Zn(ZQ)_2$ becomes more favorable. However, with TSQ, its lower affinity for Zn^{2+} prevents competitive generation of $Zn(TSQ)_2$ even in the face of reduced numbers of proteomic binding sites for Zn^{2+}. According to this hypothesis, DEA-NO reduced the number of adventitious binding sites by modifying important sulfhydryl groups. As a result, some, if not all, of the labile Zn^{2+} can be sequestered as $Zn(ZQ)_2$ (reaction 9).

$$\text{NO-S-Proteome-S-NO} + 2\ Zn^{2+} + 4\ ZQ \leftrightharpoons \text{NO-S-Proteome-S-NO} + 2\ Zn(ZQ)_2 \qquad (9)$$

A.

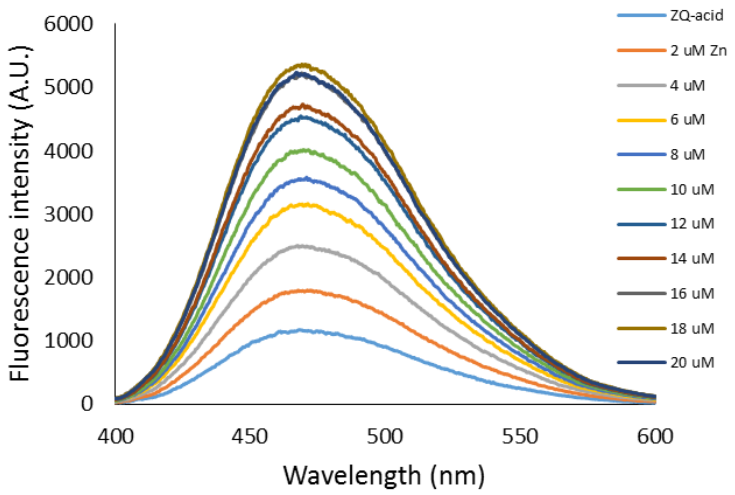
Fluorescence intensity (A.U.)
6000
5000
4000
3000
2000
1000
0
400
450
500
550
600
Wavelength (nm)
ZQ-acid
2 uM Zn
4 uM
6 uM
8 uM
10 uM
12 uM
14 uM
16 uM
18 uM
20 uM

B.

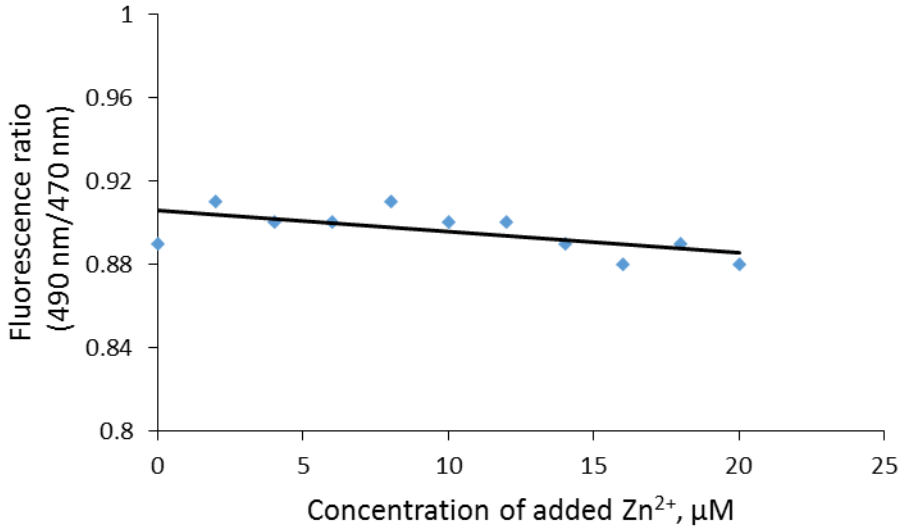
Fluorescence ratio
(490 nm/470 nm)
1
0.96
0.92
0.88
0.84
0.8
0
5
10
15
20
25
Concentration of added Zn2+, µM

C.

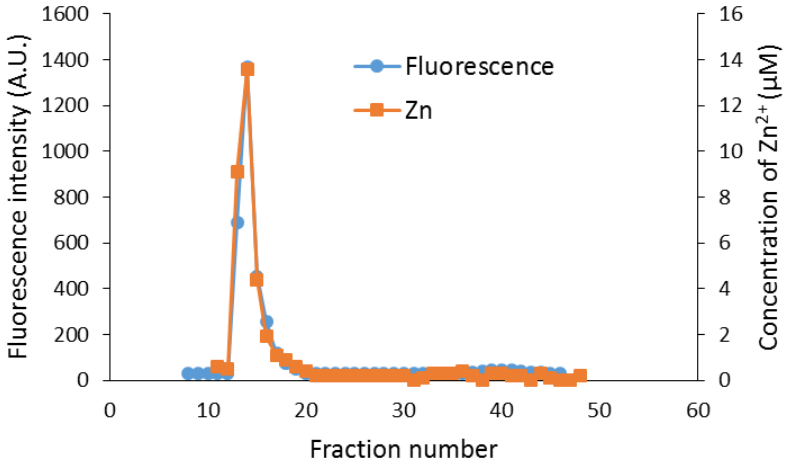

Figure 3.3.7 Titration of isolated proteome with $ZnCl_2$ in the presence of Zinquin acid. (A) Isolated proteome (8 μM Zn^{2+}) was reacted with 20 μM Zinquin acid for 30 min (the bottommost spectrum). Following on, the reaction mixture was titrated with the increasing concentration of $ZnCl_2$. (B) The change of fluorescence ratio at 490 nm to 470 nm. (C) The final reaction mixture from (A) was fractionated using Sephadex gel filtration, and the eluted fractions were analyzed for both fluorescence and zinc content.

A.

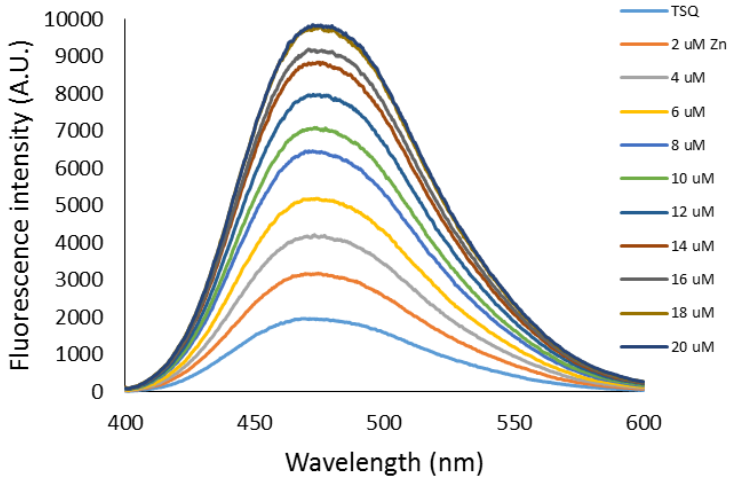
Fluorescence intensity (A.U.)
10000
9000
8000
7000
6000
5000
4000
3000
2000
1000
0
400
450
500
550
600
Wavelength (nm)
TSQ
2 uM Zn
4 uM
6 uM
8 uM
10 uM
12 uM
14 uM
16 uM
18 uM
20 uM

B.

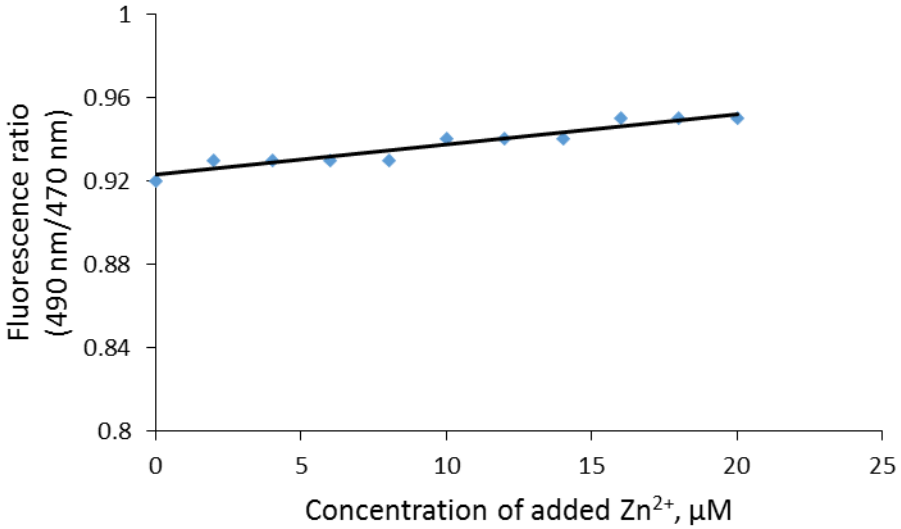
Fluorescence ratio
(490 nm/470 nm)
1
0.96
0.92
0.88
0.84
0.8
0
5
10
15
20
25
Concentration of added Zn2+, µM

C.

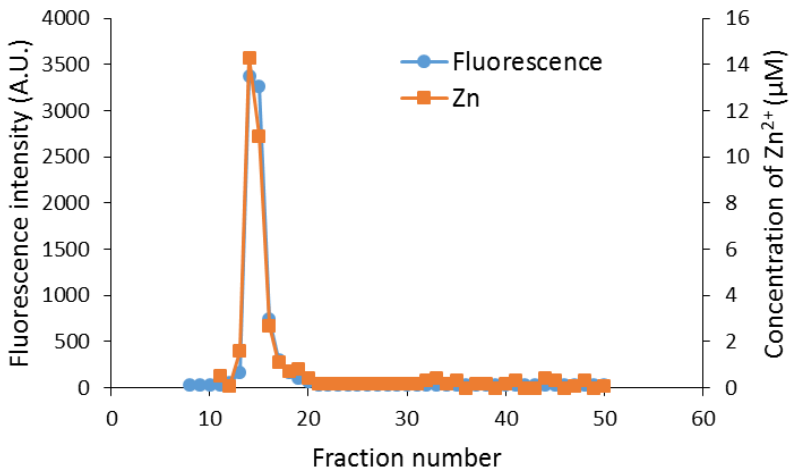

Figure 3.3.8 Titration of isolated proteome with $ZnCl_2$ in the presence TSQ. (A) Isolated proteome (8 μM Zn^{2+}) was reacted with 20 μM TSQ for 30 min (the bottommost spectrum). Following on, the reaction mixture was titrated with the increasing concentration of $ZnCl_2$. (B) The change of fluorescence ratio at 490 nm to 470 nm. (C) The final reaction mixture from (A) was fractionated using Sephadex gel filtration, and the eluted fractions were analyzed for both fluorescence and zinc content.

3.3.6. Reaction of isolated proteome with DEA-NO in the presence of FluoZin-3.

The reaction of isolated proteome (10μM Zn^{2+}) with 500 μM DEA-NO was also monitored using another Zn^{2+} sensor that does not form ternary complexes with Zn-proteins, FluoZin-3 (20 μM). The absence of any fluorescence signal during the reaction of proteome and FluoZin-3 for 20 min indicated that Zn-proteome did not react with FluoZin-3 to form any ternary adduct. However, the introduction of DEA-NO to the reaction mixture for 1 hour caused a gradual increase of fluorescence throughout this period (**Figure 3.3.9**). Interestingly, addition of 10 μM TPEN, a powerful Zn^{2+} chelator, at an intermediate time did not quench any of the enhanced fluorescence. Instead, the fluorescence signal continued increasing. This datum suggested that the increase of fluorescence was not due to the formation of Zn-FluoZin-3 complex, because its fluorescence should have been reversed upon the addition of TPEN. The proteomic sulfhydryl concentration was reduced by 41% (from 342 μM to 202 μM) after the reaction of proteome with DEA-NO. In a separate experiment, upon fractionation of the final reaction mixture of proteome (10 μM Zn^{2+}), 20 μM FluoZin-3 and 500 μM DEA-NO using a Sephadex G-75 column, no Zn-FluoZin-3 complex was found (**Figure 3.3.10**) meaning FluoZin-3 does not chelate proteomic Zn^{2+}.

To investigate the source of this fluorescence enhancement, 20 μM FluoZin-3 was reacted with 500 μM DEA-NO for 1 hour followed by 10 μM TPEN for another 10 min. A gradual increase of fluorescence even larger than in the proteome experiment was observed. Again, 10 μM TPEN could not reverse the intensification of the fluorescence. It was concluded that NO reacts with FluoZin-3 with an increase of fluorescence, independent of its reaction with Zn^{2+}. This finding is of particular importance, because the reaction of NO and FluoZin-3 may confuse the

researchers studying the induction of zinc release by nitric oxide in the presence of FluoZin-3, unless not confirmed by TPEN.

3.3.7. Reaction of isolated proteome with DEA-NO prior to FluoZin-3.

Isolated proteome containing 5 µM Zn^{2+} was incubated with 500 µM DEA-NO for an hour and subsequently, 20 µM FluoZin-3 was added for another 30 min. Fluorescence slowly increased with time and 10 µM TPEN did not reverse the fluorescence (**Figure 3.3.11 A**). This again suggests that the fluorescence enhancement is due not to the reaction of FluoZin-3 with proteomic Zn^{2+}, rather to that of FluoZin-3 and nitric oxide.

When the final reaction mixture of another experiment – reaction of isolated proteome (5 µM Zn^{2+}) pre-incubated with 500 µM DEA-NO for an hour followed by 20 µM FluoZin-3 – was fractionated using Sephadex G-75 column, neither high molecular weight fluorescence nor low molecular weight Zn-FluoZin3 was obtained (**Figure 3.3.11 B**).

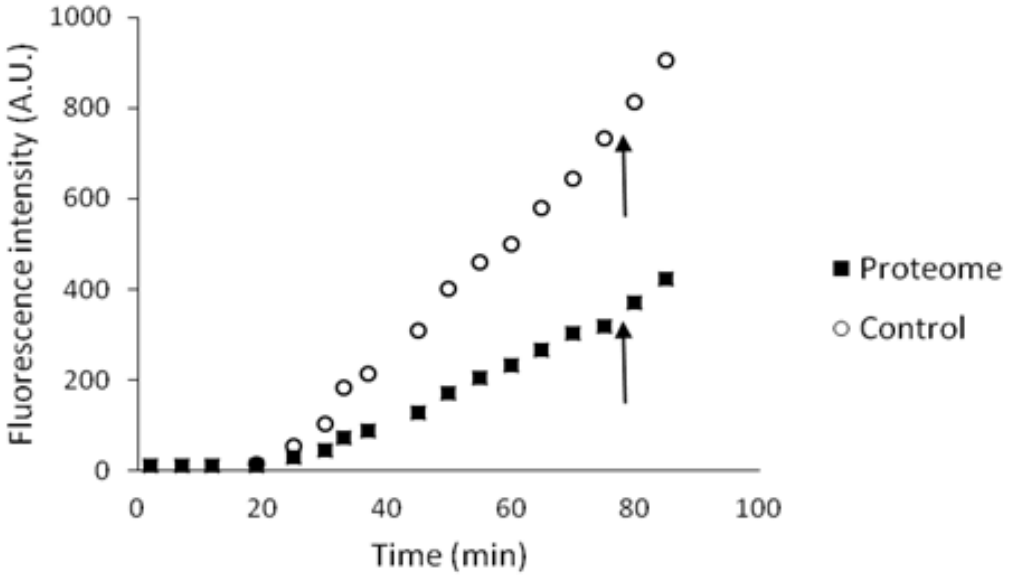

Figure 3.3.9 Reaction of isolated proteome with DEA-NO in the presence of FluoZin-3. Isolated proteome (10 µM Zn^{2+}) was reacted with 20 µM FluoZin-3 for 20 min followed by 500 µM DEA-NO for another hour. Finally 10 µM TPEN was added for 10 min. As control experiment, 20 µM FluoZin-3 in 20 mM Tris (pH 7.4) was reacted with 500 µM DEA-NO for an hour followed by 10 µM TPEN for another 10 min. The arrow indicates the time of TPEN addition.

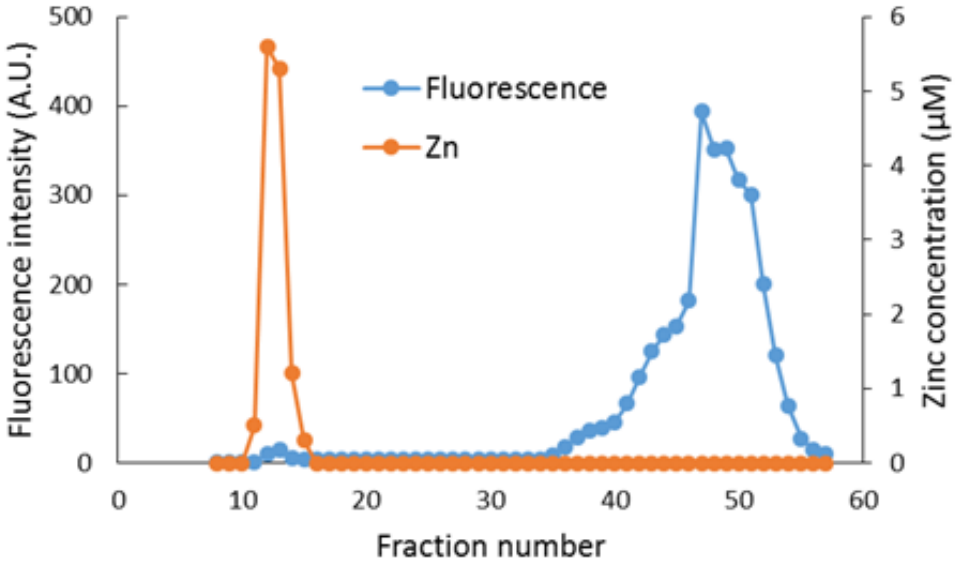

Figure 3.3.10 Sephadex gel filtration of proteome incubated with DEA-NO in the presence of FluoZin-3. Proteome (10 µM Zn^{2+}) was reacted with 20 µM FluoZin-3 for 20 min. Subsequently, 500 µM DEA-NO was introduced into the reaction mixture for an hour. Following on, the final reaction mixture was fractionated using Sephadex G-75 gel filtration chromatography. The fractions eluted with 20 mM degassed Tris buffer at pH 7.4 were analyzed for fluorescence and zinc content.

A.

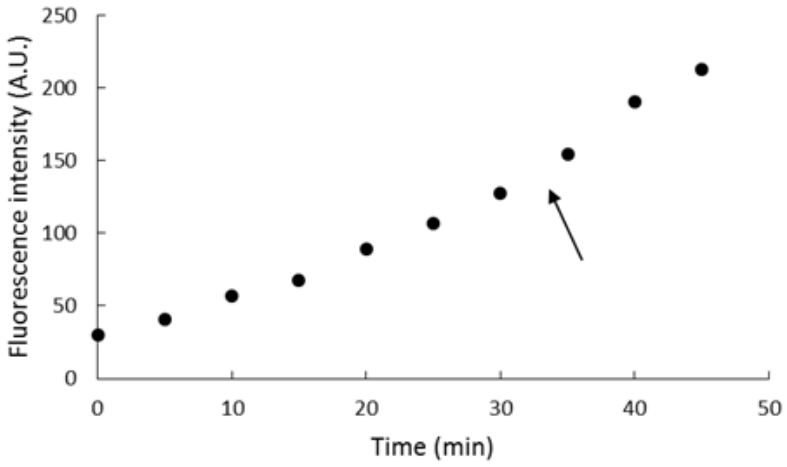

B.

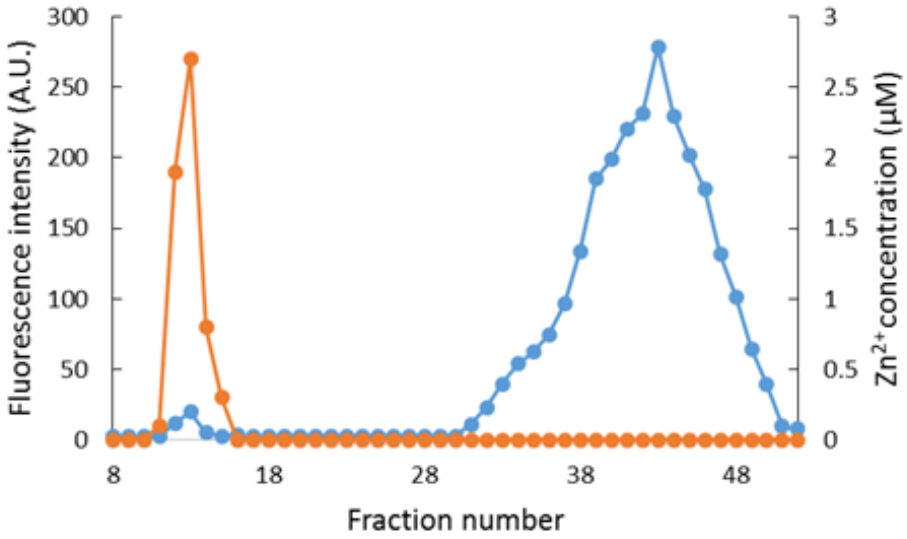

Figure 3.3.11 Reaction of isolated proteome (5 µM Zn^{2+}) with 500 µM DEA-NO followed by 20 µM FluoZin-3. (A) Proteome was incubated with 500 µM DEA-NO for one hour before 20 µM FluoZin-3 was introduced for another 30 min. At this time point, 10 µM TPEN was added for an additional 15 min. (B) Sephadex G-75 fractionation of the final reaction mixture of isolated proteome pre-incubated with 500 µM for an hour followed by 20 µM FluoZin-3.

3.3.8 Stability of Zn-FluoZin3 in the presence of proteome

The ability of FluoZin-3 to sense mobilized Zn^{2+} in the context of proteomic environment was investigated by titrating isolated proteome (12 μM Zn^{2+}) with added Zn^{2+} in the presence of 10 μM FluoZin-3. Unexpectedly, no significant change in fluorescence was observed until about 10-12 μM Zn^{2+} was added (region I), whereas a simple control titration of 10 μM FluoZin-3 in 20 mM Tris buffer (pH 7.4) with Zn^{2+} reached the maximum fluorescence at stoichiometric amount of added Zn^{2+} (**Figure 3.3.12 A**). This indicated that the initial 10-12 μM Zn^{2+} was buffered by various high affinity adventitious binding sites for Zn^{2+} within the proteome (Reaction 18), that outcompeted FluoZin-3, a relatively high affinity Zn^{2+} sensor with K_d of 1.5×10^{-8} M, for the added Zn^{2+}.[1, 2] However, as the added Zn^{2+} concentration was increased, fluorescence started increasing gradually (region II), suggesting the competition between relatively lower affinity proteomic adventitious sites and FluoZin-3 for the added Zn^{2+}. Despite the enhancement at higher added Zn^{2+} concentration, the maximum fluorescence in this experiment never reached that of control titration, which might be due to the possible lower quantum yield of Zn-FluoZin-3 complex in proteomic environment. The result of this experiment is particularly interesting, because it shows that the mobilized Zn^{2+} resulting from the reaction of nitric oxide and proteomic sulfhydryl groups in the presence of FluoZin-3 will be picked up by various high affinity adventitious proteomic binding sites instead of FluoZin-3, unless a very high concentration of Zn^{2+} is mobilized to saturate those adventitious sites before being sensed by FluoZin-3. The dissociation constant (K_{high}) of these high affinity adventitious sites corresponding to region I was calculated to be in the order of 10^{-10} M. The calculation considered 15 μM Zn^{2+} as the end point of the titration of the high affinity binding sites. The

equilibrium constant (K) of the equation 10 was calculated, and then plugged into the equation, $K = K_{Zn\text{-}FluoZin3} / K_{Proteome\bullet Zn}$, to find the dissociation constant of the high affinity sites, $K_{Proteome\bullet Zn}$. The dissociation constant of FluoZin-3, $K_{Zn\text{-}FluoZin3}$, was considered to be 1.5×10^{-8} M.

$$Proteome\bullet Zn + FluoZin3 \leftrightarrows Zn\text{-}FluoZin3 + Proteome \qquad (10)$$

$$K = ([Zn\text{-}FluoZin3]*[Proteome]) / ([Proteome\bullet Zn]*[FluoZin3]) \qquad (11)$$

The dissociation constant (K_{weak}) of the proteome with weaker Zn^{2+} binding affinity corresponding to region II was also calculated. The equilibrium concentrations of proteome and proteome•Zn were represented by the following equations.

$$[Proteome] = [C_{Total\ proteome} - (C_{added\ Zn}{}^{2+} - ((F\text{-}F_{min})/(F_{max} - F_{min}))C_{Total\ FZ\text{-}3})]$$

$$[Proteome\bullet Zn] = [C_{added\ Zn}{}^{2+} - ((F\text{-}F_{min})/(F_{max} - F_{min}))C_{Total\ FZ\text{-}3}],$$

where C represents concentration, F fluorescence and FZ-3 FluoZin-3. F_{max} and F_{min} were taken as 7000 and 336 (corresponding to 15 µM added Zn^{2+}) fluorescence units, respectively. By substituting [Proteome] and [Proteome•Zn] in equation 11, the equilibrium constant (K_{weak}) becomes as follows.

$$K_{weak} = b\,[(C_{Total\ proteome} / (C_{added\ Zn}{}^{2+} - a\,C_{Total\ FZ\text{-}3})) - 1] \qquad (12)$$

where $b = (F\text{-}F_{min}) / (F_{max} - F)$ and $a = F\text{-}F_{min} / F_{max} - F_{min}$. The equation 12 containing two unknowns, K_{weak} and $C_{Total\ proteome}$, was solved for the added Zn^{2+} concentrations of 60, 70, 80 and 90 µM, and the average K_{weak} was found to be on the order of 10^{-7} M.

The finding of the proteome's high zinc buffering capacity indicates that observing Zn^{2+} mobilization using FluoZin-3 depends not only on the release of Zn^{2+} but also masking other adventitious sites that have high affinity for Zn^{2+}.

The ability of proteome to outcompete FluoZin-3 for Zn^{2+} was further studied in another way. 10 µM Zn-FluoZin-3 complex was titrated by isolated proteome (13 µM Zn^{2+}). As expected, initial fluorescence of Zn-FluoZin-3 decreased immediately by about 21% as 365 µg/mL of proteome (final concentration) containing 1.2 µM Zn^{2+} (final concentration) was added (**Figure 3.3.12 B**).

$$\text{(Zn)-Proteome-SH} + Zn^{2+} \leftrightharpoons \text{(Zn)-Proteome.*Zn}$$

$$\text{(Zn)-Proteome-S.*Zn} + \text{FluoZin-3} \leftrightharpoons \text{(Zn)-Proteome-SH} + \text{*Zn-FluoZin-3}$$

A.

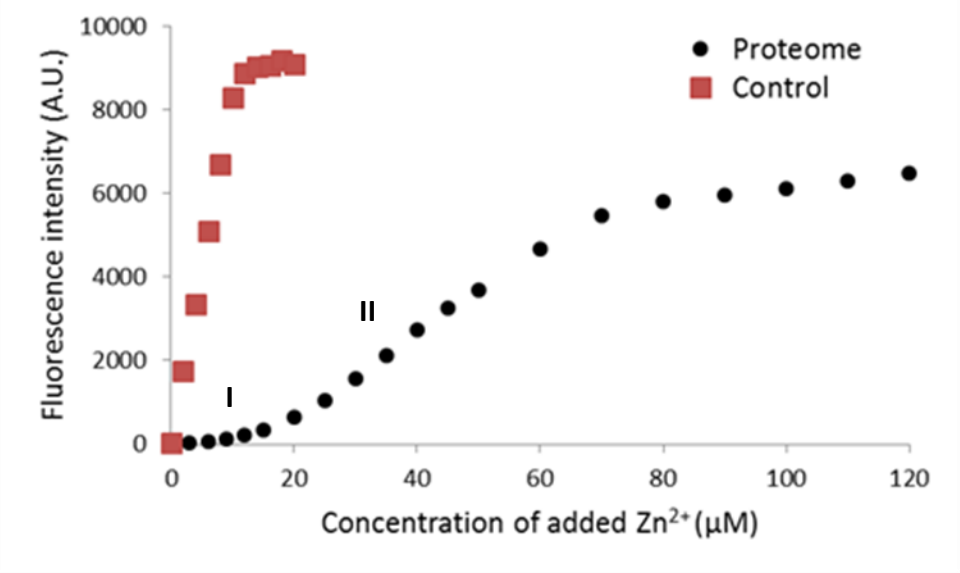

B.

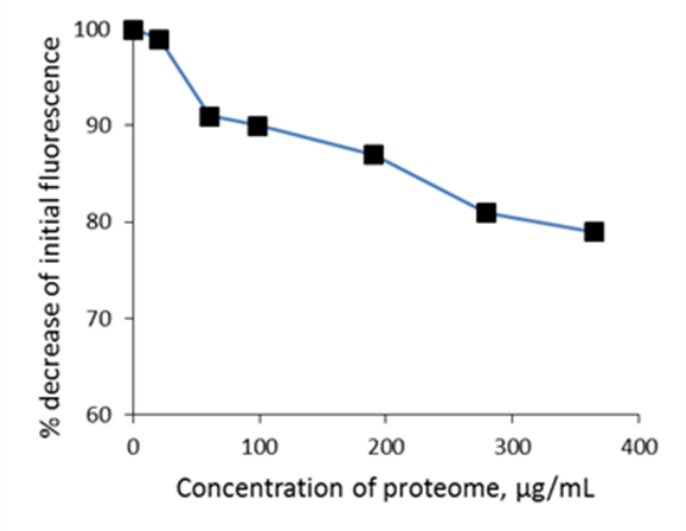

Figure 3.3.12 Stability of Zn-FluoZin3 in the presence of proteome. (A) Isolated proteome (12 µM Zn^{2+}) was incubated with 10 µM FluoZin-3 for 15 min. The reaction mixture was then titrated with increasing concentration of $ZnCl_2$. (B) 10 µM Zn-FluoZin-3 complex in Tris (pH 7.4) was titrated with isolated proteome (13 µM Zn^{2+}).

3.4 Zinc buffering of proteome and proteomic components responsible for it

According to figure 3.3.11 A, in the titration of isolated proteome (12 µM Zn^{2+}) with Zn^{2+} in the presence of 10 µM FluoZin-3, about 10 µM Zn^{2+} had to be added before any detectable Zn-FluoZin3 was formed. This indicated that the initial 10 µM Zn^{2+} bound to the various proteomic zinc binding sites having higher for Zn^{2+} affinity than FluoZin-3. This flat region where no fluorescence was seen was referred to as 'zinc buffering region I'. We wanted to investigate the proteomic sites that possess higher affinity for added Zn^{2+} than FluoZin3. Since many of the zinc binding sites in Zn-proteins utilize sulfhydryl groups as binding ligands, perhaps along with other groups, that coordinate Zn^{2+}, we hypothesized that the added Zn^{2+} binds to proteomic sulfhydryl groups and create the zinc buffering phenomenon. To test this hypothesis, proteome was incubated with different thiol binding agents, such as N-ethylmaleimide (NEM), diethylamine NONOate (DEA-NO) and 5,5-dithio-bis-(2-nitrobenzoic acid) (DTNB), followed by titration of the incubated proteome with Zn^{2+} in the presence of FluoZin-3 and Newport Green.

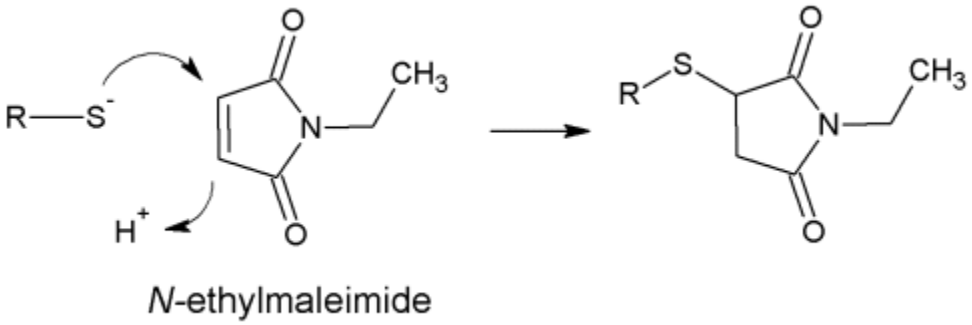

N-ethylmaleimide

Figure 3.4.1 Reaction of N-ethylmaleimide (NEM) with thiolate anion

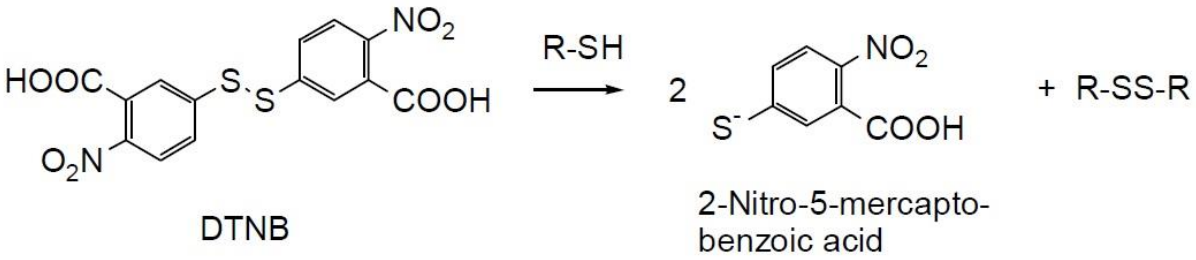

Figure 3.4.2 Reaction of DTNB with sulfhydryl group of a thiol

3.4.1 Titration of proteome incubated with N-ethylmaleimide (NEM) with Zn^{2+} in the presence of FluoZin-3

Proteome containing 10 µM Zn^{2+} was incubated with 500 µM NEM for an hour. Following the incubation, 10 µM FluoZin-3 was added to the reaction mixture for 15 min. The reaction mixture was subsequently titrated with the increasing concentration of $ZnCl_2$. The titration of proteome with $ZnCl_2$ in the presence of 10 µM FluoZin-3 without NEM incubation was used as control experiment. As zinc was added to the NEM treated proteome, fluorescence started increasing immediately, as opposed to in control experiment where about 15 µM Zn^{2+} had to be added before any increase of fluorescence could be seen (**Figure 3.4.3**). Evidently, 500 µM NEM completely neutralized the initial zinc buffering capacity of proteome. The emission maximum of the fluorescence spectra at 520 nm suggested the formation of Zn-FluoZin3 complex. The loss of initial zinc buffering capacity of proteome following 500 µM NEM incubation can be explained as follows: NEM reacted with the proteomic sulfhydryl groups and as such blocked

the binding sites for the added zinc. Therefore, the added zinc was available to be complexed by FluoZin-3 and to form Zn-FluoZin3 with an enhancement of fluorescence. However, during the second phase of the reaction (after 15 μM $ZnCl_2$ was added), the change of fluorescence was found to parallel that of the control suggesting that sulfhydryl groups were not the predominant functional groups that bind Zn^{2+} in this phase.

Control:

Phase 1: Proteome-SH + Zn^{2+} ⇆ Proteome-S-Zn

Phase 2: Proteome.Zn + FluoZin3 ⇆ Proteome + Zn-FluoZin3

NEM:

Phase 1: Proteome-SH + NEM ⇆ Proteome-S-NEM

Zn2+ + FluoZin3 ⇆ Zn-FluoZin3

Phase 2: Proteome.Zn + FluoZin3 ⇆ Proteome + Zn-FluoZin3

A.

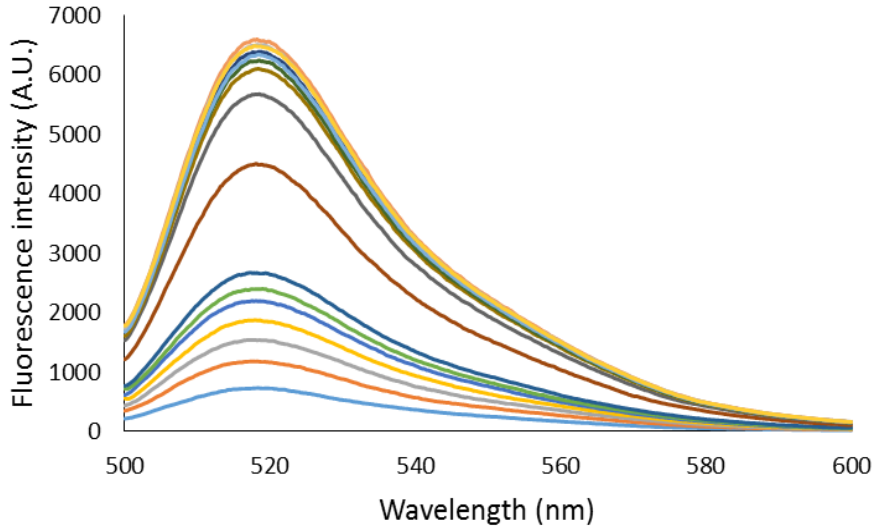
Fluorescence intensity (A.U.)
7000
6000
5000
4000
3000
2000
1000
0
500
520
540
560
580
600
Wavelength (nm)

B.

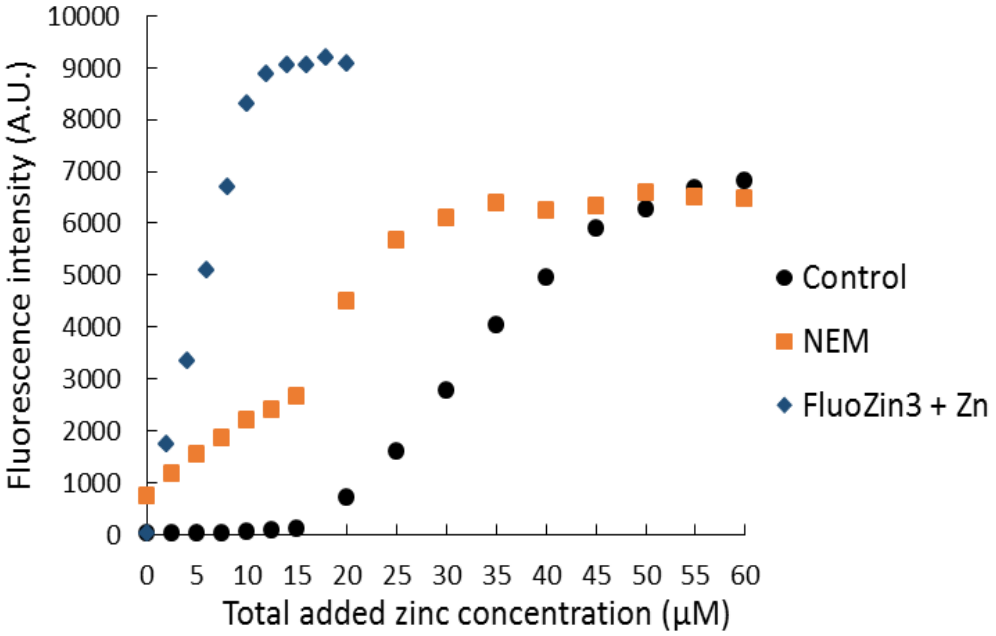
Fluorescence intensity (A.U.)
10000
9000
8000
7000
6000
5000
4000
3000
2000
1000
0
0 5 10 15 20 25 30 35 40 45 50 55 60
Total added zinc concentration (µM)
Control
NEM
FluoZin3 + Zn

C.

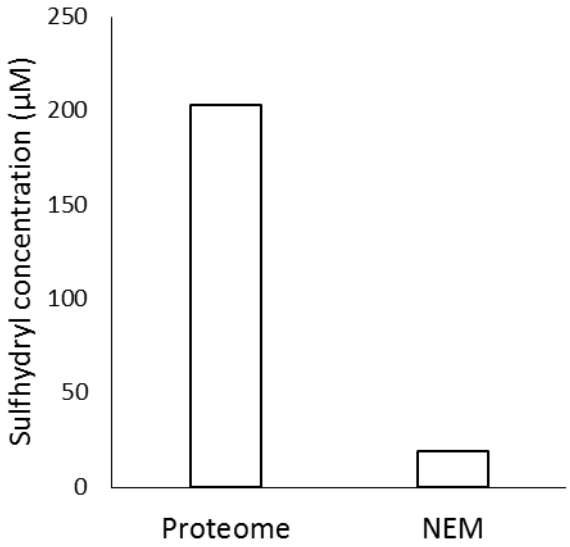

Figure 3.4.3 Titration of proteome incubated with N-methyl maleimide (NEM) with $ZnCl_2$ in the presence of FluoZin-3. (A) Fluorescence spectra of the titration of proteome (10 μM Zn^{2+}) incubated with 500 μM NEM for an hour with $ZnCl_2$ in the presence of 10 μM FluoZin-3. (B) Change of fluorescence at 520 nm with the increasing concentration of $ZnCl_2$. The control experiment involves the titration of proteome without NEM incubation with $ZnCl_2$ in the presence of 10 μM FluoZin-3. (C) The change of sulfhydryl concentration of proteome upon NEM incubation.

3.4.2 Titration of proteome incubated with N-ethylmaleimide (NEM) with $ZnCl_2$ in the presence of Newport Green (NPG)

As we have seen, the modification of proteomic sulfhydryl groups by NEM abolished the strong zinc binding affinity of proteome and thus FluoZin-3 could in part outcompete proteome for the added Zn^{2+}, we repeated the experiment with a weaker zinc sensor Newport Green (NPG). Possessing low affinity for Zn^{2+} ($K_D \sim 10^{-6}$ μM), Newport Green cannot effectively compete with the proteome's higher affinity binding sites for added Zn^{2+}. According to the control experiment in **Figure 3.4.4**, when isolated proteome containing 5 μM Zn^{2+} was titrated with the increasing concentration of $ZnCl_2$ in the presence of 10 μM Newport Green, about 25 μM Zn^{2+} had to be added before NPG was able to bind Zn^{2+} with some enhancement of fluorescence. Newport green could not compete with proteome for the initial 25 μM Zn^{2+}. During the second phase of the reaction, a competition also existed between the proteome's moderate affinity zinc binding sites and Newport Green that resulted a gradual increase of fluorescence. However, when the proteome (5 μM Zn^{2+}) was incubated with 500 μM NEM and then titrated with $ZnCl_2$ in the presence of 10 μM NPG, proteome's zinc buffering capacity was significantly reduced. Fluorescence enhancement due to the formation of Zn-NPG complex was observed after 10 μM $ZnCl_2$ was added, as opposed to about 25 μM in the control experiment. Since a slight red shift in the emission maximum was observed, the possibility of the formation of Proteome•Zn-NPG could not be ruled out. The noticeable loss of proteome's zinc buffering capacity following incubation with NEM further implicated sulfhydryl groups in the proteomic competition with the sensor for Zn^{2+}.

A.

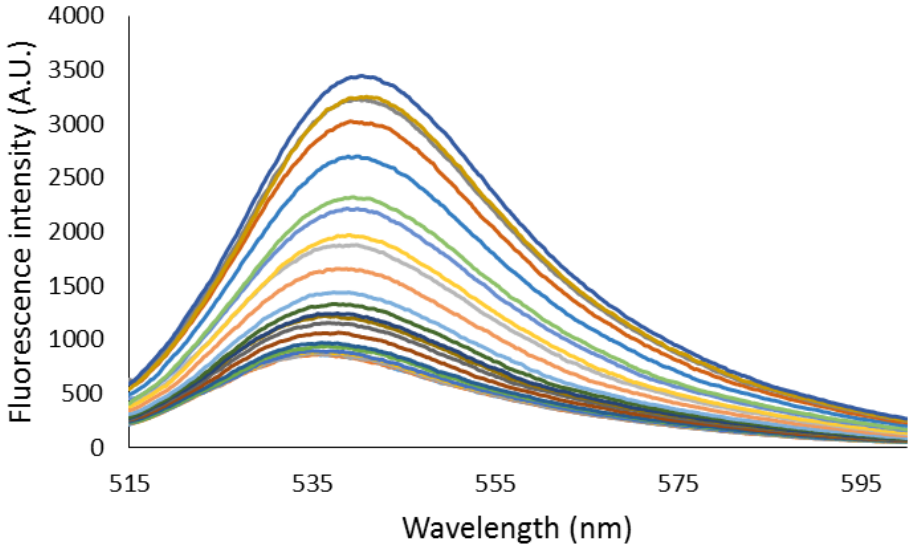
Fluorescence intensity (A.U.)
4000
3500
3000
2500
2000
1500
1000
500
0
515
535
555
575
595
Wavelength (nm)

B.

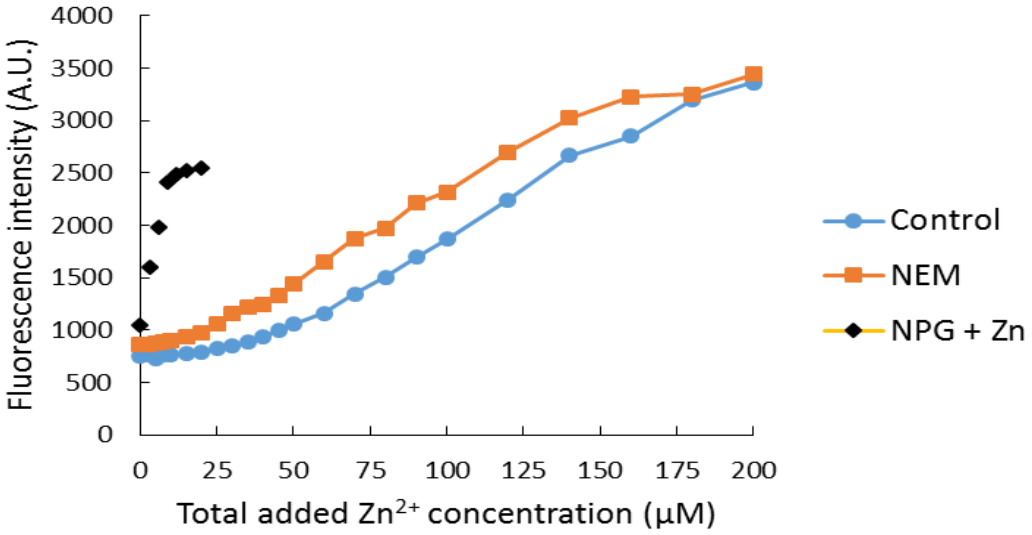
Fluorescence intensity (A.U.)
4000
3500
3000
2500
2000
1500
1000
500
0
0
25
50
75
100
125
150
175
200
Total added Zn2+ concentration (µM)
Control
NEM
NPG + Zn

C.

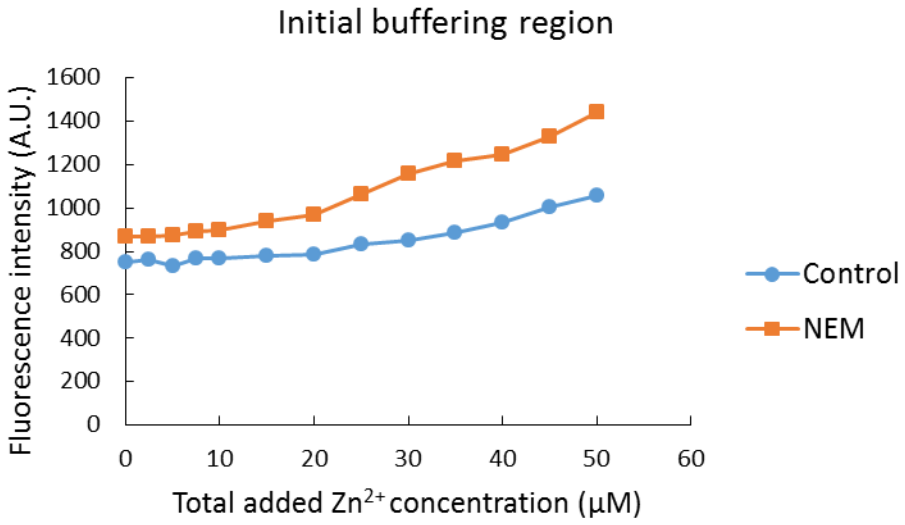

Figure 3.4.4 Titration of proteome incubated with N-methyl maleimide (NEM) with $ZnCl_2$ in the presence of Newport Green (NPG). (A) Fluorescence spectra from the titration of proteome (5 µM Zn^{2+}) incubated with 500 µM NEM with $ZnCl_2$ in the presence of 10 µM Newport Green. (B) [Control]: Isolated proteome (5 µM Zn^{2+}) was incubated with 10 µM NPG for 15 min, and then titrated with the increasing concentration of $ZnCl_2$. [NEM]: Proteome (5 µM Zn^{2+}) was reacted with 10 µM NPG for 15 min followed by 500 µM NEM for another one hour. Subsequently, the final reaction mixture was titrated with $ZnCl_2$. [NPG + Zn]: 10 µM NPG in 20 mM Tris (pH 7.4) was titrated with $ZnCl_2$. (C) The initial buffering region.

3.4.3. Titration of proteome incubated with 5,5-dithio-bis-(2-nitrobenzoic acid) (DTNB) with $ZnCl_2$ in the presence of FluoZin-3.

The involvement of proteomic sulfhydryl groups in zinc buffering capacity of proteome was investigated using another thiol binding reagent 5,5-dithio-bis-(2-nitrobenzoic acid) (DTNB). Consistent with the results from the previous experiments with NEM, the strong zinc binding affinity was obliterated in the DTNB treated proteome. According to figure 3.4.5, fluorescence enhancement due to the formation of Zn-FluoZin3 complex was observed immediately after Zn^{2+} was added. Since DTNB reacted with proteomic sulfhydryl groups and blocked their reaction with the added Zn^{2+}, FluoZin-3 was able to bind Zn^{2+} with an increment of fluorescence. By contrast, in the control experiment sigmoidal curve was seen for the increase of fluorescence with added Zn^{2+} indicating zinc buffering capacity of proteome.

$$\text{Proteome-SH} + \text{DTNB} \leftrightarrows \text{Proteome-S-TNB} + \text{TNB}$$

$$Zn^{2+} + \text{FluoZin-3} \leftrightarrows \text{Zn-FluoZin3}$$

A.

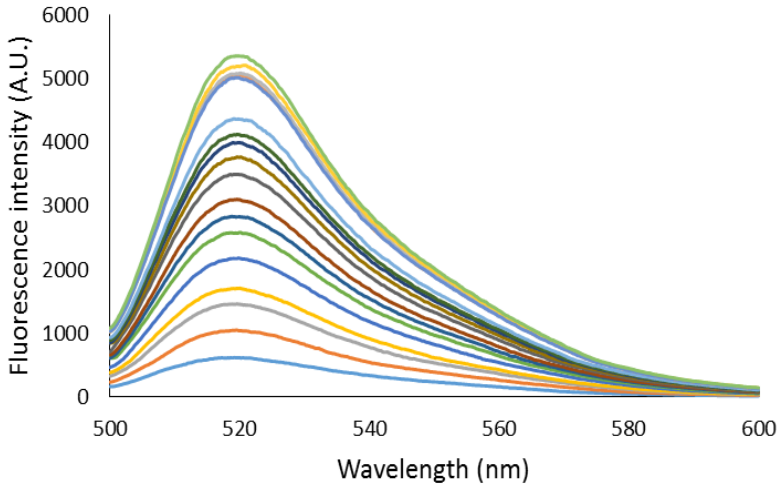

B.

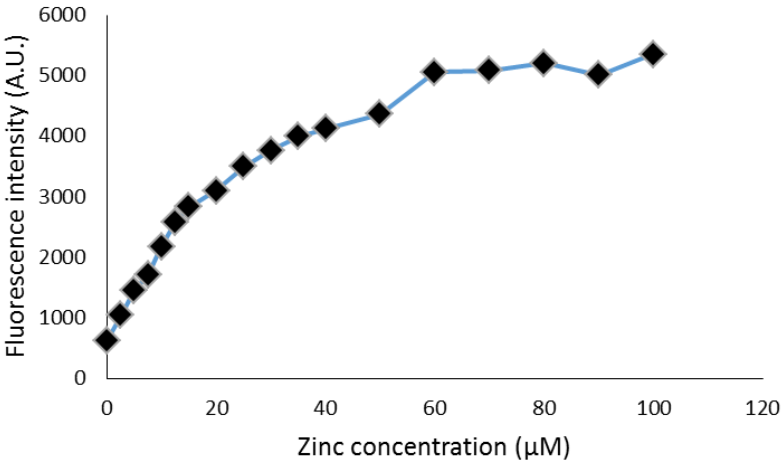

Figure 3.4.5 Titration of proteome incubated with 5,5-dithio-bis-(2-nitrobenzoic acid) (DTNB) with $ZnCl_2$ in the presence of FluoZin-3. (A) Fluorescence spectra of titration of proteome (6 µM Zn^{2+}) incubated with 5,5-dithio-bis-(2-nitrobenzoic acid) (DTNB) and 10 µM FluoZin-3 with the increasing concentration of $ZnCl_2$ (0-100 µM). (B) Change of fluorescence intensity with the concentration of $ZnCl_2$.

3.5 Status of Zn-proteome at different phases in a cell cycle

Meeusen *et al.* reported that when LLC-PK_1 cells were incubated with 30 µM TSQ for 30 min at 37 ^{0}C, the fluorescence in cells due to the formation of TSQ-Zn-Proteome ternary adduct was asymmetric, i.e., some cells showed brighter fluorescence than others (**Figure 3.5.1 A**).[65] Moreover, when 30 µM Zn^{2+} and 3 µM pyrithione was added to the TSQ incubated cells, fluorescence enhancement was asymmetric as well (**Figure 3.5.1 B**). We hypothesized that this asymmetric distribution of fluorescence was attributed to the cells being at different phases of the cell cycle, where the cells synthesize varied quantities of zinc proteins and thus, different concentrations of TSQ-Zn-proteome would be generated when incubated with TSQ. To test this hypothesis, CCRF-CEM cells were incubated with different chemical blockers (Thymidine and Nocodazole) to block the cells at different phases of the cell cycle and then reacted with fluorescent sensors, such as TSQ and Zinquin. Thymidine blocks the cells at G1 phase, while Nocodazole at G2/M phase.[99-104] The synchronization of the cells was confirmed by flow cytometry, which measures optical and fluorescence properties of single cells.[105-107] Cell populations are sort out by the physical properties of the cells, such as size (represented by forward angle light scattering) and intracellular complexity (represented by side scattering). Cells are treated with fluorescent dyes which may bind or intercalate with cellular constituents such as DNA or RNA. Stained cells suspended in buffer are drawn into a stream generated by a surrounding sheath of isotonic fluid, which permit the cells to pass one at a time through an interrogation point. At this point, the cells are intersected with a beam of monochromatic light from a laser source. Based on the intensities of the emitted light, the cell populations are resolved. We chose CCRF-CEM cells for this study because this is a suspension cell line, which

was found to be easier for cell sorting by flow cytometry than an adherent cell line, such as LLC-PK_1 used by Meeusen for his experiments.

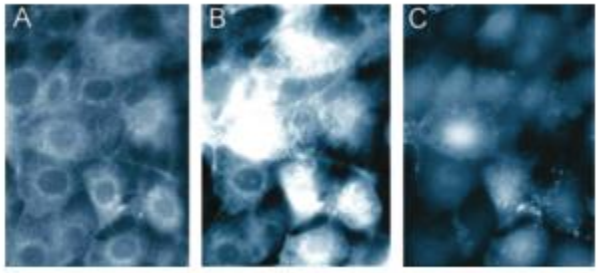

Figure 3.5.1 Fluorescence micrograph images of cellular Zn^{2+} observed after exposure to the Zn^{2+} fluorophore TSQ. (A) LLC-PK_1 cells incubated with 30 µM TSQ in DPBS for 30 min at 37 0C. (B) Fluorescence increase of A after addition of 30 µM Zn^{2+} and 3 µM pyrithione for 1 min. (C) Fluorescence reduction of B following addition of 100 µM TPEN for 10 min.

3.5.1 Cell viability assay

Cell viability of CCRF-CEM cells treated with 2 mM thymidine or 100 ng/mL nocodazole for 24 hours and control (untreated) cells was determined with Trypan Blue exclusion assay. Thymidine treated cells were found to be 90% viable, whereas nocodazole incubated cells showed about 80% viability. Control cells were almost 100% viable.

3.5.2 Reaction of TSQ and CCRF-CEM cells blocked at G1 phase by thymidine

In order to block the cells at G1 phase, CCRF-CEM cells were treated with 2 mM thymidine for 24 hours, and the synchronization of the cells at G1 phase was confirmed using Flow Cytometry. 13.05 x 10^6 thymidine-blocked cells were washed and resuspended in DPBS and then reacted with 20 µM TSQ, which resulted in gradual increase of fluorescence centered at 470 nm indicating the formation of TSQ-Zn-Proteome (**Figure 3.5.2 B**). As a control experiment, 10.5 x 10^6 untreated cells distributed throughout the cell cycle were reacted with 20 µM TSQ, which also showed fluorescence intensity with an emission maximum of 470 nm (**Figure 3.5.2 A**). However, when the fluorescence intensity was normalized, the intensity per million cells for thymidine-blocked cells (187 units) were found to be 42% greater than that (132 units) of control cells. This greater fluorescence intensity for CCRF-CEM cells blocked at G1 phase suggests that cells at G1 phase synthesize greater concentration of zinc proteins than at other phases of a cell cycle and that the greater availability of zinc proteins allows TSQ to generate more TSQ-Zn-Proteome ternary adduct. After the reaction, both control and thymidine-blocked cells were sonicated, centrifuged and the cell lysates were analyzed for fluorescence. Consistent with the fluorescence intensities of the whole cells, the cell lysates also showed unequal normalized fluorescence (**Figure 3.5.3**). The cell lysate from the thymidine-blocked cells (170 fluorescence units per million cells) displayed 70% greater fluorescence intensities than that from the control cells (100 fluorescence units per million cells). Consequently, both the whole cells and the cell lysates support the hypothesis that cells at G1 phase synthesize a greater concentration of zinc proteins than at other stages of the cell cycle.

A.

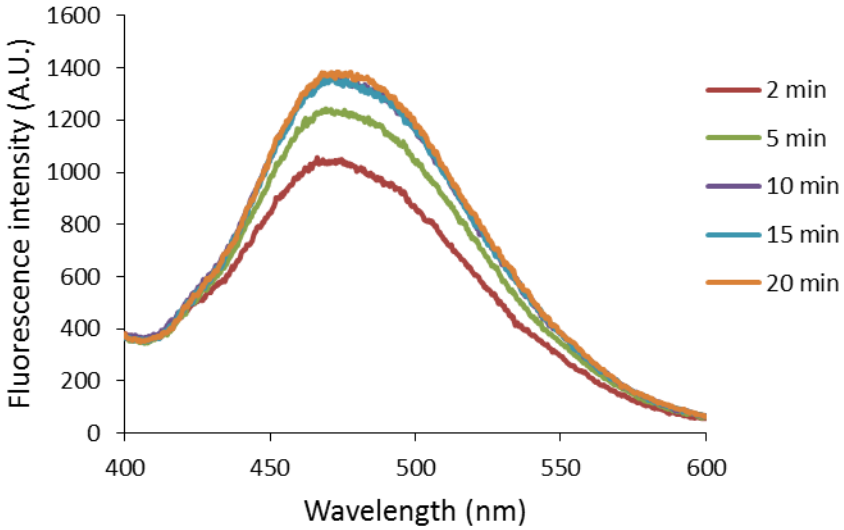
1600
1400
1200
1000
800
600
400
200
0
Fluorescence intensity (A.U.)
400
450
500
550
600
Wavelength (nm)
2 min
5 min
10 min
15 min
20 min

B.

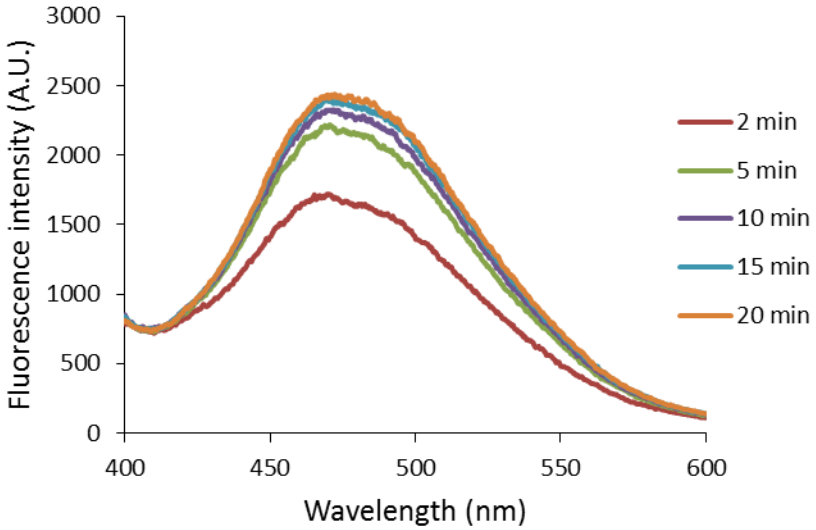
3000
2500
2000
1500
1000
500
0
Fluorescence intensity (A.U.)
400
450
500
550
600
Wavelength (nm)
2 min
5 min
10 min
15 min
20 min

C.

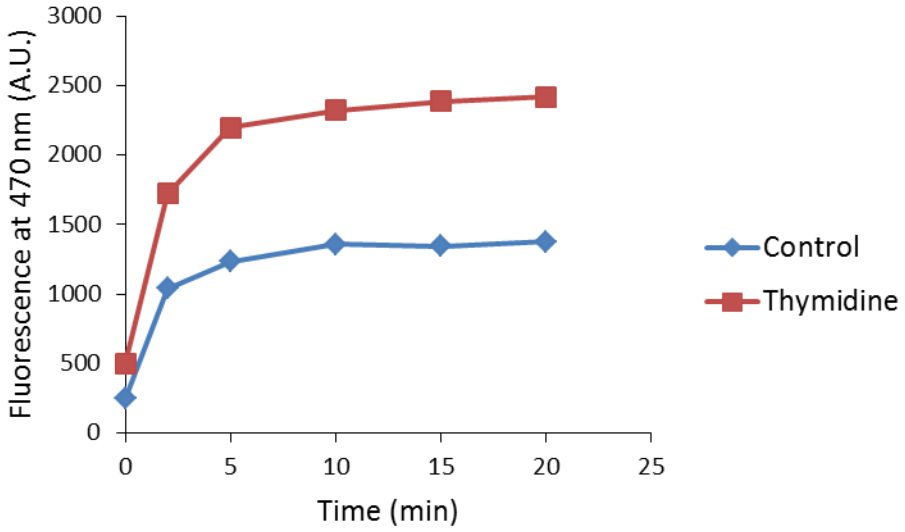

Figure 3.5.2 Reaction of TSQ and CCRF-CEM cells blocked at G1 phase by thymidine. (A) Control: 10.5 x 10^6 CCRF-CEM cells were harvested, resuspended in DPBS and then reacted with 20 µM TSQ for 20 min. The fluorescence spectra was recorded every 5 min. (B) 13.05 x 10^6 CCRF-CEM cells incubated with 2 mM thymidine for 24 hours were harvested, resuspended in DPBS and then reacted with 20 µM TSQ for 20 min. (C) Comparison of kinetics of both reaction.

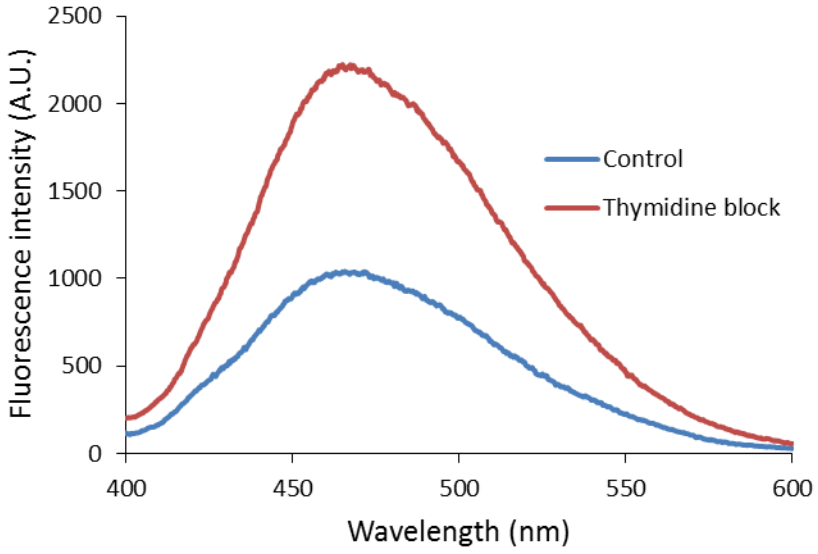

Figure 3.5.3 Fluorescence spectrum of the cell lysate collected from CCRF-CEM cells (TSQ). Cells were incubated with 2 mM thymidine for 24 hours and then reacted with 20 µM TSQ for 20 min. Cell lysates of both control and thymidine blocked cells were collected by the sonication of the cells followed by centrifugation.

3.5.3 Reaction of Zinquin (ZQ) and CCRF-CEM cells blocked at G1 phase by thymidine

CCRF-CEM cells synchronized at G1 phase by thymidine were also reacted with Zinquin (ZQ). 18.55 x 10^6 cells blocked at G1 phase by 2 mM thymidine for 24 hours were washed and resuspended in DPBS, and subsequently reacted with 20 µM Zinquin (**Figure 3.5.4 B**). Like TSQ, Zinquin also formed ZQ-Zn-Proteome ternary adduct, as evident from the gradual enhancement of fluorescence intensity with a λ_{max} of 470 nm. The reaction of 16.75 x 10^6 untreated cells with 20 µM Zinquin was also performed as a control experiment. The control cells, like thymidine-blocked cells, also showed fluorescence intensity centered at 470 nm (**Figure 3.5.4 A**). However, as the fluorescence intensities for both control and synchronized cells were normalized, the intensity from blocked cells (75 fluorescence units per million cells) was 47% greater than that from untreated cells (51 units per million cells). The cells lysates from both control and synchronized cells were collected following the reaction. As the fluorescence of the lysates was read, they also showed unequal normalized fluorescence intensities. The cell lysate from thymidine-blocked cells gave 139 fluorescence units per million cells, as opposed to 103 units for the cell lysate from control cells – 35% greater fluorescence intensity for the synchronized cells (**Figure 3.5.5**). The reaction of CCRF-CEM cells blocked at G1 phase with Zinquin once again supports the hypothesis that cells produce more zinc proteins during G1 phase of its life cycle than at other phases.

A.

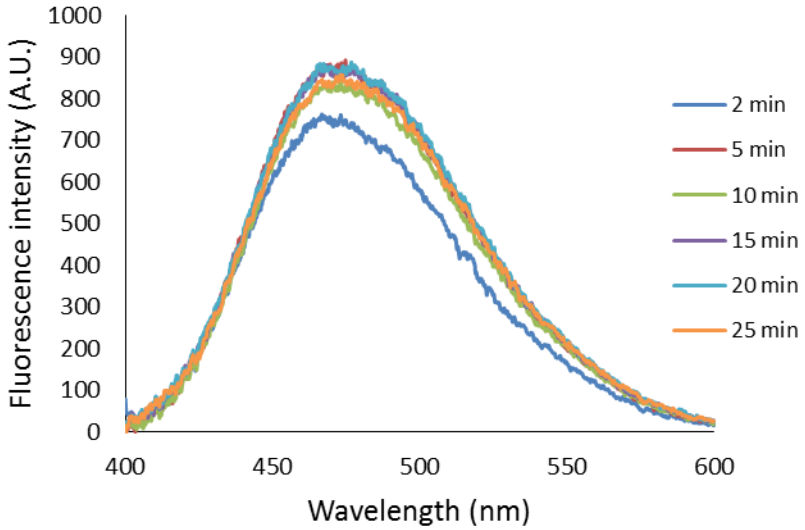
Fluorescence intensity (A.U.)
1000
900
800
700
600
500
400
300
200
100
0
400
450
500
550
600
Wavelength (nm)
2 min
5 min
10 min
15 min
20 min
25 min

B.

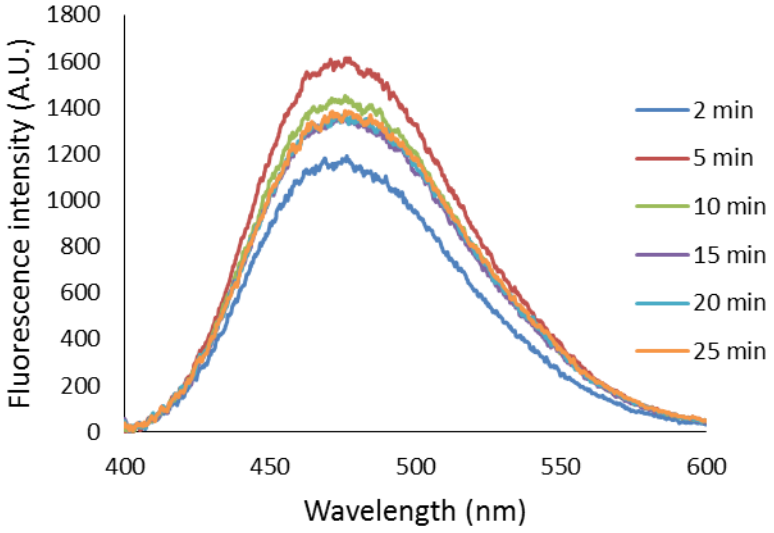
Fluorescence intensity (A.U.)
1800
1600
1400
1200
1000
800
600
400
200
0
400
450
500
550
600
Wavelength (nm)
2 min
5 min
10 min
15 min
20 min
25 min

C.

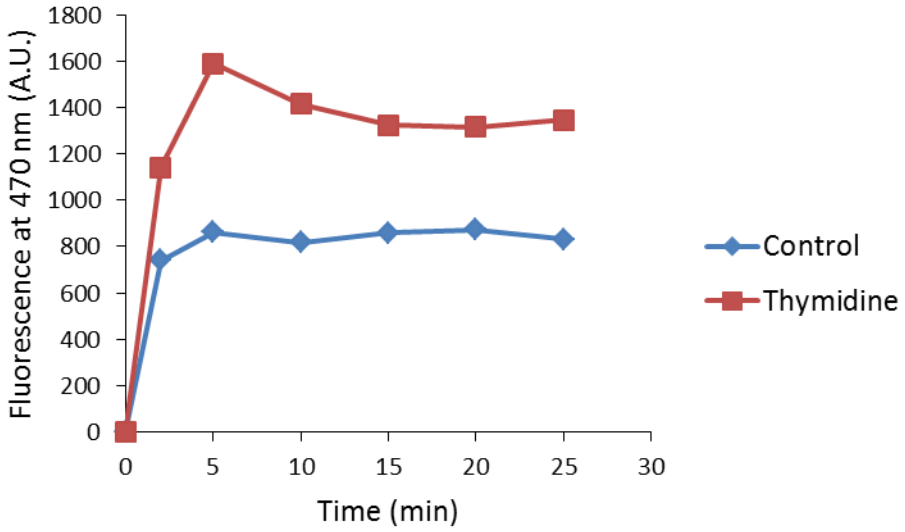

Figure 3.5.4 Reaction of Zinquin (ZQ) and CCRF-CEM cells blocked at G1 phase by thymidine. (A) Control: 16.75 x 10^6 CCRF-CEM cells were harvested, resuspended in DPBS and then reacted with 20 µM ZQ for 25 min. (B) 18.55 x 10^6 CCRF-CEM cells incubated with 2 mM thymidine for 24 hours were harvested, resuspended in DPBS and then reacted with 20 µM ZQ for 25 min. (C) Comparison of kinetics of both reactions.

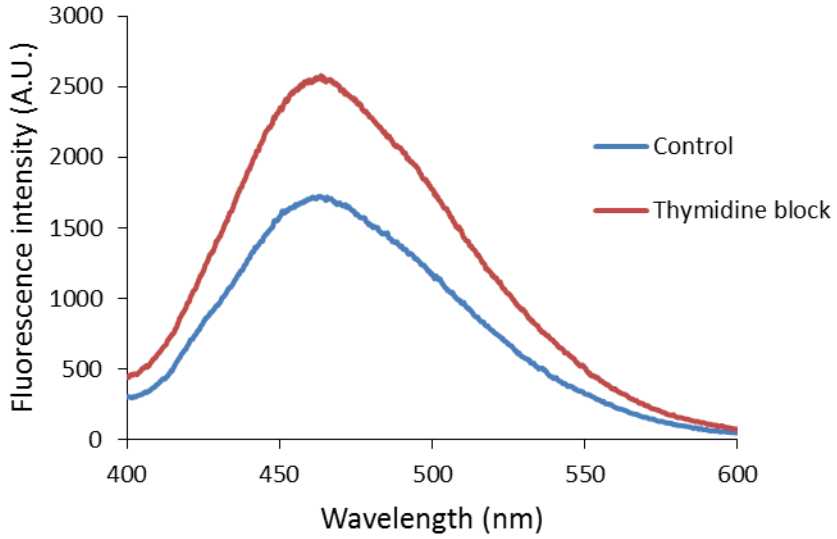

Figure 3.5.5 Fluorescence spectrum of the cell lysate collected from CCRF-CEM cells (ZQ). Cells were incubated with 2 mM thymidine for 24 hours and then reacted with 20 µM Zinquin ethyl ester (ZQee) for 20 min. Cell lysates of both control and thymidine blocked cells were collected by the sonication of the cells followed by centrifugation.

3.5.4 Reaction of TSQ and proteome isolated from CCRF-CEM cells blocked at G1 phase by thymidine

We have seen that the reaction of CCRF-CEM cells blocked at G1 phase by thymidine with TSQ or Zinquin, when compared with the untreated cells, suggests that cells synthesize greater concentration of Zn-proteins during G1 phase than any other phases of the cell cycle. To further verify this hypothesis, proteome was isolated from CCRF-CEM cells treated with 2 mM thymidine for 24 hours and then reacted with 20 μM TSQ. As the reaction progressed, fluorescence centered at 470 nm increased, indicative of the formation of TSQ-Zn-Proteome ternary adducts (**Figure 3.5.6 B**). The control experiment was done with the proteome isolated from the untreated CCRF-CEM cells. The reaction of control proteome with 20 μM TSQ also displayed fluorescence enhancement with λ_{max} of 470 nm (**Figure 3.5.6 A**). Again, consistent with the whole cells results, the normalized fluorescence intensity resulting from the reaction of proteome and TSQ was significantly different for control cell proteome and thymidine-blocked cell proteome. The fluorescence intensity per million cells synchronized in G1 phase was found to be double of that for control cells (**Table 3.5.1**). Moreover, the zinc content per million cells for thymidine-blocked cells was also 50% greater than that for untreated cells (**Table 3.5.1**). Therefore, the hypothesis that cells at G1 phase synthesize greater concentration of zinc proteins than at other phases of cell cycle is supported by experiments with both whole cells and isolated proteome.

A.

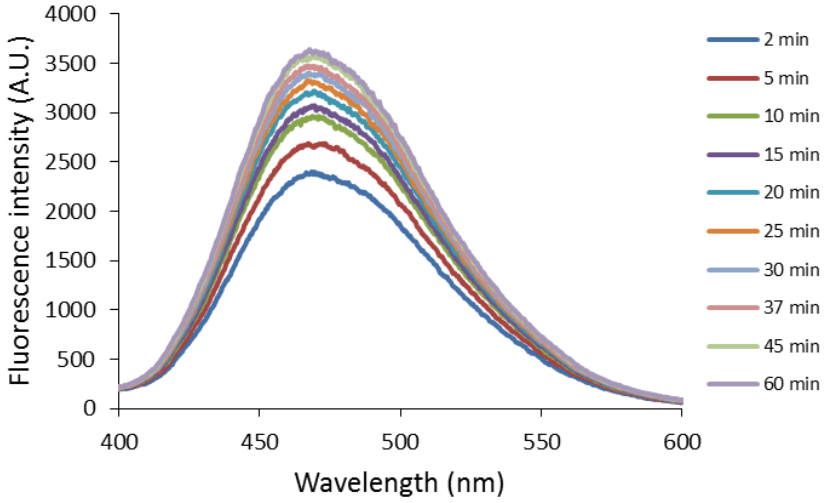
Fluorescence intensity (A.U.)
4000
3500
3000
2500
2000
1500
1000
500
0
400
450
500
550
600
Wavelength (nm)
2 min
5 min
10 min
15 min
20 min
25 min
30 min
37 min
45 min
60 min

B.

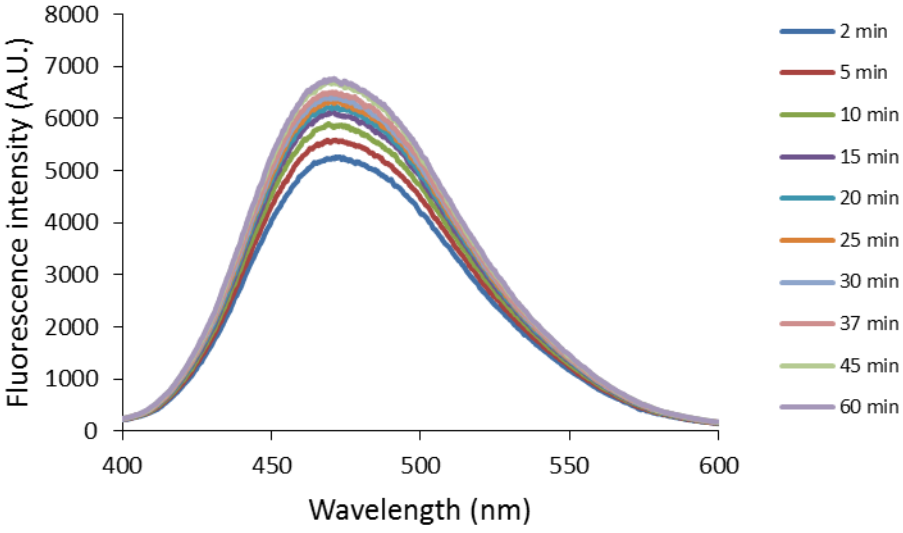
Fluorescence intensity (A.U.)
8000
7000
6000
5000
4000
3000
2000
1000
0
400
450
500
550
600
Wavelength (nm)
2 min
5 min
10 min
15 min
20 min
25 min
30 min
37 min
45 min
60 min

C.

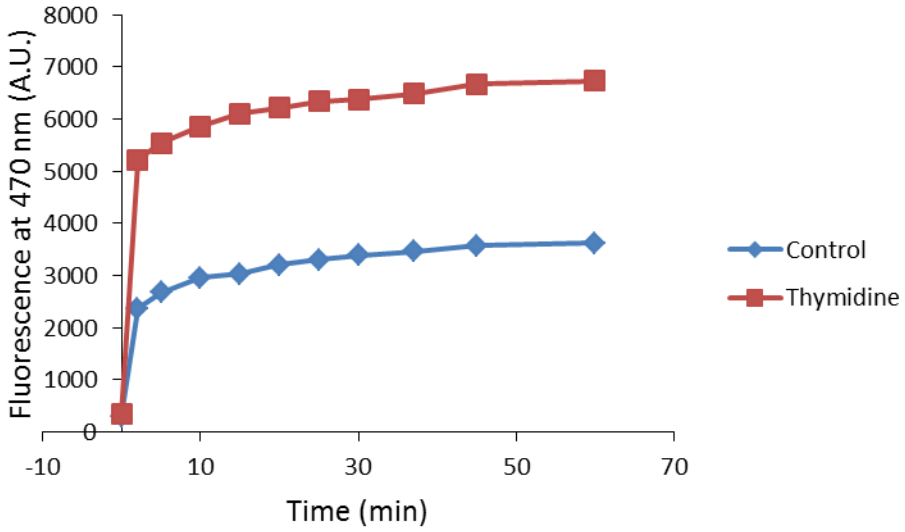

Figure 3.5.6 Reaction of TSQ and proteome isolated from CCRF-CEM cells blocked at G1 phase by thymidine. (A) Control: 1.25 x 10^8 cells were harvested, sonicated and centrifuged. The cell lysate was then loaded onto a Sephadex G-75 column to collect the proteome. Following on, proteome was reacted with 20 µM TSQ for an hour. (B) Proteome was isolated from 1.2 x 10^8 CCRF-CEM cells treated with 2 mM thymidine for 24 hours. Isolated proteome was subsequently reacted with 20 µM TSQ for an hour. (C) Comparison of kinetics of both reactions.

Table 3.5.1: Comparison of the normalized fluorescence intensities from TSQ reaction and zinc contents of proteome isolated from control (untreated) CCRE-CEM cells and thymidine blocked cells

			Ratio (Blocked/control)
Fluorescence intensity per million cells (A.U.)	Control	29	2
	Blocked	57	
Zinc content per million cells (nmol)	Control	0.10	1.5
	Blocked	0.16	

3.5.5 Reaction of Zinquin (ZQ) and proteome isolated from CCRF-CEM cells blocked at G1 phase by thymidine

The reaction of proteome isolated from CCRF-CEM cells that had been synchronized at G1 phase was investigated with Zinquin (ZQ) as well. To do this, proteome was collected from 1.2 x 10^8 CCRF-CEM cells treated with 2 mM thymidine for 24 hours, and subsequently reacted with 20 µM Zinquin. Like TSQ, Zinquin also reacted with isolated proteome with an enhancement of fluorescence with an emission maximum of 470 nm (**Figure 3.5.7 B**). Control proteome isolated from 1.25 x 10^8 untreated CCRF-CEM cells was also reacted with 20 µM Zinquin. The control reaction also showed gradual increase of fluorescence with λ_{max} of 470 nm (**Figure 3.5.7 A**). The results were comparable to those of the TSQ experiment. The normalized fluorescence intensity from the reaction of proteome isolated from CCRF-CEM cells blocked at G1 phase (41 fluorescence units per million cells) was found to be almost double that for control (untreated) cells (22 units per million cells) (**Table 3.5.2**). The normalized zinc content was also found to be about 40% greater in case of synchronized cells – 0.15 nmol per million cells as opposed to 0.11 nmol in control cells (**Table 3.5.2**). This experiment further strengthens the hypothesis that more proteome-bound Zn exists in cells at G1 phase than at any other phases of the cell cycle. Since ZQ and TSQ qualitatively bind to different Zn-proteins, these results imply that a broad range of Zn-proteins undergoes concentration changes during the course of the cell cycle.

A.

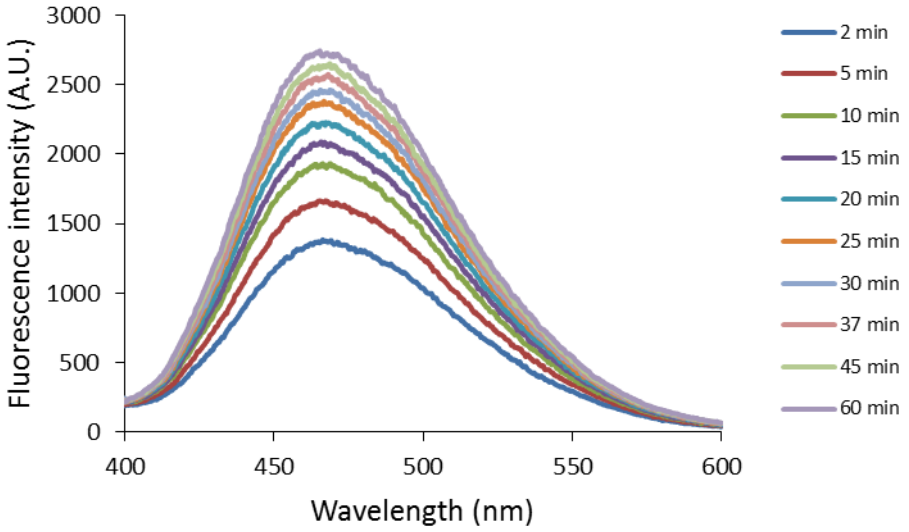
Fluorescence intensity (A.U.)
3000
2500
2000
1500
1000
500
0
400
450
500
550
600
Wavelength (nm)
2 min
5 min
10 min
15 min
20 min
25 min
30 min
37 min
45 min
60 min

B.

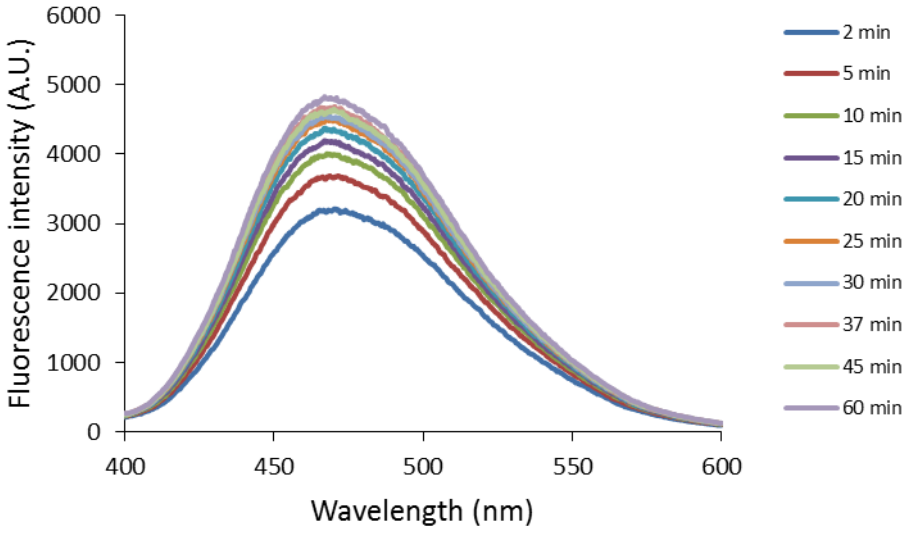
Fluorescence intensity (A.U.)
6000
5000
4000
3000
2000
1000
0
400
450
500
550
600
Wavelength (nm)
2 min
5 min
10 min
15 min
20 min
25 min
30 min
37 min
45 min
60 min

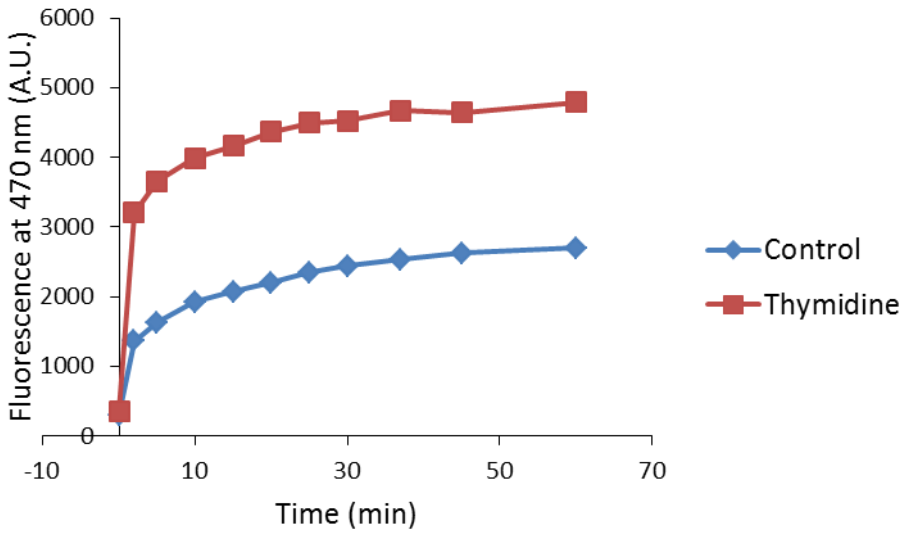

Figure 3.5.7 Reaction of Zinquin (ZQ) and proteome isolated from CCRF-CEM cells blocked at G1 phase by thymidine. (A) Control: 1.25 x 10^8 cells were harvested, sonicated and centrifuged. The cell lysate was then loaded onto a Sephadex G-75 column to collect the proteome. Following on, proteome was reacted with 20 µM Zinquin for an hour. (B) Proteome was isolated from 1.2 x 10^8 CCRF-CEM cells treated with 2 mM thymidine for 24 hours. Isolated proteome was subsequently reacted with 20 µM Zinquin for an hour. (C) Comparison of kinetics of both reactions.

Table 3.5.2: Comparison of the normalized fluorescence intensities from Zinquin reaction and zinc contents of proteome isolated from control (untreated) CCRE-CEM cells and thymidine blocked cells

			Ratio (Blocked/Control)
Fluorescence intensity per million cells (A.U.)	Control	22	1.9
	Blocked	41	
Zinc content per million cells (nmol)	Control	0.11	1.4
	Blocked	0.15	

3.5.6 Reaction of TSQ and proteome isolated from CCRF-CEM cells blocked at G2/M phase by nocodazole

The reactions of CCRF-CEM cells synchronized at G1 phase by thymidine or the isolated proteome from blocked cells with TSQ or Zinquin showed that cells synthesize more Zn-proteins in G1 phase than in other phases of the cell cycle. Next, we wanted to investigate the status of cellular zinc proteins at other phases of the cell cycle to extend the above findings. Logically, cells should produce fewer number of Zn-proteins at other phases than at G1 phase in order that the average for the divinding cell population be less than for G1. To probe this, another cell blocker nocodazole was chosen, which blocks the cells at G2/M phase. CCRF-CEM cells were treated with 100 ng/mL nocodazole for 24 hours to synchronize the cells at G2/M phase. Cell synchronization at G2/M phase was verified using Flow Cytometry. For this experiment, proteome was isolated from 5.5 x 10^7 CCRF-CEM cells treated with 100 ng/mL nocodazole for 24 hours, and then reacted with 20 μM TSQ. As expected, fluorescence enhancement with an emission maximum of 470 nm was found (**Figure 3.5.8 B**). Proteome was isolated from 5.8 x 10^7 untreated cells and reacted with 20 μM TSQ as a control experiment (**Figure 3.5.8 A**). When normalized, the fluorescence intensity for the blocked cells at G2/M phase (32 fluorescence units per million cells) was found to be about half of that for control cells (69 fluorescence units per million cells) (**Table 3.5.3**). The normalized zinc content in synchronized cells was also found to be 67% of the control – 0.08 nmol zinc per million cells as opposed to 0.12 nmol in control cells (**Table 3.5.3**). These results indicate that cells at G2/M phase synthesize less zinc containing proteins than at other phases of the cell cycle.

A.

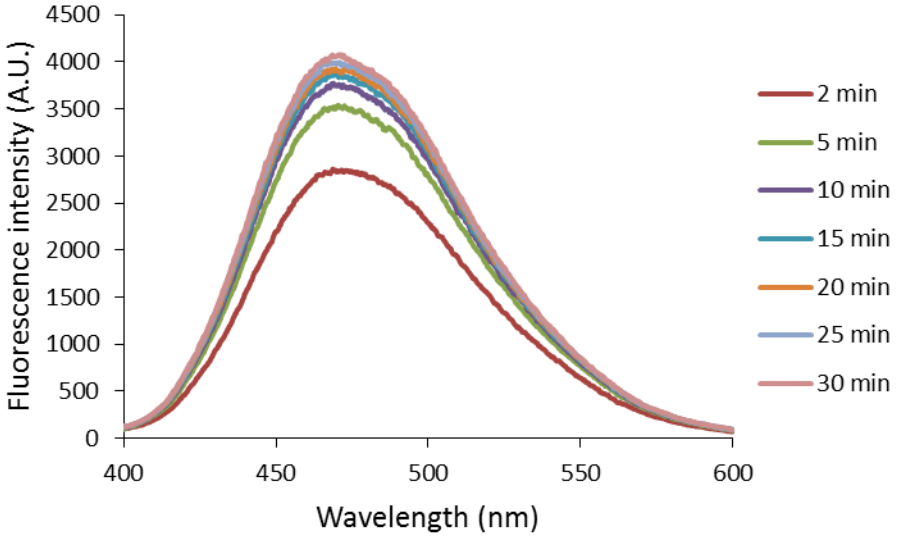
Fluorescence intensity (A.U.)
4500
4000
3500
3000
2500
2000
1500
1000
500
0
400
450
500
550
600
Wavelength (nm)
2 min
5 min
10 min
15 min
20 min
25 min
30 min

B.

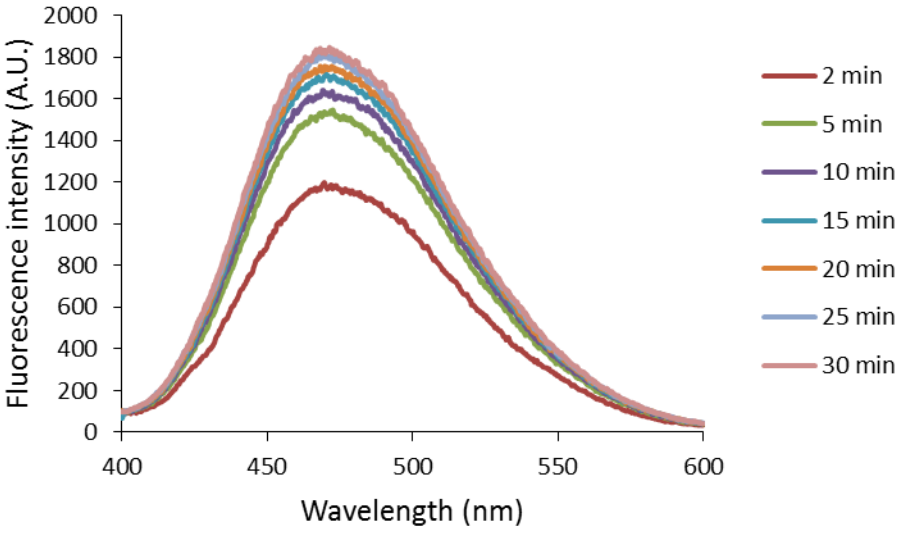
Fluorescence intensity (A.U.)
2000
1800
1600
1400
1200
1000
800
600
400
200
0
400
450
500
550
600
Wavelength (nm)
2 min
5 min
10 min
15 min
20 min
25 min
30 min

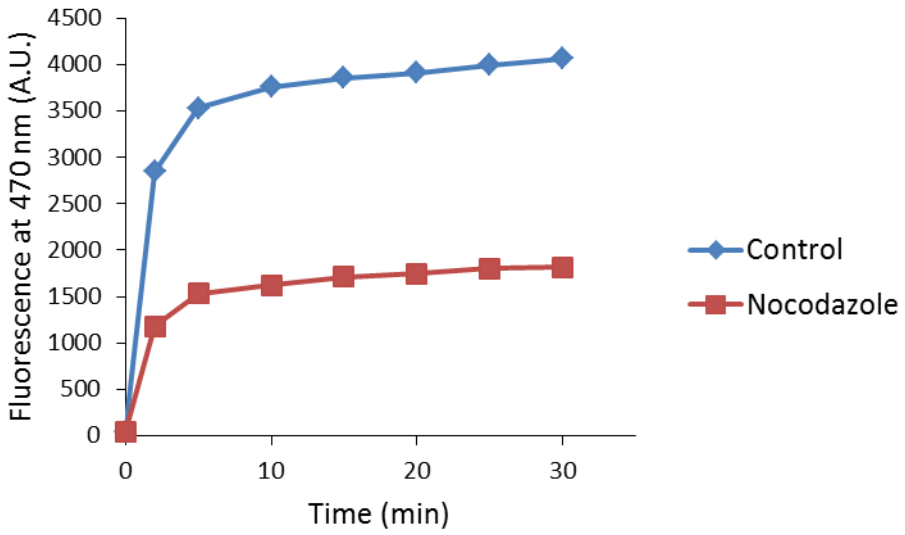

Figure 3.5.8 Reaction of TSQ and proteome isolated from CCRF-CEM cells blocked at G2/M phase by nocodazole. (A) Control: 5.8 x 10^7 cells were harvested, sonicated and centrifuged. The cell lysate was then loaded onto a Sephadex G-75 column to collect the proteome. Following on, proteome was reacted with 20 µM TSQ for 30 min. (B) Proteome was isolated from 5.5 x 10^7 CCRF-CEM cells treated with 100 ng/mL nocodazole for 24 hours. Isolated proteome was subsequently reacted with 20 µM TSQ for 30 min. (C) Comparison of kinetics of both reactions.

Table 3.5.3: Comparison of the normalized fluorescence intensities from TSQ reaction and zinc contents of proteome isolated from control (untreated) CCRE-CEM cells and nocodazole blocked cells

			Ratio (Blocked/control)
Fluorescence intensity per million cells (A.U.)	Control	69	0.5
	Blocked	32	
Zinc content per million cells (nm)	Control	0.12	0.67
	Blocked	0.08	

3.5.7 Reaction of Zinquin (ZQ) and proteome isolated from CCRF-CEM cells blocked at G2/M phase by nocodazole

The previous experiment - the reaction of TSQ and proteome collected from CCRF-CEM cells synchronized at G2/M phase by nocodazole - was compared with another that utilized ZQ in place of TSQ. In doing so, proteome was isolated from 5.8 x 10^7 CCRF-CEM cells treated with 100 ng/mL nocodazole for 24 hours and then reacted with 20 µM Zinquin for 30 min. As expected, gradual increase of fluorescence centered at 470 nm was observed due to formation of ZQ-Zn-Proteome ternary complex (**Figure 3.5.9 B**). The result of this experiment was compared with a control experiment in which 20 µM Zinquin was reacted with proteome isolated from 5.5 x 10^7 untreated CCRF-CEM cells (**Figure 3.5.9 A**). Like TSQ, Zinquin reaction also showed that the normalized fluorescence intensity and zinc content are dissimilar for synchronized and control cells. The fluorescence intensity per million cells for blocked cells at G2/M phase (19 arbitrary units) was found to be 50% of that for control cells (40 arbitrary units) (**Table 3.5.4**). Consistently, zinc content per million cells for synchronized cells (0.08 nmol) was 67% of that for control cells (0.12 nmol) (**Table 3.5.4**). This experiment again indicates that cells make relatively fewer number of zinc proteins during G2/M phase than at other phases of the cell cycle.

A.

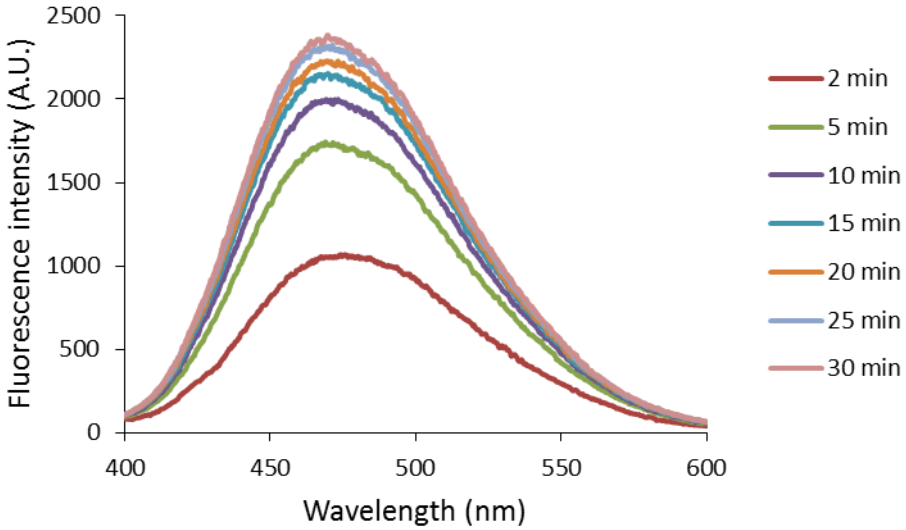
Fluorescence intensity (A.U.)
2500
2000
1500
1000
500
0
400
450
500
550
600
Wavelength (nm)
2 min
5 min
10 min
15 min
20 min
25 min
30 min

B.

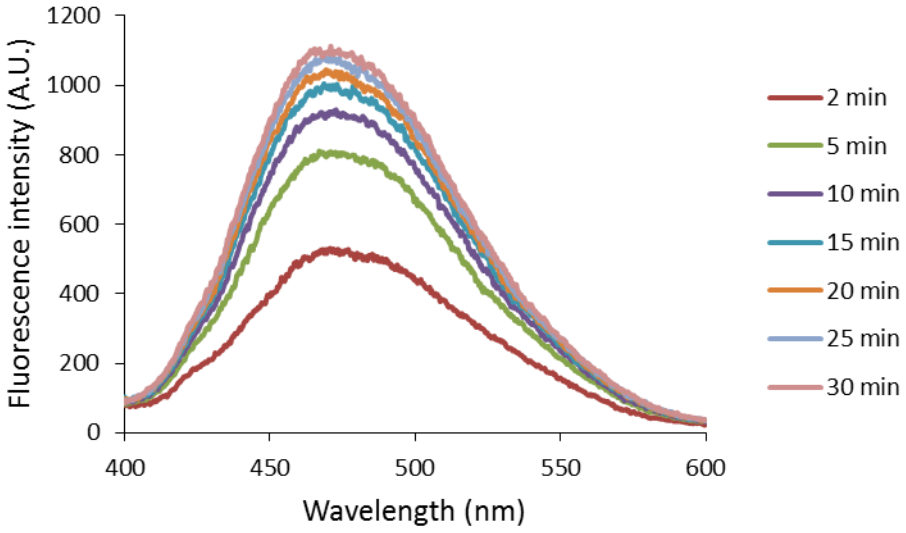
Fluorescence intensity (A.U.)
1200
1000
800
600
400
200
0
400
450
500
550
600
Wavelength (nm)
2 min
5 min
10 min
15 min
20 min
25 min
30 min

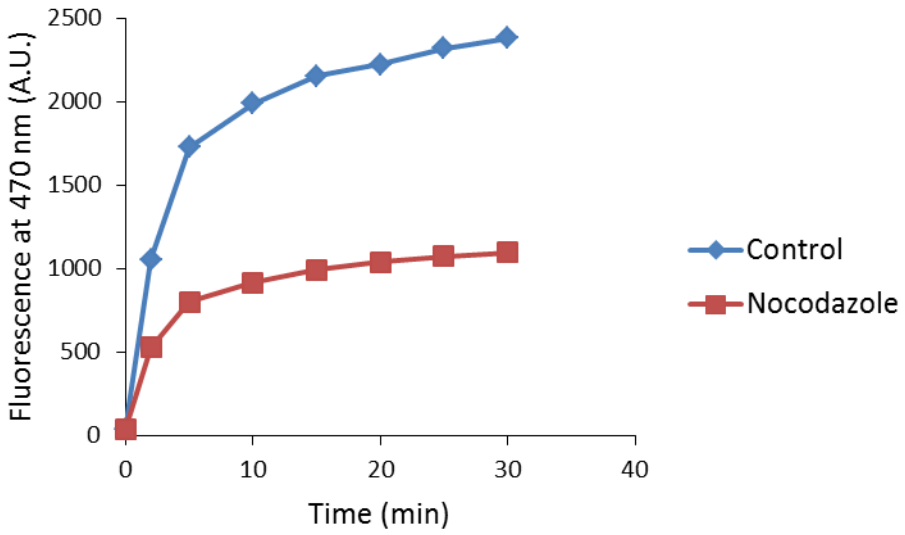

Figure 3.5.9 Reaction of Zinquin (ZQ) and proteome isolated from CCRF-CEM cells blocked at G2/M phase by nocodazole. (A) Control: 5.8 x 10^7 cells were harvested, sonicated and centrifuged. The cell lysate was then loaded onto a Sephadex G-75 column to collect the proteome. Following on, proteome was reacted with 20 µM Zinquin (ZQ) for 30 min. (B) Proteome was isolated from 5.5 x 10^7 CCRF-CEM cells treated with 100 ng/mL for 24 hours. Isolated proteome was subsequently reacted with 20 µM Zinquin (ZQ) for an hour. (C) Comparison of kinetics of both reactions.

Table 3.5.4: Comparison of the normalized fluorescence intensities from Zinquin reaction and zinc contents of proteome isolated from control (untreated) CCRE-CEM cells and thymidine blocked cells

			Ratio (Blocked/Control)
Fluorescence intensity per million cells (A.U.)	Control	40	0.5
	Blocked	19	
Zinc content per million cells (nmol)	Control	0.12	0.67
	Blocked	0.08	

4. DISCUSSION

Zinc is involved in a wide array of biological functions, including its structural and catalytic roles in various Zn-proteins.[1, 2] Recent studies have revealed that Zn^{2+} also serves as a signaling molecule and a secondary messenger.[41, 42] With the aim of studying the zinc trafficking across the cell membrane and within the cell, a number of fluorescent sensors with a wide range of stability constants have been designed and synthesized.[1, 2] Conventionally, the appearance of a fluorescence microscopic signal following the incubation of cells with a cell permeable sensor, and its disappearance in the presence of the powerful membrane permeant chelator, TPEN, are interpreted as indicating the presence of *labile*, *available* Zn^{2+} in the cellular process under study. However, in most cases, the chemical interaction between the fluorescent dye and various cellular components, and the sensor's influence on the equilibria between the Zn-proteins and the sensor itself have not been thoroughly studied. If the available free Zn^{2+} concentration is not comparable with the stability constant and the concentration of the sensor used, the conclusions drawn from the studies that employed the sensor may be ambiguous. Therefore, the biological chemistry of these fluorescent sensors needs to be properly understood.

A number of studies have used the fluorescent sensor Newport Green (NPG) to image intracellular labile Zn^{2+}.[67-72] A sensor with a low Zn^{2+} binding affinity ($K_d \sim 10^{-5}$-10^{-6} M), NPG_A, its acid form, binds Zn^{2+} *in vitro* with a 1:1 stoichiometry and displays a two-fold enhancement of fluorescence upon binding Zn^{2+}, which is readily reversed by TPEN. However, some limitations of NPG include its high background fluorescence and the unaltered emission maximum of 530 nm following Zn^{2+} binding. Moreover, both NPG_A and Zn-NPG_A show non-linear growth of

fluorescence at increasing concentrations, possibly, due to the π-stacking of fluorescein reporters of the sensor. This property complicates its use in quantitative measurements. In addition, because of its small binding constant for Zn^{2+}, it may encounter cellular ligands, including proteins and small molecules such as glutathione, that compete with NPG for intracellular labile Zn^{2+}. This study examined the effectiveness of NPG as a zinc sensor within the cellular environment.

When LLC-PK_1 cells were reacted with the cell permeable, non-fluorescent ester form NPG_E, a slow increase of fluorescence was observed, which continued growing despite the addition of TPEN. This suggested that the fluorescence enhancement originated from the slow hydrolysis of the non-fluorescent ester NPG_E to the fluorescent acid NPG_A catalyzed by cellular esterases. NPG_A did not react with the native distribution of Zn^{2+} to produce any measurable Zn-NPG or NPG-Zn-Proteome ternary adduct, unlike TSQ and Zinquin (ZQ).[50, 65] Strangely, much of the NPG_A generated following hydrolysis of NPG_E was found in the extracellular medium, indicating the efflux of NPG_E or NPG_A by some unknown mechanism. This finding indicated that the fluorescence enhancement attributed to the imaging of intracellular Zn^{2+} reported in some studies might involve the extracellular Zn^{2+}.

Filtration the cell lysate collected from LLC-PK_1 cells incubated with NPG_E showed that NPG_A made non-specific interactions with proteome, as majority of fluorescence was associated with the high molecular weight retentate and was unaffected when TPEN was added. Similar results obtained from the reaction of isolated proteome with NPG_E or NPG_A further supported the non-specific interaction of NPG_A with proteome. When reacted with individual Zn-proteins instead of the whole proteome, such as alcohol dehydrogenase (Zn-ADH) and carbonic anhydrase (Zn-

CA), NPG_E slowly converted to NPG_E, accompanied by a slow increase of fluorescence, meaning that both Zn-proteins acted as esterases which catalyzed the conversion. TPEN could not reverse the course of fluorescence increase, which suggested that no NPG-Zn-ADH or NPG-Zn-CA ternary adduct formed. However, filtration of the final reaction mixtures demonstrated that NPG_A interacted non-specifically with both Zn-ADH and Zn-CA, consistent with the proteome results. By contrast, both TSQ and Zinquin (ZQ) form ternary adducts TSQ/ZQ-Zn-(CA/ADH) with both Zn-proteins.[50, 65] Both NPG_A and Zn-NPG_A showed significant interaction with bovine serum albumin, which has a well-defined zinc binding site, as well. As NPG_A or Zn-NPG_A was reacted with BSA, a noticeable enhancement of fluorescence was observed and the emission maximum shifted from 532 nm to 538 nm. Following filtration of the final reaction mixtures, all of the fluorescence intensity was found associated with BSA, which further confirmed the interaction of BSA and NPG_A or Zn-NPG_A. This random binding of NPG_A to proteome, further supported by the reactions with individual proteins, including alcohol dehydrogenase, carbonic anhydrase and bovine serum albumin, is an undesired property of a cellular metal binding sensor. A recent paper also reported the interaction of NPG with proteomic fractions following gel filtration.[108]

From the reactions of NPG with the whole cells, isolated proteome and individual proteins, it was concluded that NPG is not reactive with the static distribution of cellular zinc. Next, proteome, including Zn-proteome, together with NPG_A was titrated with Zn^{2+} to model the cellular dynamic Zn^{2+} pool to examine if NPG_A with its low zinc binding constant can bind to the mobile Zn^{2+} within the proteomic environment. No Zn-NPG_A formed even after the addition of about five times Zn^{2+} concentration of the native proteome, meaning that proteome contains a

large number of Zn^{2+} binding sites with zinc binding affinity much higher than NPG, which effectively outcompete NPG for the added Zn^{2+} (reaction 1). This property of proteome is referred to as its zinc buffering capacity.

$$\text{Proteome} + NPG_A + Zn^{2+} \rightleftharpoons \text{Proteome}\bullet Zn + NPG_A \qquad (1)$$

Beyond this buffering region, NPG_A could weakly compete with the proteome, indicating that proteome has additional binding sites with zinc binding stability constants comparable to NPG_A (reaction 2).

$$\text{Proteome}\bullet Zn + NPG_A \rightleftharpoons \text{Proteome} + Zn\text{-}NPG_A \qquad (2)$$

Proteome could also chelate Zn^{2+} from pre-incubated Zn-NPG_A complex to form Proteome•Zn, further substantiating its additional zinc binding sites with greater stability constants than NPG. Together, these titration experiments implied that Zn-NPG_A complex is not stable enough to survive within the proteomic environment, where a large number of proteomic ligands can outcompete NPG_A for Zn^{2+}. This finding is very significant, because it brings forth the question of how NPG_A acts an intracellular sensor to image mobile Zn^{2+} reported in many studies by surpassing the high zinc buffering capacity of proteome. Possibly, the proteome's zinc buffering capacity is cellular compartment specific, i.e. the proteins with high zinc buffering capacity are limited to certain cellular organelles such that NPG_A can bind free or labile pool of Zn^{2+} in some parts of the cell. However, when subcellular proteome, including cytosolic, mitochondrial and nuclear proteome, were collected and subsequently, titrated with Zn^{2+}, buffering capacity was observed in all of them, regardless of the compartment. Besides proteome, glutathione,

another potential Zn^{2+} binding small molecule ligand that exists in mM concentration in eukaryotic cells and has an apparent stability constant for Zn^{2+} at pH 7 of $10^{4.2}$, also competed with NPG_A for Zn^{2+}.[81] In addition, Zn-NPG_A showed weak stability in the presence of micromolar concentration of glutathione, suggesting that there are plethora of potential ligands, both proteome and small molecules, including glutathione, which compete with NPG_A to bind labile Zn^{2+}. So under this circumstance, NPG_A's efficacy as an intracellular zinc sensor is questionable.

The finding that Zn-NPG_A complex is inadequately stable observed from *in vitro* experiments (proteome and glutathione) was in agreement with *in vivo* observations. When LLC-PK_1 cells pre-incubated with NPG_E were treated with $Zn(pyrithione)_2$, Zn^{2+} complexed with the ionophore pyrithione, an immediate increase fluorescence was observed. However, the cell impermeable strong Zn^{2+} chelator, EDTA, almost completely quenched the increased fluorescence, revealing that the signal enhancement originated from extracellular Zn-NPG_A formation. The extracellular NPG_A may have resulted from the efflux of NPG_A following the conversion from NPG_E described earlier. Although pyrithione shuttled into cells a significant amount of Zn^{2+} - almost equal to 50% of the total proteomic Zn^{2+} concentration – the intracellular NPG_A could not compete with the cellular competitors to generate any Zn-NPG_A, because no measurable intracellular fluorescence enhancement could be detected. This experiment once again encourages the possibility that the fluorescence enhancement which was attributed to intracellular Zn-NPG_A formation reported in various studies may partly originate from the extracellular Zn-NPG_A.

To further substantiate the observation that NPG_A cannot effectively compete with the competitive proteomic and small molecule ligands for the mobile Zn^{2+}, isolated proteome pre-treated with NPG_A was reacted with two thiol binding reagents, a nitric oxide donor

diethylamine NONOate (DEA-NO) and N-ethylmaleimide (NEM), which react with proteomic sulfhydryl groups and liberate Zn^{2+} coordinated by thiolate ligands in native Zn-proteins. Following the reaction with DEA-NO, no detectable Zn-NPG_A was formed, implying that the liberated Zn^{2+} from native Zn^{2+} binding sites was captured by competitive proteomic and/or small molecule ligands. Interestingly, NPG_A reacted independently with nitric oxide (NO) accompanied by fluorescence enhancement and unaltered emission maximum, meaning that NPG_A acts also as a nitric oxide (NO) sensor. Therefore, previous studies that employed NPG_A to detect Zn^{2+} liberated upon reaction with nitric oxide might have to be re-examined, since the fluorescence increase perhaps stemmed from NPG_A's binding to nitric oxide (NO), not from Zn-NPG_A.

The other thiol binding reagent NEM reacted with about 50% of the proteomic sulfhydryl groups and resulted in a small increase of fluorescence. However, TPEN could only partially reverse the fluorescence enhancement, indicating that an insignificant amount of Zn-NPG_A had formed. By contrast, Zinquin, a higher affinity zinc sensor than NPG, binds Zn^{2+} mobilized from proteome following the reaction with NEM as $Zn(ZQ)_2$.[83] Apparently, proteomic ligands bind the newly liberated Zn^{2+} with higher affinity than NPG_A, further questioning NPG_A's ability to image free Zn^{2+} in the cellular environment.

Although a number of studies used NPG to image intracellular free Zn^{2+}, this present work questions the stability of Zn-NPG_A in all cellular compartments. Newport Green, because of its small stability constant for Zn^{2+}, has to compete with a host of adventitious proteomic sites with higher affinity for Zn^{2+}. Therefore, these results bring into the question what pools of intracellular or extracellular Zn^{2+} are imaged by Newport Green.

Having found that Newport green with a modest stability constant for Zn^{2+} cannot serve as a good sensor for imaging Zn^{2+} within the cellular environment, next we studied the biological chemistry of another fluorescent Zn^{2+} sensor Zinpyr-1 (ZP1) that has a stability constant higher than Newport Green. The ZP1 structure possesses two di-(2-picolyl)amine chelators that bind Zn^{2+} ions (Figure 1.2). It binds the first Zn^{2+} with much higher affinity (K_d 0.7 nM) but with very weak fluorescence, while the weaker binding of the second Zn^{2+} (K_d 85 μM) is associated with much higher increase of fluorescence.[1] Moreover, the half-saturated complex ZP1-Zn displays an emission maximum of 535 nm, but shifts to 525 nm as the fully saturated complex ZP1$(Zn)_2$ is generated. Since the strong binding of first Zn^{2+} results in very weak fluorescence and the weak binding of second Zn^{2+} gives larger fluorescence increase, the gradual binding of Zn^{2+} to ZP1 produces a sigmoidal shaped titration curve. This property – production of weak fluorescence upon strong binding of the first Zn^{2+} - makes its use as a cellular sensor complicated.

The incubation of LLC-PK_1 cells with ZP1 resulted in very weak fluorescence with an emission maximum of 535 nm. Neither TPEN, a cell permeable strong Zn^{2+} chelator, nor EDTA, a cell impermeable strong Zn^{2+} chelator, could quench the fluorescence. This apparently indicated no reaction between ZP1 and intracellular, native Zn^{2+} or extracellular Zn^{2+}. However, since the strong binding of Zn^{2+} to ZP1 gives very weak fluorescence, it is difficult to conclude definitively that no reaction occurred between ZP1 and cellular Zn^{2+}. When the cell lysate obtained following the incubation of LLC-PK_1 cells with ZP1 was separated using size exclusion chromatography, a significant pool of high molecular weight fluorescence was observed that

co-existed with most of the Zn^{2+} concentration in the cell lysate. This suggested the formation of ternary adduct, ZP1-Zn-Proteome, between ZP1 and native Zn-Proteome.

To further investigate the possibility of the formation of ZP1-Zn-Proteome ternary adduct, ZP1 was reacted with isolated Zn-Proteome. The fluorescence with 540 nm emission maximum generated from the reaction was reduced by 44% by TPEN. Moreover, upon gel filtration of the final reaction mixture of ZP1 and isolated Zn-proteome, the majority of the fluorescence was found in the high molecular weight, proteome region. TPEN quenched the integrated fluorescence intensity of the proteome fractions by about 25%. Together, these experiments again pointed to the production of ZP1-Zn-Proteome ternary adduct.

As another evidence of its reaction with Zn-proteome, ZP1 displaced TSQ from TSQ-Zn-Proteome ternary adduct generated by the reaction of TSQ and Zn-Proteome and formed new ternary adduct species ZP-Zn-Proteome. This was quite evident from the disappearance of fluorescence intensity of TSQ-Zn-Proteome at 470 nm, and the emergence of 540 nm fluorescence due to the formation of ZP1-Zn-Proteome. TPEN caused significant reduction of the integrated fluorescence of proteome at 540 nm.

Besides its reaction with native Zn-proteome, ZP1 forms a ternary adduct, Proteome•Zn-ZP1, with isolated proteome and added Zn^{2+} as well. As isolated proteome was titrated with Zn^{2+} in the presence of ZP1, a progressive increase of fluorescence was observed immediately, which resulted in a hyperbolic graph of fluorescence increase vs. added Zn^{2+}, unlike the titration of ZP1 with Zn^{2+} that gives a sigmoidal shaped fluorescence vs. Zn^{2+} binding curve due to the unequal binding affinities of two Zn^{2+} ions for ZP1 and their distinct fluorescence properties.

Moreover, throughout the titration the emission maximum remained unaltered at 535-540 nm. Gel filtration of the final reaction mixture showed that almost all of the fluorescence intensity and Zn^{2+} were found in the high molecular weight fractions. In addition, TPEN reversed the integrated fluorescence intensity of the proteome fractions almost by 50%. These results imply that ZP1 reacts with Zn^{2+} that adventitiously binds proteome, and forms Proteome•Zn-ZP1 ternary adduct.

The generation of ternary adduct, Proteome•Zn-ZP1, was further supported from the reaction between isolated proteome and $ZP1(Zn)_2$. The reaction caused a red-shift of the emission maximum to 540 nm from $ZP(Zn)_2$'s 525 nm peak. Furthermore, following gel filtration of the final reaction mixture, most of the fluorescence and almost all of the zinc were located in the high molecular weight fractions. TPEN reduced the integrated fluorescence intensity of the high molecular weight fractions by almost 82%.

The titration of ZP1 with alcohol dehydrogenase (Zn-ADH), used as a model Zn-protein, displayed a gradual enhancement of fluorescence at 536 nm, which was reversed almost completely by TPEN. This suggested the generation of ternary adduct ZP1-Zn-ADH between ZP1 and alcohol dehydrogenase followed by the possible displacement of ZP1 by TPEN to form TPEN-Zn-ADH. The TPEN reaction is consistent with the previous studies which demonstrated that it binds Zn-ADH in the form of TPEN-Zn-ADH.[67] However, the continuing increase of fluorescence even at the concentration of alcohol dehydrogenase that contained Zn^{2+} six times higher than the concentration of ZP1 indicated that the interaction between ZP1 and Zn-ADH to form ZP1-Zn-ADH is weak. The location of the majority of the fluorescence in the low molecular

weight fractions – which resulted from ZP1's intrinsic fluorescence - following the gel filtration of the final reaction mixture of the reaction between ZP1 and alcohol dehydrogenase further supported the weak interaction ZP1 and Zn-ADH that was disrupted during the gel filtration.

Taken together, the reactions of ZP1 with LLC-PK_1 cells, isolated proteome and model proteins, such as alcohol dehydrogenase in the absence or presence of externally added Zn^{2+} suggested that ZP1 reacts with Zn-Proteome and results in the formation of ternary adduct ZP1-Zn-Proteome with native Zn-Proteome or Proteome•Zn-ZP1 with externally added Zn^{2+} and proteome. Therefore, the use of ZP1 to image cellular free or labile Zn^{2+} is complicated as it also images Zn-protein. Thus, careful investigations are required in the studies that employ ZP1 to image free or labile Zn^{2+}.

The titrations of isolated proteome with externally added Zn^{2+} in the presence of Newport Green or Zinpyr-1 were carried out as model reactions to mimic the release of Zn^{2+} from various intracellular Zn^{2+} stores such as endoplasmic reticulum, vesicles etc. which have been imaged by different fluorescent sensors in various studies. However, we have seen that in those model reactions, NPG_A cannot compete with proteome for the added Zn^{2+} until very high concentrations of Zn^{2+} were added. And ZP1 formed ternary adduct, Proteome•Zn-ZP1, with Zn^{2+} that is adventitiously bound to proteome. In neither case did the sensor image free Zn^{2+} as various studies claimed. Therefore, the studies which used a fluorescent Zn^{2+} sensor to sense Zn^{2+} released from intracellular stores or liberated from Zn-proteome followed by the introduction of a physiological or pathological agent that induced the liberation of Zn^{2+} need further study.

To put the results of those model Zn^{2+} release experiments into cellular context, we studied the reaction of nitric oxide (NO) with cellular or isolated Zn-proteome. A number of studies reported the imaging of free Zn^{2+} liberated following the incubation of cells with NO by fluorescent sensors.[54, 56, 109, 110] In one early study, sheep pulmonary alveolar endothelial cells (SPAEC) exposed to the NO donor, S-NO-cysteine, and ZQ displayed a 25% increase in fluorescence compared with controls, which led to the conclusion that Zn^{2+} mobilized by NO plays a key role in NO-dependent vessel constriction.[56] The present work examines the reaction of LLC-PK_1 cells or isolated proteome with another NO donor, diethylamine NONOate (DEA-NO), with fluorescent sensors having varied binding affinities for Zn^{2+}.

The reaction of LLC-PK_1 cells with Zinquin (ZQ) reacted with 15-20% of Zn-proteome as expected and generated the ternary adduct species ZQ-Zn-Proteome – evident from the appearance of 470 nm emission maximum. Upon the subsequent introduction of DEA-NO, fluorescence further increased at 470 nm, indicating the formation of additional ternary adduct species. In addition, along with 470 nm, 490 nm emission, characteristic of $Zn(ZQ)_2$ complex formation, appeared. The gel filtration of the cell lysate once again supported the generation of both ternary adduct species and the $Zn(ZQ)_2$ complex. Together, these results suggested that Zn^{2+} mobilized from Zn-proteome upon NO exposure binds adventitiously to various proteomic sites possessing zinc binding affinity. The excess ZQ then makes additional ternary adduct species Proteome•Zn-ZQ, which accounts for the fluorescence increase at 470 nm. Due to its high stability constant of Zn^{2+} binding, ZQ can also generate some $Zn(ZQ)_2$ complex through ligand substitution. These results can be described by the following equations:

$$\text{Zn-S-Proteome} + \text{NO} \rightleftharpoons \text{NO-S-Proteome} + \text{Zn}^{2+}$$

$$\text{Proteome} + \text{Zn}^{2+} \rightleftharpoons \text{Proteome•Zn}$$

$$\text{Proteome•Zn} + \text{ZQ} \rightleftharpoons \text{Proteome•Zn-ZQ (470 nm)}$$

$$\text{Proteome•Zn} + 2\text{ZQ} \rightleftharpoons \text{Proteome} + \text{Zn(ZQ)}_2 \text{ (490 nm)}$$

The results were verified with the reaction of isolated proteome with ZQ followed by DEA-NO. When the reaction was repeated with another zinc sensor TSQ, closely related to ZQ structure, along with TSQ-Zn-Proteome ternary adduct generated from the reaction of TSQ and 15-20% of the native Zn-proteome, additional ternary adduct species Proteome•Zn-TSQ formed through similar mechanism as of ZQ. However, because it is a weaker sensor than ZQ, TSQ could not form any $Zn(TSQ)_2$ complex by chelating Zn^{2+} from Proteome•Zn. This explanation is consistent with our previous result of the reaction of proteome with DEA-NO in the presence of Newport Green. Since Newport Green is a weak zinc sensor, it could not compete with proteome for the liberated Zn^{2+}, and thus was unable to form any measurable Zn-NPG. However, in both cases, proteomic sulfhydryl concentration were significantly reduced, confirming the reaction of NO and proteomic sulfhydryl groups, which resulted the liberation of proteomic Zn^{2+}.

To further validate the results of ZQ and TSQ experiments, isolated proteome pre-treated with ZQ or TSQ was titrated with Zn^{2+}, a model used to mimic liberation of Zn^{2+} following NO exposure. As anticipated in both cases, additional ternary adduct Proteome•Zn-ZQ/TSQ was generated from the reaction of ZQ/TSQ and Zn^{2+} adventitiously bound to proteome, Proteome•Zn. However, unlike NO experiment with ZQ, no $Zn(ZQ)_2$ complex was produced. This implied that proteome's adventitious zinc binding sites perhaps involve sulfhydryl groups. Since

a significant number of these sulfhydryl groups are modified by NO in the DEA-NO experiment, some of the mobilized Zn^{2+} may be unable to bind these sites and become accessible to ZQ to produce the $Zn(ZQ)_2$ complex. By contrast, in this titration experiment, due to the absence of added sulfhydryl binding agent, most of the proteomic sulfhydryl groups are unmodified and thus prevent ZQ from binding any added Zn^{2+} to form $Zn(ZQ)_2$ complex.

Having found that ZQ and TSQ, due to their difference in zinc binding affinity, reacted differently with proteome exposed to DEA-NO, we turned to a third sensor FluoZin-3, another zinc sensor with intermediate binding affinity (15 nM) between TSQ and ZQ.[1] Unlike ZQ and TSQ, FluoZin-3 does not react with native Zn-proteome. Following exposure of proteome incubated with FluoZin-3 to DEA-NO, a gradual increase of fluorescence insensitive to TPEN was observed, suggesting that the fluorescence increase due to the modification of the fluorophore, not because of the binding of Zn^{2+}. Evidently, FluoZin-3, like Newport Green, reacts independently with nitric oxide (NO) accompanied by fluorescence enhancement. In this case, neither Proteome•Zn-FluoZin3 ternary adduct nor Zn-FluoZin3 could be detected. This suggested that FluoZin-3 cannot effectively competed for Zn^{2+} with modified or adventitious proteomic binding sites.

Thus, three different results were obtained from the reaction of proteome with the nitric oxide donor, DEA-NO, depending on the zinc binding affinity of the fluorescent sensor used. This clearly demonstrates that the Zn^{2+} binding properties of proteome under different cellular conditions, e.g. proteomic sulfhydryl groups modified by NO in this case play an important role to determine how the zinc sensor will function. For example, among the three sensors used in

this study, ZQ could effectively compete with proteome for the mobilized Zn^{2+}, only when the proteomic zinc binding sites were modified by NO. Therefore, the imaging of Zn^{2+} labilized by the exposure of NO depends on the zinc binding characteristics of the proteome and the relative zinc binding affinity of the sensor compared with that of proteome's adventitious sites. That proteome has numerous high affinity Zn^{2+} binding sites as revealed in the above titration experiment suggests that Zn^{2+} may be transported to native Zn-proteins via ligand substitution involving these non-specific high affinity sites.

Apart from doubting the effectiveness of a large number of zinc sensors to image labile Zn^{2+} within the proteomic environment, the apparent strong affinity of mobilizable Zn^{2+} for the above mentioned non-specific proteomic binding sites raises other important questions. For example, if the proteome provides a strong buffer for Zn^{2+}, how does intracellular Zn^{2+} signaling take place?

From a number of experiments, including the titration of proteome with Zn^{2+} in the presence of Newport Green, ZP1, TSQ, Zinquin and FluoZin-3, it is convincingly evident that beside the strong Zn^{2+} binding sites in native Zn-proteins, proteome has a large number of high affinity adventitious zinc binding sites. However, as was seen in the reaction of proteome incubated with ZQ and DEA-NO, nitric oxide (NO) significantly modified the proteomic sulfhydryl groups, which coincided with the proteome's reduction of zinc buffering capacity and as such ZQ could effectively compete with proteome to generate $Zn(ZQ)_2$ complex. This observation led us to the hypothesis that proteomic sulfhydryl groups are primarily involved in these adventitious high affinity Zn^{2+} binding sites. To examine this idea further, proteomic sulfhydryl groups were modified by thiol binding reagents, such as N-ethylmaleimide (NEM) and 5,5-dithio-bis-(2-

nitrobenzoic acid) (DTNB), before treatment with Zn^{2+}. Interestingly, when the proteome was incubated with NEM or DTNB, its high affinity Zn^{2+} binding sites were significantly reduced, as monitored by both FluoZin-3 and Newport Green. This finding clearly implicated proteomic sulfhydryl (-SH) groups as the high affinity zinc binding sites that outcompeted FluoZin-3 for the added Zn^{2+}. This discovery takes us one step further into understanding the mechanism of cellular zinc trafficking. Moreover, this finding once again draws attention to the fact that the ability of the sensor to image free or labile Zn^{2+} is contingent on the proteome's Zn^{2+} binding characteristics. For example, reaction of nitric oxide (NO) with the proteomic sulfhydryl (SH) groups reduces their availability to bind Zn^{2+} in the presence of ZQ and other sensors, and this proteomic condition allows the sensors to bind Zn^{2+} accompanied by a fluorescence enhancement. Various studies reported that the release of Zn^{2+}, induced by the exposure of nitric oxide donors, precedes a Zn-dependent regulatory/signaling process, often inferred from the fluorescence increase of the zinc sensor used. However, the sensor's ability to bind Zn^{2+} might be dependent on the diminished zinc buffering capacity of proteome resulting from the modification of the sulfhydryl groups by NO. We know this because in unperturbed condition of the proteome, most of the fluorescent zinc sensors, including high affinity sensors Zinquin and FluoZin-3, are unable to bind mobile Zn^{2+}. The pioneering discovery by Meeusen *et al.* that inspired this investigation of the chemical biology of fluorescent zinc sensors, such as Newport Green and Zinpyr-1, was that TSQ images Zn-proteins, not free Zn^{2+}, through the formation of ternary adduct TSQ-Zn-Protein – evident from its signature emission maximum of 470 nm, unlike the $Zn(TSQ)_2$ complex that displays 490 nm emission maximum. The incubation of LLC-PK_1 cells with TSQ followed by $Zn(Pyrithione)_2$ resulted in bright fluorescence, as observed

under fluorescence microscope, due to the formation of TSQ-Zn-Proteome ternary adduct and TPEN, a strong Zn^{2+} chelator, reversed the fluorescence to a significant measure. However, the bright fluorescence following the introduction of TSQ and $Zn(Pyrithione)_2$ was not symmetrically distributed among the cells – some showed much more intense fluorescence than others. Seeking the reason for this asymmetric fluorescence among the cells led us to the hypothesis that cells at different stages of the cell cycle make unequal concentrations of particular Zn-proteins. In turn, this may account for the unequal brightness of fluorescence in different cells within a normal population of dividing cells.

CCRF cells were synchronized at G1 phase by the treatment with thymidine and subsequently reacted with TSQ/Zinquin. Cells showed twice as much fluorescence and zinc content per cell as the untreated population. The proteome isolated from thymidine treated CCRF cells displayed similar results. By contrast, proteome isolated from cells synchronized at G2/M phase by the incubation with nocodazole and its subsequent reaction with TSQ/ZQ resulted in about half of the fluorescence intensity and two-third of the zinc content as the untreated cells. Together, these findings supported the hypothesis that cells synthesize different amounts of zinc proteins at different stages of its cell cycle. The results explain the non-uniform brightness of fluorescence among the neighboring cells following the treatment with TSQ and $Zn(Pyrithione)_2$ observed by Meeusen *et al*.[65]

5. SUMMARY

Taken altogether, this study has yielded some important discoveries, which are significant to the understanding of the biological chemistry of the fluorescent zinc sensors, particularly Newport Green and Zinpyr-1, and also, of cellular zinc trafficking. We have shown that due to its modest Zn^{2+} binding affinity and as such its inability to outcompete proteome for Zn^{2+}, Newport Green, by itself, cannot act as an effective sensor to image labile Zn^{2+} within the proteomic environment. Moreover, some of its unwanted properties, such as the slow hydrolysis of its weakly fluorescent ester form into the strongly fluorescent acid form, and its efflux into the extracellular medium, further complicate its use as a cellular Zn^{2+} sensor. The study of Zinpyr-1 has exposed its ability to generate ZP1-Zn-Proteome ternary adduct – both with native Zn-Proteome and with proteome and the added Zn^{2+}. In addition, the weaker fluorescence signal resulting from the first Zn^{2+} binding with higher affinity makes its use as a cellular sensor even more convoluted.

The reaction of the proteome with diethylamine NONOate (DEA-NO) monitored by three different sensors – Zinquin, TSQ and FluoZin-3 – revealed that the formation of Zn-Sensor complex following the liberation of Zn^{2+} from Zn-proteome is dependent on the relative binding affinity of the sensor used. The reaction with Zinquin (ZQ), a high affinity sensor, yielded a significant quantity of $Zn(ZQ)_2$, whereas no measurable $Zn(TSQ)_2$ or Zn-FluoZin3 was formed from the reactions of DEA-NO modified Zn-proteome with TSQ or FluoZin-3, relatively lower affinity sensors than Zinquin.

The titration experiment of proteome incubated with FluoZin-3 with Zn^{2+} resulted in the important finding that proteome possesses a large concentration of high affinity Zn^{2+} binding sites having K_d for Zn^{2+} on the order of 10^{-10} M. These high affinity Zn^{2+} binding sites may serve as intermediate carriers of Zn^{2+}, following entry into the cell, to convey Zn^{2+} to apo-proteins to form native Zn-proteins - a pathway still not well understood. Following on, we have discovered that these high affinity Zn^{2+} binding sites of proteome use sulfhydryl groups to bind Zn^{2+}, evident from the abolition of these sites when proteome was reacted with sulfhydryl binding reagents, such as N-ethylmaleimide (NEM) and 5,5-dithio-bis-(2-nitrobenzoic acid) (DTNB). This finding will drive us further into the understanding of the intermediate pathway of Zn-protein formation. Last but not least, the cell cycle study has resulted in another important revelation that cells synthesize varied amount of zinc proteins at different stages of the cell cycle. All these findings will, surely, enhance the overall understanding of the cellular zinc trafficking between and within the cellular compartments.

6. REFERENCES

[1] Que, E. L., Domaille, D. W., and Chang, C. J. (2008) Metals in neurobiology: probing their chemistry and biology with molecular imaging, *Chemical Reviews 108*, 1517-1549.

[2] Carter, K. P., Young, A. M., and Palmer, A. E. (2014) Fluorescent sensors for measuring metal ions in living systems, *Chemical reviews 114*, 4564-4601.

[3] Outten, C. E., and O'Halloran, T. V. (2001) Femtomolar sensitivity of metalloregulatory proteins controlling zinc homeostasis, *Science 292*, 2488-2492.

[4] Andreini, C., Banci, L., Bertini, I., and Rosato, A. (2006) Counting the zinc-proteins encoded in the human genome, *Journal of proteome research 5*, 196-201.

[5] Andreini, C., Banci, L., Bertini, I., and Rosato, A. (2006) Zinc through the three domains of life, *Journal of proteome research 5*, 3173-3178.

[6] Andreini, C., Bertini, I., and Rosato, A. (2009) Metalloproteomes: a bioinformatic approach, *Accounts of chemical research 42*, 1471-1479.

[7] Christianson, D. W., and Cox, J. D. (1999) Catalysis by metal-activated hydroxide in zinc and manganese metalloenzymes, *Annual review of biochemistry 68*, 33-57.

[8] McCall, K. A., Huang, C.-c., and Fierke, C. A. (2000) Function and mechanism of zinc metalloenzymes, *The Journal of nutrition 130*, 1437S-1446S.

[9] Sousa, S. F., Lopes, A. B., Fernandes, P. A., and Ramos, M. J. (2009) The Zinc proteome: a tale of stability and functionality, *Dalton Transactions*, 7946-7956.

[10] Trewavas, A. (2006) A Brief History of Systems Biology “Every object that biology studies is a system of systems.” Francois Jacob (1974), *The Plant Cell 18*, 2420-2430.

[11] Bruggeman, F. J., and Westerhoff, H. V. (2007) The nature of systems biology, *Trends in microbiology 15*, 45-50.

[12] Tyers, M., and Mann, M. (2003) From genomics to proteomics, *Nature 422*, 193-197.

[13] Krężel, A., and Maret, W. (2006) Zinc-buffering capacity of a eukaryotic cell at physiological pZn, *JBIC Journal of Biological Inorganic Chemistry 11*, 1049-1062.

[14] Eide, D. J. (2006) Zinc transporters and the cellular trafficking of zinc, *Biochimica et Biophysica Acta (BBA)-Molecular Cell Research 1763*, 711-722.

[15] Zhu, J., Meeusen, J., Krezoski, S., and Petering, D. H. (2010) Reactivity of Zn-, Cd-, and apo-metallothionein with nitric oxide compounds: in vitro and cellular comparison, *Chemical research in toxicology 23*, 422-431.

[16] Vinkenborg, J. L., Nicolson, T. J., Bellomo, E. A., Koay, M. S., Rutter, G. A., and Merkx, M. (2009) Genetically encoded FRET sensors to monitor intracellular Zn2+ homeostasis, *Nature methods 6*, 737-740.

[17] Huffman, D. L., and O'Halloran, T. V. (2001) Function, structure, and mechanism of intracellular copper trafficking proteins, *Annual review of biochemistry 70*, 677-701.

[18] Puig, S., and Thiele, D. J. (2002) Molecular mechanisms of copper uptake and distribution, *Current opinion in chemical biology 6*, 171-180.

[19] O'Halloran, T. V., and Culotta, V. C. (2000) Metallochaperones, an intracellular shuttle service for metal ions, *Journal of Biological Chemistry 275*, 25057-25060.

[20] Nowakowski, A., Karim, M., and Petering, D. Zinc Proteomics, *Encyclopedia of Inorganic and Bioinorganic Chemistry*.

[21] Otvos, J. D., and Armitage, I. M. (1980) Structure of the metal clusters in rabbit liver metallothionein, *Proceedings of the National Academy of Sciences 77*, 7094-7098.

[22] Robbins, A., McRee, D., Williamson, M., Collett, S., Xuong, N., Furey, W., Wang, B., and Stout, C. (1991) Refined crystal structure of Cd, Zn metallothionein at 2.0 Åresolution, *Journal of molecular biology 221*, 1269-1293.

[23] Namdarghanbari, M. A., Meeusen, J., Bachowski, G., Giebel, N., Johnson, J., and Petering, D. H. (2010) Reaction of the zinc sensor FluoZin-3 with Zn 7-metallothionein: inquiry into the existence of a proposed weak binding site, *Journal of inorganic biochemistry 104*, 224-231.

[24] Pinter, T. B., and Stillman, M. J. (2014) The zinc balance: Competitive zinc metalation of carbonic anhydrase and metallothionein 1A, *Biochemistry 53*, 6276-6285.

[25] Li, T.-Y., Kraker, A. J., Shaw, C. F., and Petering, D. H. (1980) Ligand substitution reactions of metallothioneins with EDTA and apo-carbonic anhydrase, *Proceedings of the National Academy of Sciences 77*, 6334-6338.

[26] Kraker, A. J., Krakower, G., Shaw, C. F., Petering, D. H., and Garvey, J. S. (1988) Zinc metabolism in Ehrlich cells: properties of a metallothionein-like zinc-binding protein, *Cancer research 48*, 3381-3388.

[27] Maret, W., and Li, Y. (2009) Coordination dynamics of zinc in proteins, *Chemical reviews 109*, 4682-4707.

[28] Kochańczyk, T., Drozd, A., and Krężel, A. (2015) Relationship between the architecture of zinc coordination and zinc binding affinity in proteins–insights into zinc regulation, *Metallomics 7*, 244-257.

[29] Colvin, R. A., Bush, A. I., Volitakis, I., Fontaine, C. P., Thomas, D., Kikuchi, K., and Holmes, W. R. (2008) Insights into Zn2+ homeostasis in neurons from experimental and modeling studies, *American Journal of Physiology-Cell Physiology 294*, C726-C742.

[30] Colvin, R. A., Holmes, W. R., Fontaine, C. P., and Maret, W. (2010) Cytosolic zinc buffering and muffling: their role in intracellular zinc homeostasis, *Metallomics 2*, 306-317.

[31] Karim, M. R., and Petering, D. H. (2016) Newport Green, a fluorescent sensor of weakly bound cellular Zn 2+: competition with proteome for Zn 2+, *Metallomics*.

[32] Maret, W. (2009) Molecular aspects of human cellular zinc homeostasis: redox control of zinc potentials and zinc signals, *Biometals 22*, 149-157.

[33] Maret, W., and Krężel, A. (2007) Cellular zinc and redox buffering capacity of metallothionein/thionein in health and disease, *Molecular medicine 13*, 371.

[34] Andrews, G. K. (2001) Cellular zinc sensors: MTF-1 regulation of gene expression, In *Zinc Biochemistry, Physiology, and Homeostasis*, pp 37-51, Springer.

[35] Petering, D. H., Zhu, J., Krezoski, S., Meeusen, J., Kiekenbush, C., Krull, S., Specher, T., and Dughish, M. (2006) Apo-metallothionein emerging as a major player in the cellular activities of metallothionein, *Experimental Biology and Medicine 231*, 1528-1534.

[36] Zhang, B., Georgiev, O., Hagmann, M., Günes, Ç., Cramer, M., Faller, P., Vasák, M., and Schaffner, W. (2003) Activity of metal-responsive transcription factor 1 by toxic heavy metals and H2O2 in vitro is modulated by metallothionein, *Molecular and cellular biology 23*, 8471-8485.

[37] Laity, J. H., and Andrews, G. K. (2007) Understanding the mechanisms of zinc-sensing by metal-response element binding transcription factor-1 (MTF-1), *Archives of biochemistry and biophysics 463*, 201-210.

[38] Langmade, S. J., Ravindra, R., Daniels, P. J., and Andrews, G. K. (2000) The transcription factor MTF-1 mediates metal regulation of the mouse ZnT1 gene, *Journal of Biological Chemistry 275*, 34803-34809.

[39] Günther, V., Lindert, U., and Schaffner, W. (2012) The taste of heavy metals: gene regulation by MTF-1, *Biochimica et Biophysica Acta (BBA)-Molecular Cell Research 1823*, 1416-1425.

[40] Bozym, R. A., Chimienti, F., Giblin, L. J., Gross, G. W., Korichneva, I., Li, Y., Libert, S., Maret, W., Parviz, M., and Frederickson, C. J. (2010) Free zinc ions outside a narrow

concentration range are toxic to a variety of cells in vitro, *Experimental Biology and Medicine 235*, 741-750.

[41] Paoletti, P., Vergnano, A., Barbour, B., and Casado, M. (2009) Zinc at glutamatergic synapses, *Neuroscience 158*, 126-136.

[42] Li, H., Cao, R., Wasserloos, K. J., Bernal, P., Liu, Z. Q., Pitt, B. R., and St Croix, C. M. (2010) Nitric oxide and zinc homeostasis in pulmonary endothelium, *Annals of the New York Academy of Sciences 1203*, 73-78.

[43] Frederickson, C. J., and Bush, A. I. (2001) Synaptically released zinc: physiological functions and pathological effects, *Biometals 14*, 353-366.

[44] Budde, T., Minta, A., White, J. A., and Kay, A. (1997) Imaging free zinc in synaptic terminals in live hippocampal slices, *Neuroscience 79*, 347-358.

[45] Kay, A. R., and Tóth, K. (2008) Is zinc a neuromodulator?, *Science signaling 1*, re3.

[46] Petering, D. H. (2004) Zinc Fluorescence Probes (Commentary), *Chemtacts–Inorganic Chemistry 17*, 569-580.

[47] Pluth, M. D., Tomat, E., and Lippard, S. J. (2011) Biochemistry of mobile zinc and nitric oxide revealed by fluorescent sensors, *Annual review of biochemistry 80*, 333.

[48] Domaille, D. W., Que, E. L., and Chang, C. J. (2008) Synthetic fluorescent sensors for studying the cell biology of metals, *Nature chemical biology 4*, 168-175.

[49] Jiang, P., and Guo, Z. (2004) Fluorescent detection of zinc in biological systems: recent development on the design of chemosensors and biosensors, *Coordination Chemistry Reviews 248*, 205-229.

[50] Nowakowski, A. B., and Petering, D. H. (2011) Reactions of the fluorescent sensor, Zinquin, with the zinc-proteome: adduct formation and ligand substitution, *Inorganic chemistry 50*, 10124-10133.

[51] Koh, J.-Y., Suh, S. W., Gwag, B. J., He, Y. Y., Hsu, C. Y., and Choi, D. W. (1996) The role of zinc in selective neuronal death after transient global cerebral ischemia, *Science 272*, 1013-1016.

[52] Tønder, N., Johansen, F., Frederickson, C., Zimmer, J., and Diemer, N. (1990) Possible role of zinc in the selective degeneration of dentate hilar neurons after cerebral ischemia in the adult rat, *Neuroscience letters 109*, 247-252.

[53] Tsuchiya, D., Hong, S., Suh, S. W., Kayama, T., Panter, S. S., and Weinstein, P. R. (2002) Mild hypothermia reduces zinc translocation, neuronal cell death, and mortality after transient global ischemia in mice, *Journal of Cerebral Blood Flow & Metabolism 22*, 1231-1238.

[54] Croix, C. M. S., Wasserloos, K., Dineley, K., Reynolds, I., Levitan, E., and Pitt, B. (2002) Nitric oxide-induced changes in intracellular zinc homeostasis are mediated by metallothionein/thionein, *American Journal of Physiology-Lung Cellular and Molecular Physiology 282*, L185-L192.

[55] Tang, Z.-L., Wasserloos, K., Croix, C. M. S., and Pitt, B. R. (2001) Role of zinc in pulmonary endothelial cell response to oxidative stress, *American Journal of Physiology-Lung Cellular and Molecular Physiology 281*, L243-L249.

[56] Pearce, L. L., Wasserloos, K., Croix, C. M. S., Gandley, R., Levitan, E. S., and Pitt, B. R. (2000) Metallothionein, nitric oxide and zinc homeostasis in vascular endothelial cells, *The Journal of nutrition 130*, 1467S-1470S.

[57] Frederickson, C. J., Kasarskis, E., Ringo, D., and Frederickson, R. (1987) A quinoline fluorescence method for visualizing and assaying the histochemically reactive zinc (bouton zinc) in the brain, *Journal of neuroscience methods 20*, 91-103.

[58] Haase, H., and Beyersmann, D. (2002) Intracellular zinc distribution and transport in C6 rat glioma cells, *Biochemical and biophysical research communications 296*, 923-928.

[59] Kaltenberg, J., Plum, L. M., Ober-Blöbaum, J. L., Hönscheid, A., Rink, L., and Haase, H. (2010) Zinc signals promote IL-2-dependent proliferation of T cells, *European journal of immunology 40*, 1496-1503.

[60] Truong-Tran, A. Q., Ruffin, R. E., and Zalewski, P. D. (2000) Visualization of labile zinc and its role in apoptosis of primary airway epithelial cells and cell lines, *American Journal of Physiology-Lung Cellular and Molecular Physiology 279*, L1172-L1183.

[61] Zalewski, P. D., Forbes, I. J., and Betts, W. (1993) Correlation of apoptosis with change in intracellular labile Zn (II) using zinquin [(2-methyl-8-p-toluenesulphonamido-6-quinolyloxy) acetic acid], a new specific fluorescent probe for Zn (II), *Biochemical Journal 296*, 403-408.

[62] Zalewski, P. D., Millard, S. H., Forbes, I. J., Kapaniris, O., Slavotinek, A., Betts, W. H., Ward, A. D., Lincoln, S. F., and Mahadevan, I. (1994) Video image analysis of labile zinc in viable pancreatic islet cells using a specific fluorescent probe for zinc, *Journal of Histochemistry & Cytochemistry 42*, 877-884.

[63] Haase, H., and Beyersmann, D. (1999) Uptake and intracellular distribution of labile and total Zn (II) in C6 rat glioma cells investigated with fluorescent probes and atomic absorption, *Biometals 12*, 247-254.

[64] Thompson, R. B. (2005) Studying zinc biology with fluorescence: ain't we got fun?, *Current opinion in chemical biology 9*, 526-532.

[65] Meeusen, J. W., Tomasiewicz, H., Nowakowski, A., and Petering, D. H. (2011) TSQ (6-methoxy-8-p-toluenesulfonamido-quinoline), a common fluorescent sensor for cellular zinc, images zinc proteins, *Inorganic chemistry 50*, 7563-7573.

[66] Nowakowski, A. B., Meeusen, J. W., Menden, H., Tomasiewicz, H., and Petering, D. H. (2015) Chemical–Biological Properties of Zinc Sensors TSQ and Zinquin: Formation of Sensor-Zn-Protein Adducts versus Zn (Sensor) 2 Complexes, *Inorganic chemistry*.

[67] Meeusen, J. W., Nowakowski, A., and Petering, D. H. (2012) Reaction of metal-binding ligands with the zinc proteome: zinc sensors and N, N, N', N'-tetrakis (2-pyridylmethyl) ethylenediamine, *Inorganic chemistry 51*, 3625-3632.

[68] Strober, W. (2001) Trypan blue exclusion test of cell viability, *Current protocols in immunology*, A3. B. 1-A3. B. 3.

[69] Avelar-Freitas, B., Almeida, V. G., Pinto, M. C. X., Mourão, F. A. G., Massensini, A. R., Martins-Filho, O. A., Rocha-Vieira, E., and Brito-Melo, G. (2014) Trypan blue exclusion assay by flow cytometry, *Brazilian Journal of Medical and Biological Research 47*, 307-315.

[70] El-Sayed, I. H., Huang, X., and El-Sayed, M. A. (2006) Selective laser photo-thermal therapy of epithelial carcinoma using anti-EGFR antibody conjugated gold nanoparticles, *Cancer letters 239*, 129-135.

[71] Lowry, O. H., Rosebrough, N. J., Farr, A. L., and Randall, R. J. (1951) Protein measurement with the Folin phenol reagent, *J biol Chem 193*, 265-275.

[72] Peterson, G. L. (1977) A simplification of the protein assay method of Lowry et al. which is more generally applicable, *Analytical biochemistry 83*, 346-356.

[73] Petering, D. H., Loftsgaarden, J., Schneider, J., and Fowler, B. (1984) Metabolism of cadmium, zinc and copper in the rat kidney: the role of metallothionein and other binding sites, *Environmental health perspectives 54*, 73.

[74] Ellman, G., and Lysko, H. (1979) A precise method for the determination of whole blood and plasma sulfhydryl groups, *Analytical biochemistry 93*, 98-102.

[75] Priel, T., Aricha-Tamir, B., and Sekler, I. (2007) Clioquinol attenuates zinc-dependent β-cell death and the onset of insulitis and hyperglycemia associated with experimental type I diabetes in mice, *European journal of pharmacology 565*, 232-239.

[76] Stork, C. J., and Li, Y. V. (2006) Measuring cell viability with membrane impermeable zinc fluorescent indicator, *Journal of neuroscience methods 155*, 180-186.

[77] Stork, C. J., and Li, Y. V. (2006) Intracellular zinc elevation measured with a "calcium-specific" indicator during ischemia and reperfusion in rat hippocampus: a question on calcium overload, *The Journal of neuroscience 26*, 10430-10437.

[78] Lukowiak, B., Vandewalle, B., Riachy, R., Kerr–Conte, J., Gmyr, V., Belaich, S., Lefebvre, J., and Pattou, F. (2001) Identification and purification of functional human β-cells by a new specific zinc-fluorescent probe, *Journal of Histochemistry & Cytochemistry 49*, 519-527.

[79] Stork, C. J., and Li, Y. V. (2010) Zinc release from thapsigargin/IP3-sensitive stores in cultured cortical neurons, *Journal of molecular signaling 5*, 5.

[80] Ohana, E., Hoch, E., Keasar, C., Kambe, T., Yifrach, O., Hershfinkel, M., and Sekler, I. (2009) Identification of the Zn2+ binding site and mode of operation of a mammalian Zn2+ transporter, *Journal of Biological Chemistry 284*, 17677-17686.

[81] Walsh, M. J., and Ahner, B. A. (2013) Determination of stability constants of Cu (I), Cd (II) & Zn (II) complexes with thiols using fluorescent probes, *Journal of inorganic biochemistry 128*, 112-123.

[82] Masuoka, J., Hegenauer, J., Van Dyke, B., and Saltman, P. (1993) Intrinsic stoichiometric equilibrium constants for the binding of zinc (II) and copper (II) to the high affinity site of serum albumin, *Journal of Biological Chemistry 268*, 21533-21537.

[83] Nowakowski, A., and Petering, D. (2012) Sensor specific imaging of proteomic Zn 2+ with zinquin and TSQ after cellular exposure to N-ethylmaleimide, *Metallomics 4*, 448-456.

[84] Woodroofe, C. C., Masalha, R., Barnes, K. R., Frederickson, C. J., and Lippard, S. J. (2004) Membrane-permeable and-impermeable sensors of the Zinpyr family and their application to imaging of hippocampal zinc in vivo, *Chemistry & biology 11*, 1659-1666.

[85] Sinclair, S. A., Sherson, S. M., Jarvis, R., Camakaris, J., and Cobbett, C. S. (2007) The use of the zinc-fluorophore, Zinpyr-1, in the study of zinc homeostasis in Arabidopsis roots, *New Phytologist 174*, 39-45.

[86] Malavolta, M., Costarelli, L., Giacconi, R., Muti, E., Bernardini, G., Tesei, S., Cipriano, C., and Mocchegiani, E. (2006) Single and three-color flow cytometry assay for intracellular zinc ion availability in human lymphocytes with Zinpyr-1 and double immunofluorescence: Relationship with metallothioneins, *Cytometry Part A 69*, 1043-1053.

[87] Lim, N. C., Freake, H. C., and Brückner, C. (2005) Illuminating zinc in biological systems, *Chemistry–A European Journal 11*, 38-49.

[88] Tomat, E., Nolan, E. M., Jaworski, J., and Lippard, S. J. (2008) Organelle-specific zinc detection using zinpyr-labeled fusion proteins in live cells, *Journal of the American Chemical Society 130*, 15776-15777.

[89] You, Y., Tomat, E., Hwang, K., Atanasijevic, T., Nam, W., Jasanoff, A. P., and Lippard, S. J. (2010) Manganese displacement from Zinpyr-1 allows zinc detection by fluorescence microscopy and magnetic resonance imaging, *Chemical Communications 46*, 4139-4141.

[90] Vallee, B. L., and Auld, D. S. (1990) Zinc coordination, function, and structure of zinc enzymes and other proteins, *Biochemistry 29*, 5647-5659.

[91] Stamler, J. S., Singel, D. J., and Loscalzo, J. (1992) Biochemistry of nitric oxide and its redox-activated forms, *SCIENCE-NEW YORK THEN WASHINGTON- 258*, 1898-1898.

[92] Habib, S., and Ali, A. (2011) Biochemistry of nitric oxide, *Indian journal of clinical biochemistry 26*, 3-17.

[93] Gladwin, M. T., Crawford, J. H., and Patel, R. P. (2004) The biochemistry of nitric oxide, nitrite, and hemoglobin: role in blood flow regulation, *Free Radical Biology and Medicine 36*, 707-717.

[94] Wink, D. A., and Mitchell, J. B. (1998) Chemical biology of nitric oxide: insights into regulatory, cytotoxic, and cytoprotective mechanisms of nitric oxide, *Free Radical Biology and Medicine 25*, 434-456.

[95] Jourd'heuil, D., Jourd'heuil, F. L., and Feelisch, M. (2003) Oxidation and nitrosation of thiols at low micromolar exposure to nitric oxide evidence for a free radical mechanism, *Journal of Biological Chemistry 278*, 15720-15726.

[96] Kroncke, K.-D., Fehsel, K., Schmidt, T., Zenke, F. T., Dasting, I., Wesener, J. R., Bettermann, H., Breunig, K. D., and Kolbbachofen, V. (1994) Nitric oxide destroys zinc-sulfur clusters inducing zinc release from metallothionein and inhibition of the zinc finger-type yeast transcription activator LAC9, *Biochemical and biophysical research communications 200*, 1105-1110.

[97] Katakai, K., Liu, J., Nakajima, K., Keefer, L. K., and Waalkes, M. P. (2001) Nitric oxide induces metallothionein (MT) gene expression apparently by displacing zinc bound to MT, *Toxicology letters 119*, 103-108.

[98] Schwarz, M. A., Lazo, J. S., Yalowich, J. C., Allen, W. P., Whitmore, M., Bergonia, H. A., Tzeng, E., Billiar, T. R., Robbins, P. D., and Lancaster, J. R. (1995) Metallothionein protects against the cytotoxic and DNA-damaging effects of nitric oxide, *Proceedings of the National Academy of Sciences 92*, 4452-4456.

[99] Harper, J. V. (2005) Synchronization of Cell Populations in G1/S and G 2/M Phases of the Cell Cycle, *Cell Cycle Control: Mechanisms and Protocols*, 157-166.

[100] Li, F., Ambrosini, G., Chu, E. Y., Plescia, J., Tognin, S., Marchisio, P. C., and Altieri, D. C. (1998) Control of apoptosis and mitotic spindle checkpoint by survivin, *Nature 396*, 580-584.

[101] Gong, J., Traganos, F., and Darzynkiewicz, Z. (1995) Growth imbalance and altered expression of cyclins B1, A, E, and D3 in MOLT-4 cells synchronized in the cell cycle by inhibitors of DNA replication, *Cell growth & differentiation: the molecular biology journal of the American Association for Cancer Research 6*, 1485-1493.

[102] Wei, W., Ayad, N. G., Wan, Y., Zhang, G.-J., Kirschner, M. W., and Kaelin, W. G. (2004) Degradation of the SCF component Skp2 in cell-cycle phase G1 by the anaphase-promoting complex, *Nature 428*, 194-198.

[103] Zhu, X., Kumar, R., Mandal, M., Sharma, N., Sharma, H. W., Dhingra, U., Sokoloski, J. A., Hsiao, R., and Narayanan, R. (1996) Cell cycle-dependent modulation of telomerase activity in tumor cells, *Proceedings of the National Academy of Sciences 93*, 6091-6095.

[104] Samake, S., and Smith, L. C. (1996) Synchronization of cell division in eight-cell bovine embryos produced in vitro: Effects of nocodazole, *Molecular reproduction and development 44*, 486-492.

[105] Brown, M., and Wittwer, C. (2000) Flow cytometry: principles and clinical applications in hematology, *Clinical chemistry 46*, 1221-1229.

[106] Davies, D. (2007) Cell sorting by flow cytometry, In *Flow Cytometry*, pp 257-276, Springer.

[107] Mandy, F. F., Bergeron, M., and Minkus, T. (1995) Principles of flow cytometry, *Transfusion Science 16*, 303-314.

[108] Figueroa, J. A. L., Vignesh, K. S., Deepe, G. S., and Caruso, J. (2014) Selectivity and specificity of small molecule fluorescent dyes/probes used for the detection of Zn 2+ and Ca 2+ in cells, *Metallomics 6*, 301-315.

[109] Kruczek, C., Görg, B., Keitel, V., Pirev, E., Kröncke, K. D., Schliess, F., and Häussinger, D. (2009) Hypoosmotic swelling affects zinc homeostasis in cultured rat astrocytes, *Glia 57*, 79-92.

[110] Jang, Y., Wang, H., Xi, J., Mueller, R. A., Norfleet, E. A., and Xu, Z. (2007) NO mobilizes intracellular Zn2+ via cGMP/PKG signaling pathway and prevents mitochondrial oxidant damage in cardiomyocytes, *Cardiovascular research 75*, 426-433.

CURRICULUM VITAE

Mohammad R. Karim

Education

PhD in Chemistry - August 2016

University of Wisconsin-Milwaukee

Advisor: Distinguished Professor David H. Petering

Dissertation: The Role of Proteome in the Cellular Zn^{2+} Trafficking and in the Ability of the Zinc Fluorescent Sensors to Image Intracellular Zn^{2+}.

Masters of Science (M.S) in Chemistry – 2009

University of Dhaka, Bangladesh

Result: First Class

Thesis: Analysis of organochlorine pesticide DDT and its derivatives in poultry meat and feed using GC-MS.

Bachelor of Science (B.S.) in Chemistry – 2008

University of Dhaka, Bangladesh

Result: First Class

Experiences

Research Assistant at University of Wisconsin-Milwaukee

September 2010 – December 2010; June – August of 2011, 2012 & 2013; June 2014 – June 2016 (3 years 2 months)

- Performed a plethora of experiments to study the role of proteome in cellular Zn^{2+} trafficking resulting in the formation of native Zn-Proteins, and to investigate how zinc fluorescent sensors, such as Newport Green and Zinpyr-1, interact with the cellular constituents.

- Gained expertise in operating analytical instruments including fluorometer, UV-Visible spectrophotometer, Flame Atomic Absorption Spectrophotometer, inductively coupled plasma mass spectrometer (ICP-MS), isothermal titration calorimetry (ITC), and cell culture.

- Mentored three students for undergraduate research.

Teaching Assistant at University of Wisconsin – Milwaukee

September 2009 – May 2010; January – May 2011; September 2011 – May 2012; September 2012 – May 2012; September 2012 – May 2013; September 2013 – May 2014 (4 years 2 months)

- Taught discussion and laboratory classes of undergraduate chemistry courses, including general chemistry for pre-medical and pre-nursing majors, and organic chemistry.
- Worked as a mentor for new teaching assistants to help with teaching discussion and laboratory classes of undergraduate chemistry courses.

Instructor at S@ifu's, Dhaka - Bangladesh

August 2008 – July 2009

- Taught GRE, TOEFL, GMAT and SAT in classrooms to the students aspiring for higher study abroad.

Scholarship and Awards

- Chancellor's Fellowship Award, University of Milwaukee - Wisconsin (September 2009 – May 2014)
- Dean's Award, University of Dhaka (2008)

Selected Presentations

- **Mohammad R. Karim** and David H. Petering. How does Newport Green act as a fluorescent sensor for weakly bound cellular Zn^{2+}? *248th ACS National Meeting and Exposition*, August 2014.

- **Mohammad R. Karim** and David H. Petering. Reaction of Zn-proteome with diethylamine NONOate (DEA-NO): measurement of labilized zinc by TSQ, Zinquin and FluoZin-3 is sensor dependent. *5th Georgian Bay International Conference on Bioinorganic Chemistry*, 2015.

- **Mohammad R. Karim** and David H. Petering. Zinc sensors reveal that proteomic zinc buffering is dependent on sulfhydryl groups. *251st ACS National Meeting and Exposition*, May 2016.

Publications

- **Mohammad R. Karim** and David H. Petering. Newport Green, a Fluorescent Sensor of Weakly Bound Cellular Zn^{2+}: Competition with Proteome for Zn^{2+}. *Metallomics*, 2016, 8 (2), 201 – 210.

- Andrew Nowakowski, **Mohammad Karim**, and David Petering. Zinc Proteomics. *Encyclopedia of inorganic and bioinorganic chemistry*, 2015, 1-10.

- **Mohammad R. Karim** and David H. Petering. Transient Zn^{2+} Release in NO treated Cells and Proteome: Dependence on Fluorescent Sensor and Modulation of Proteomic SH groups. *Submitted*.

Manuscripts in progress

- **Mohammad R. Karim** and David H. Petering. Zinc Sensors Reveal that Proteomic Zinc Buffering is Dependent on Sulfhydryl Groups. *Manuscript in progress*.

- **Mohammad R. Karim** and David H. Petering. The zinc fluorescent sensor Zinpyr-1 forms ternary adduct with proteome and mobile Zn^{2+}. *Manuscript in progress*.